



This is to certify that the

dissertation entitled

Dielectric Study of the Glass Transition in Orientationally-Disordered Crystals

presented by

Matthew A. Miller

has been accepted towards fulfillment of the requirements for

Ph.D. degree in Physics

Major professor
Norman O. Birge

Date 6/19/98

MSU is an Affirmative Action/Equal Opportunity Institution

0-12771



PLACE IN RETURN BOX to remove this checkout from your record. TO AVOID FINES return on or before date due.

DATE DUE	DATE DUE	DATE DUE

1/98 c/CIRC/DateDue.p65-p.14

DIELECTRIC STUDY OF THE GLASS TRANSITION IN ORIENTATIONALLY-DISORDERED CRYSTALS

By

Matthew A. Miller

A DISSERTATION

Submitted to
Michigan State University
in partial fulfillment of the requirements
for the degree of

DOCTOR OF PHILOSOPHY

Department of Physics and Astronomy

1998

ABSTRACT

DIELECTRIC STUDY OF THE GLASS TRANSITION IN ORIENTATIONALLY-DISORDERED CRYSTALS

By

Matthew A. Miller

The glass transition in supercooled liquids occurs when the time required for equilibration processes in the liquid exceeds some experimental timescale. Below the glass transition temperature T_g, the material is designated a *glass* and displays thermodynamic properties more appropriate for a solid than a liquid. Despite considerable theoretical and experimental effort in the past century, a fundamental description of the microscopic mechanisms underlying glass formation has not been realized. Alternative approaches are welcomed which offer the possibility of studying the glass transition in systems displaying reduced structural complexity.

This thesis focuses on studying the glass transition dynamics in a class of materials known as Orientationally-Disordered Crystals (ODC's). The molecules of ODC's possess translational order while retaining orientational degrees of freedom, giving rise to an orientational glass transition which displays the same characteristic features of the glass transition in fully-disordered liquids. Thus, ODC's are of great interest as model glass systems.

Using the technique of dielectric spectroscopy, we have investigated the dynamical behavior of two particular ODC's near their respective glass transitions: Cyclo-Octanol and Ethanol. We find that the orientational glass transition in each material displays the same two characteristic features of the structural glass transition in

fully-disordered liquids: 1) rapidly increasing relaxation times as the temperature is lowered toward the glass transition temperature T_g, and 2) increasingly non-Debye relaxation behavior with decreasing temperature. For ethanol in particular, we have performed a quantitative comparison of the dynamics in the supercooled liquid (SCL) and rotator crystal (RP) phases, and find that rotational motion is the dominant dynamical process governing the glass transition in both phases, and that diffusive processes contribute to a lesser extent.

Finally, we have performed a detailed examination of the shape of the α -relaxation in the SCL and RP crystal phases of ethanol for a frequency range covering ten decades. We find that the high frequency power-law behavior in the RP crystal is consistent with the expectations of a well-known scaling form used for structural glasses, while the limited amount of SCL data appears to show steeper power-law behavior than expected.

To my wife, Lori.

ACKNOWLEDGEMENTS

First and foremost, I would like to thank my advisor, Norman Birge. Without his friendship, guidance, and tireless efforts to obtain financial support for my research, I surely would not have completed this journey.

I thank Charles Moreau for his friendship, engaging conversations, and our competitive "death-matches". I thank David Hoadley for teaching me nearly everything I know about computers and securing a job outside of academia.

I also would like to thank the machine shop guys – Jim Muns, Tom Hudson, and Tom Palazollo - for their highly professional work and endless patience with us graduate students. I am also indebted to Scott and Manfred over in the chemistry glass shop for all their fabrication - and repair - work on the many sample cells that I provided them with.

I thank Monica Jimenez-Ruiz and Javier Bermejo for their extensive contributions to the ethanol work, and Rod Lambert and Diandra Leslie-Pelecky for guidance and contributions to the cyclo-octanol studies.

Of course, a great deal of thanks goes to my family – my wife, Lori, in particular – for supporting me along the way and putting up with me during the difficult times. I would like to thank my parents for constantly encouraging me to achieve goals that sometimes seemed beyond my reach.

Last, but certainly not least, I would like to acknowledge the persistent efforts of my mother-in-law, JoAnn, whose well-worn quote of "Matthew, just put it in HIGH!" no doubt had a significant impact on my success as a graduate student.

TABLE OF CONTENTS

LIST OF TA	BLES.	ix
LIST OF FIG	GURES	x
Chapter 1: II	NTROI	DUCTION1
Chapter 2: C	BLASS	PHENOMENOLOGY7
I.	Supe	rcooled Liquids7
II.	The (Glass Transition in Supercooled Liquids8
	a.	Thermodynamic Aspects8
	b.	Dynamics of Supercooled Liquids near Tg11
		1. Rapidly increasing timescales for motion11
		2. Non-Debye Relaxation14
III.	Over	view of Experimental Studies of the Glass Transition18
IV.	Theo	ries of the Glass Transition in Supercooled Liquids21
	a.	Introduction21
	b.	Theories postulating low temperature phase transitions22
	c.	Theories predicting critical behavior at $T > T_g$ 28
V.	Conc	lusions31
Chapter 3: C	RIENT	CATIONALLY-DISORDERED CRYSTALS34
I.	The r	need for Model Glass Systems34
II.	Histo	ry35
III.	Struc	ture and Dynamics of ODC's36
IV.	Exan	nple ODC's38

V.	Motiv	vation	41
Chapter 4: E	EXPERI	MENTAL TECHNIQUES	44
I.	Diele	ectric Spectroscopy	44
II.	Revie	ew of Dielectric Theory	44
	a.	Polarization Mechanisms Dielectrics	44
	b.	Behavior in Static Fields - Static Dielectric Constant	46
	c.	Time-Varying Fields - Complex Dielectric Constant	52
III.	Diele	ectric Measurement System	57
	a.	Goals of Dielectric Spectroscopy	57
	b.	The Dielectric Sample Cell	58
	c.	Low Frequency Measurement Circuit	59
	d.	High Frequency Measurement Circuit	61
	e.	Cryostat and Temperature Control	63
IV.	Samp	ole Fabrication Methods	64
	a.	Fractional Vacuum Distillation	64
	b.	Nitrogen Atmosphere Loading	66
Chapter 5: D	DIELEC	TRIC STUDIES OF CYCLO-OCTANOL	68
I.	Motiv	vation	68
II.	Diele	ectric Measurement of Cyclo-Octanol	68
	a.	Experimental Notes	68
	b.	Summary of Low Frequency (1mHz - 10kHz) Measuremen	ts70
	c.	High Frequency (1kHz - 10 MHz) Measurements	74
III	Disco	ussion of Results	82

Chapter 6: D	IELECTRIC MEASUREMENT OF ETHANOL85	
I.	Motivation85	
II.	Dielectric Measurement of Ethanol	
	a. Experimental Notes86	
	b. Dielectric Response of SCL and RP Crystal Phases87	
III.	Detailed Study of Shape of the Relaxation in Ethanol97	
	a. Motivation97	
	b. High Frequency Power-Law Behavior98	
	c. Dixon Scaling of Ethanol Dielectric Data106	
Chapter 7: NONLINEAR DIELECTRIC MEASUREMENT109		
I.	Motivation and Background109	
II.	Nonlinear Measurement Circuit111	
III.	Present Status of Experimental Work112	
Chapter 8: SUMMARY AND FUTURE DIRECTIONS114		
Annendix A:	DATA CORRECTION METHODS	

LIST OF TABLES

Table 6.1.	Cole-Davidson fitting parameters for the RP crystal phase of ethanol in the temperature range 96 – 110 K.	92
Table 6.2.	Cole-Davidson fitting parameters for the SCL (96 – 100 K) and high-temperature liquid (164 – 181 K)	92
Table 6.3.	VTF fit parameters of the mean relaxation time in the RP crystal and SCL phases of ethanol	96
Table 6.4.	Parameters obtained in the double CD fitting of the RP crystal phase of ethanol	.100
Table 6.5.	Parameters obtained in the double CD fitting of the SCL phase of ethanol.	.100
Table 6.6.	Measured relaxation widths and comparison of scaling-predicted and actual high-frequency power laws for the RP crystal phase of ethanol	.105
Table 6.7.	Measured relaxation widths and comparison of scaling-inferred and actual high-frequency power laws for the SCL phase of ethanol.	.105

LIST OF FIGURES

Figure 2.1.	Thermodynamic signatures of the glass transition	.9
Figure 2.2.	The use of slower cooling rates results in the glass transition occurring at successively lower temperatures	10
Figure 2.3.	The curvature of the mean relaxation time on an Arrhenius plot varies widely among materials. "Fragile" liquids show strong curvature, while "strong" liquids display nearly arrhenius behavior	13
Figure 2.4.	Imaginary part of the dielectric constant of supercooled ethanol at $T=102$ K. Fits to the Debye, Cole-Davidson ($\alpha=0.796$), and KWW ($\beta=0.850$) functions have been included for reference	16
Figure 2.6.	Graphical illustration of the Kauzmann Paradox	22
Figure 3.1.	The translational order and rotational disorder of molecules in a typical rotator phase crystal	37
Figure 3.2.	Schematic diagram of the phases of cyclohexanol	38
Figure 3.3.	Experimental heat capacity of cyclohexanol in the supercooled S1 phase. The sudden drop in C_p at ~ 150 K is due to the orientational glass transition. (Data from: M. Mizukami <i>et al.</i> , Solid. St. Comm. 100 , 83-88 (1996))	.40
Figure 4.1.	Polar molecules in an external electric field	.45
Figure 4.2.	The response of induced and orientational polarization mechanisms to a constant electric field turned on at $t = 0$.54
Figure 4.3.	Frequency response of a dielectric obeying the Debye equations. This example assumes $\epsilon_0=10,\epsilon_\infty=2.0,$ and $\tau=1.0$.56
Figure 4.4.	Dielectric sample cell used for measurements	58
Figure 4.5	Circuit used for low-frequency (1mHz – 10kHz) measurements	59

Figure 4.6.	Schematic of Four-Terminal-Pair Measurement61
Figure 4.7.	Fractional Distillation System65
Figure 5.1.	Schematic diagram illustrating the various phases of cyclo-octanol69
Figure 5.2.	a) ε' and b) ε'' for the supercooled S1 phase of cyclo-octanol as measured by Leslie-Pelecky et al. in the low-frequency regime71
Figure 5.3.	Temperature dependence of parameters extracted from the KWW fitting of Figure 5.2 data. (a) "streching exponent", β, and (b) mean relaxation time τ
Figure 5.4.	Scaling of the dielectric data using a form given by Dixon, et al Cyclo-octanol begins to show slight deviations from structural glass formers (e.g. glycerol) at high frequencies
Figure 5.5.	The imaginary part of dielectric response of cyclo-octanol covering a frequency range of ten decades. The appears of the high temperature β-relaxation is readily apparent at high frequencies
Figure 5.6.	Some additional examples of high-temperature β relaxation processes similar to those observed in cyclo-octanol. (Data from: G. P. Johari, J. Chem. Phys. 58 , 1776 (1973))
Figure 5.7.	The dielectric loss (ε") curves for cyclo-octanol as obtained by R. Brand. The inset to the figure contains dielectric measurements of the stable crystalline phase S3 at the four lowest temperatures shown on the main plot. (Data from: R. P. Brand <i>et al.</i> , Phys. Rev. B 56 , 5713 (1997))78
Figure 5.8.	The dielectric loss (ϵ'') at a temperature of 160 K as obtained by R. Brand. In contrast to our measurements, Brand identifies three separate processes labeled as α , β , and γ . (Data from: R. P. Brand <i>et al</i> , Phys. Rev. B 56 , 5713 (1997))
Figure 5.9.	Plot of the mean relaxation times for the α , β , and γ processes shown in Figure 5.7. Similar to the results of Leslie-Pelecky <i>et al</i> [3], the behavior of the α -process was found to be non-Arrhenius. The β and γ processes exhibit thermally activated (Arrhenius) behavior. (Data from: R. P. Brand <i>et al</i> , Phys Rev. B 56 , 5713 (1997))
Figure 6.1.	The various phases of ethanol85

Figure 6.2.	(a) ε' and (b) ε'' versus frequency for temperatures of 96, 98, and 100 K in the supercooled liquid phase of ethanol. Solid lines are fits to the Cole-Davidson function
Figure 6.3.	(a) ε' and (b) ε'' versus frequency for temperatures of 96, 98, 100, 102, 104, 106, 108, and 110 K in the RP crystal phase of ethanol. Solid lines are fits to the Cole-Davidson function90
Figure 6.4.	(a) ϵ' and (b) ϵ'' versus frequency for temperatures of 164, 173, and 181 K in the high temperature liquid phase of ethanol. Solid lines are fits to the Cole-Davidson function plus a term of the form $4\pi\sigma_{dc}/\omega$ in ϵ'' due to dc conductivity
Figure 6.5.	Plot of the Cole-Davidson width exponent, α, versus temperature for the SCL and RP crystal phases of ethanol93
Figure 6.6.	Plot of $\varepsilon_0 - \varepsilon_\infty$ versus temperature. The observed decrease in ε_0 - ε_∞ at low temperatures is not due to partial crystallization of the sample94
Figure 6.7.	Temperature dependence of the mean relaxation time for the liquid (above T _M), supercooled liquid, and rotator crystal phases of ethanol
Figure 6.8.	Double CD fitting of 98 K (top) and 100 K (bottom) RP crystal ethanol. Single CD fit is included for reference
Figure 6.9.	Double CD fitting of 102 K (top) and 104 K (bottom) RP crystal data. Fits to the single CD form are included for reference
Figure 6.10	Double CD fitting of 106 K RP (top) and 98 K SCL (bottom). Fits to the single CD form are included for reference
Figure 6.11	. Double CD fitting of 100 K SCL data. Fits to the single CD form are included for reference
Figure 6.12	2. Dixon scaling of the RP crystal and SCL ethanol dielectric data. The RP crystal scales in accordance with structural glasses (represented here by glycerol) while the SCL shows systematic deviations at high frequencies
Figure 7.1.	Circuit for nonlinear measurement111
Figure A.1	Circuit diagram for impedance measurement using HP4192A123

Figure A.2.	Transmission line correction of capacitance data for a 511 pF Air capacitor. Correction of the data obtained at 1 meter should match the data obtained at the instrument front panel (L=0 meters). Clearly, the capacitance data is being over-corrected	127
Figure A.3.	Transmission line correction of conductance data for a 511 pF Air capacitor. Correction of the data obtained at 1 meter should match the data obtained at the instrument front panel (L=0 meters).	
	Instead, the conductance data is being under-corrected	128

Chapter 1

INTRODUCTION

Around 3000 BC, Mesopotamian potters discovered, quite by accident, that common desert sand could be liquified and subsequently cooled to reveal a smooth, shiny substance that we now call silicate *glass*. Today, in addition to these pioneering silicates, there exists a great many glassy materials that find use in applications ranging from the mundane to the complex. Decorative glassware for dining, extremely pure optical communication fibers, and high strength, heat resistant window panes for the Space Shuttle are just a few examples illustrating the wide range of applications [1]. In fact, the manufacture and sale of glassy materials has developed over the last 200 years into a multi-billion dollar industry. This reflects the fact that few other materials can claim to have a similar impact on human cultural and technological development.

Achieving the glassy phase can be accomplished by any of several routes, but the simplest and most technologically useful glasses result from the vitrification of liquids. The process of glass formation begins by cooling a liquid from a temperature well above its crystallization point. The primary requirement to be satisfied is that the liquid must be cooled sufficiently fast so as to avoid the onset of crystallization at the liquid's freezing point. This process is called *supercooling* the liquid and the resultant product designated a *supercooled liquid*. The amorphous glassy phase is produced by continuing to cool the supercooled liquid until it falls out of equilibrium, and measurement of the material's thermodynamic properties will yield values more appropriate to a solid than a liquid. The

point at which the liquid falls out of equilibrium is called the glass transition temperature, T_g, and corresponds roughly to a liquid viscosity of 10¹³ poise.

Detailed study of the glass formation process began well over 100 years ago, and has grown to be a subject of great interest to the physicist, chemist, and material scientist. This long period of study has led to a number of technological improvements, and we have become extremely proficient at manipulating the chemical, electrical, and optical properties of glass to fit a wide range of applications. However, many people are surprised to learn that the actual microscopic mechanisms of glass formation are only poorly understood, and remain largely a mystery.

There are several reasons for why a fundamental understanding of the glass transition has not yet been achieved. First, the glassy state is amorphous in nature and lacks a periodic crystalline lattice that can be treated analytically using the powerful mathematical techniques developed during solid state physics research in the 1950's and 60's. Secondly, the glass transition is not an equilibrium phenomena, making theoretical treatment more difficult. Finally, despite the existence of certain general features characterizing real glasses, there is no universal agreement on which features are considered essential to glassy behavior.

Numerical modeling of the glass transition is also difficult, resulting in computer simulations that occur on picosecond timescales. Experimental studies, on the other hand, are carried out on the order of seconds to minutes, and invariably encounter an equilibration timescale that increases extremely rapidly near the transition. The net effect is that present-day theory and experiment are separated by a wide gap. The lack of a consistent theory that encompasses the experimentally observed features of the transition

to the glassy state continues to provide motivation for scientific study. Perhaps the best way to summarize the current state of glass transition research and expectations for the future is to quote Nobel Laureate W. P Anderson, who, in a recent issue of Science [2] stated the following:

"...perhaps the deepest unsolved problem facing condensed matter physics is the nature of glass and the glass transition. This could be the next major breakthrough..."

In this thesis, the glass transition problem is approached through experimental examination of the dynamical behavior of a class of materials known as Orientationally-Disordered Crystals (ODC's). In addition to possessing a true structural glass transition in the liquid state, these materials also display an orientational glass transition in a state where the molecular centers of mass are arranged on a periodic lattice. Thus, with their restricted degrees of freedom, ODC's are of great interest as model glass-forming systems. Specifically, the technique of dielectric spectroscopy is used is to study the glassy behavior of two ODC's in detail: Cyclo-Octanol (C₈H₁₅OH) and Ethanol (C₂H₅OH).

The first issue addressed in this thesis is the feasibility of ODC's as model glass systems. This thesis will show that model glass systems, with their restricted degrees of freedom, are a useful tool for both experimental and theoretical investigations of glass transition phenomena.

The second major goal of this work is to provide a quantitative comparison of the dynamical behavior in two structurally different phases near their respective glass transition points in a single material. Our recently published work on ethanol [3] allows

one to identify which degrees of freedom – orientational or translational – are most relevant to the glass transition process. Until now, such a comparison has never been carried out due to lack of an appropriate material having sufficient polymorphism and phase stability to allow thorough experimental investigation.

Finally, the last portion of this thesis addresses the question of whether or not a true phase transition underlies the glass transition, which is a question that presently has no definitive answer. To date, there is no experimental evidence to suggest that the glass transition results from anything more than kinetic slowing of the liquid. However, based on thermodynamic arguments, some theories predict the existence of a second order phase transition at or near the glass transition point, and thus the question remains open. To address this question, we are attempting to measure the *nonlinear* dielectric constant of the orientationally-disordered phase of ethanol. The nonlinear dielectric constant is sensitive to the growth of a correlation length, which is a prime indicator of the presence of a second order phase transition.

The remainder of this document takes the following organizational form: Chapter 2 provides a detailed introduction to the phenomenology of the glass transition in supercooled liquids, and reviews the most relevant theoretical and experimental progress to date. Theories of the glass transition involving free volume, excess entropy, and the more recent "mode coupling" approach will be examined. Results from dielectric, specific heat, light scattering, x-ray diffraction, and neutron diffraction studies of the glass transition are also summarized and discussed. Chapter 3 covers the history and structural properties of Orientationally-Disordered Crystals. Experimental aspects are treated in Chapter 4, including dielectric spectroscopy, measurement instrumentation and

sample preparation techniques. Chapter 5 begins with a review of dielectric studies of Cyclo-Octanol, and then presents high-frequency measurements as an extension of previous data. A comparison of the results is made with a similar study carried out simultaneously by another research group. Chapter 6 focuses exclusively on the dielectric spectroscopy of ethanol, and results are presented and discussed. The background and strategy of the nonlinear measurement of ethanol is treated in Chapter 7. Finally, Chapter 8 summarizes the results of these experiments and discusses their relevance to current and future glass transition research.

REFERENCES

- [1] Education Department, The Corning Museum of Glass, One Museum Way Corning, NY 14830. [Online] Available. http://www.corningglasscenter.com, March 27, 1997.
- [2] P.W. Anderson, Science 267, 1616 (1995).
- [3] M. A. Miller, M. J. Ruiz, F. J. Bermejo, and N. O. Birge, Phys. Rev. B 57, June 1 (1998).

Chapter 2

GLASS PHENOMENOLOGY

I. Supercooled Liquids.

The process of glass formation from the liquid state depends critically on the ability to bypass first-order crystallization that normally intervenes and results in an ordered, low energy crystalline phase. The process of avoiding crystallization by using high rates of cooling is called "supercooling" the liquid. Thus, the general term "supercooled liquid" refers to any liquid that exists below its thermodynamic freezing temperature T_m . The thermodynamic properties of the supercooled liquid state are exactly those that would be expected upon extrapolation of the equilibrium liquid properties to temperatures below T_m . It should be emphasized that the supercooled liquid phase is metastable in nature, and is susceptible to crystallization in the presence of a proper catalytic event.

The degree to which a given liquid can be effectively supercooled depends strongly on the rate at which crystal nucleation and growth occurs in the liquid. The liquid will fully crystallize when small regions of crystalline material (called crystallites) form in the liquid and grow beyond a certain critical size. The nucleation of crystallites can occur either heterogeneously or homogeneously, however in practice the dominant process is heterogeneous nucleation, in which crystallites develop in the presence of a catalyst (e.g. suspended impurities or defects in the walls of the container housing the liquid). Typical liquids contain anywhere from 10⁵ to 10⁶ impurities per cm³ [1] and nucleation occurs via the most effective "seed" impurity present. Homogeneous

nucleation, which occurs even in pure liquids free from impurities, results when a fluctuation in the liquid brings together a critical number of molecules into crystalline configuration. This nucleation mechanism is almost never responsible for crystallization as observed in the laboratory, as all real world samples and containers exhibit both impurities and defects to some extent.

Turnbull [2] has identified several factors influencing the crystallization process, some of which are directly controllable in the laboratory. The most critical factors are the prevailing cooling rate -dT/dt, the viscosity of the liquid at the crystallization temperature T_m, the purity of the liquid, and volume of the liquid sample. These factors work in combination to determine the material's overall susceptibility to crystallization. Rapid cooling and high viscosity are effective at suppressing crystallization because the molecules lack the sufficient time and mobility necessary for rearrangement onto a crystalline lattice. Pure liquids provide few sites for nucleation, and small volumes allow for efficient removal of thermal energy from the sample.

II. The Glass Transition in Supercooled Liquids.

II. a. Thermodynamic Aspects.

Continuing to cool the supercooled liquid at a rate prohibiting crystallization will eventually result in the occurrence, at a temperature denoted T_g , of a phenomenon known as the *glass transition*. Figure 2.1 shows the typical behavior of a supercooled liquid near T_g . As the material is cooled through T_g , derivative thermodynamic quantities such as the specific heat $C_p = T\left(\frac{\partial S}{\partial T}\right)_p$ and thermal expansion coefficient $\alpha = \frac{1}{V}\left(\frac{\partial V}{\partial T}\right)_p$ will decreases more or less suddenly from values characteristic of the liquid to values more

appropriate for a solid. Quantities such as the entropy S and specific volume V show a characteristic "leveling off" at $T_{\rm g}$.

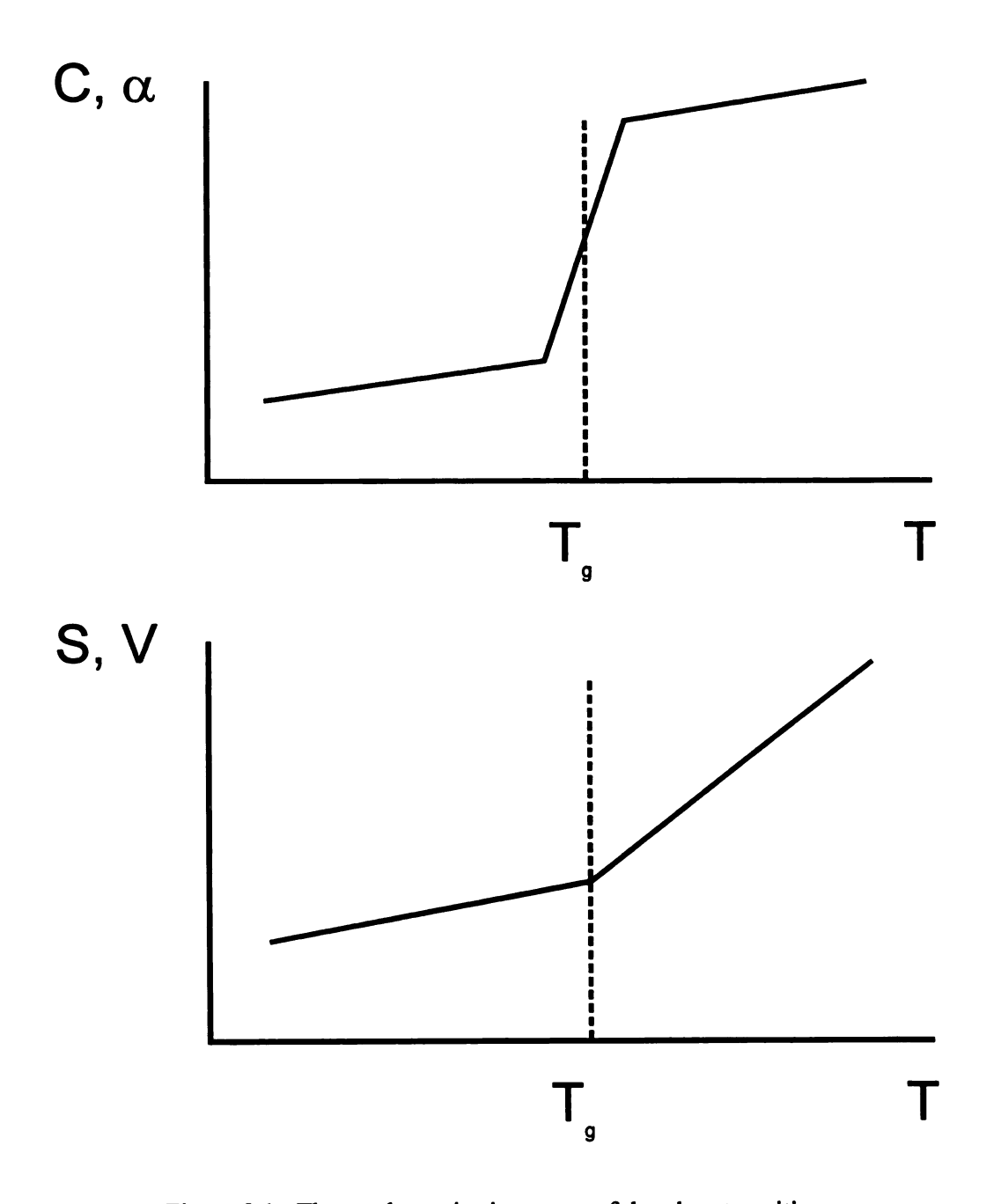


Figure 2.1. Thermodynamic signatures of the glass transition.

Kauzmann [3] pointed out that for a given liquid, the temperature T_g at which the glass transition occurs is not a rigidly defined quantity and instead locates the center of a temperature *interval* over which the observed changes occur. Figure 2.2 shows how the location of T_g and the width of the temperature interval characterizing the transition depend on the rate of cooling used in the experiment. The use of high cooling rates will result in the glass transition occurring at a slightly higher temperature $(T_g^{\ 1})$ and encompassing a broader temperature range relative to what would be observed using slower cooling rates $(T_g^{\ 2}, T_g^{\ 3})$.

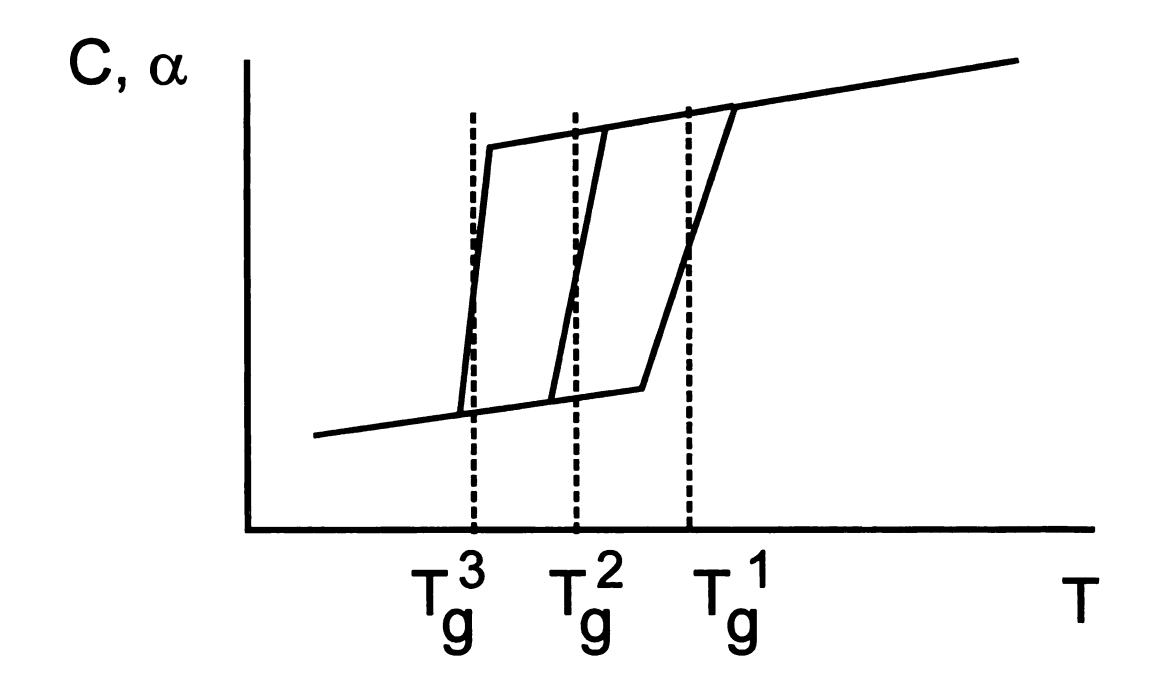


Figure 2.2. The use of slower cooling rates results in the glass transition occurring at successively lower temperatures.

At first glance, the characteristic signatures of the glass transition might resemble the appearance of a second order thermodynamic phase transition. However, as observed in the laboratory, the glass transition is most certainly not a thermodynamic phase transition of any kind. Rather, it is an entirely kinetic phenomenon reflecting the fact that at T_g the time required for structural relaxation processes in the liquid becomes greater than some experimental timescale. In other words, if measurement of some material property reflects the contribution of some structural degree of freedom, then a meaningful contribution will occur only if that degree of freedom has been given the necessary time to fully "relax" and attain equilibrium during the duration of the measurement.

II. b. Dynamics of Supercooled Liquids near Tg.

Experimental data suggest that glass forming liquids display two nearly universal dynamical features near the glass transition: 1) a rapidly increasing timescale for reorientational and diffusional motion, and 2) relaxation behavior which is *non-exponential* (or equivalently, *non-Debye*) in nature. These features will be described in the following sections.

II. b. 1. Rapidly Increasing Timescales for Molecular Motion near Tg.

The response of a material to an externally applied perturbation such as an electric field, heat pulse, or mechanical shear can provide insight into the dynamical processes occurring within the supercooled liquid. The response of the material is a superposition of several relaxation processes that occur on varying timescales. The primary " α -relaxation" of the material is a structural relaxation, and roughly corresponds to overall molecular rotation. Secondary relaxation processes called β -relaxations [4,5] occur above and below T_g , and are representative of intramolecular conformation changes as well as relaxation of interstitial regions between clusters of molecules. These β -processes usually occur at temperatures below T_g where α -relaxation is frozen out, and

provide contributions which are much smaller in magnitude than the α -process. β relaxation processes of intramolecular origin are divided into two categories depending
on the timescale on which they occur: slow processes (β_s) due to internal molecular
conformations and nearly temperature-independent fast processes (β_s) associated with the
vibrational properties of the material.

The most striking feature of the glass transition in supercooled liquids is related to the "freezing out" of the α -relaxation at T_g . This is manifested by an enormous increase (~ 13 orders of magnitude) in the viscosity η and structural relaxation time τ which occurs between the melting temperature T_m and the glass transition temperature T_g . The two quantities η and τ are usually assumed to be proportional to one another as described by the Maxwell theory of viscosity, where the proportionality constant is the high frequency shear modulus:

$$(2.1) \tau = \frac{\eta}{G_n}$$

Figure 2.3 shows the temperature dependence of the structural relaxation time for the α -relaxation process for two typical glass forming liquids. The temperature dependence of τ is often non-Arrhenius, and is often described by the Vogel-Tamman-Fulcher (VTF) [6] phenomenological fitting form given by

(2.2)
$$\tau(T) = \tau_0 \exp(A/(T-T_0))$$

Except in the high and low temperature extremes, the VTF form has successfully characterized the temperature dependence of the relaxation time and viscosity for a wide variety of glass forming liquids, and provides a quantitative measure of a material's departure from Arrhenius-like behavior ($T_0 = 0$). It is interesting to note that the VTF

form predicts that a divergence should occur at $T_0 < T_g$, which has resulted in theoretical models suggesting the possible existence of an "ideal glass transition" having thermodynamic origin at or near T_0 . Theories of the glass transition in supercooled liquids will be reviewed in section IV of this chapter.

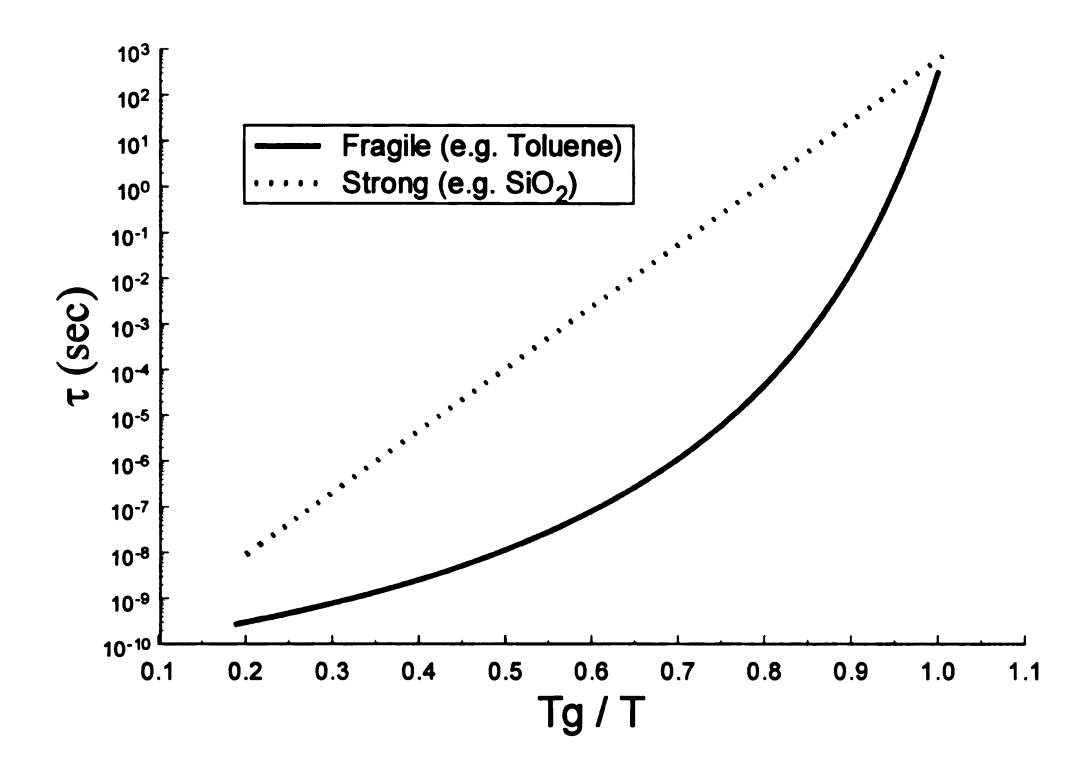


Figure 2.3. The curvature of the mean relaxation time on an Arrhenius plot varies widely among materials. "Fragile" liquids show strong curvature, while "strong" liquids display nearly Arrhenius behavior.

Angell [7] has suggested classifying glass formers based on the degree of curvature exhibited on an Arrhenius plot of the relaxation times. As shown in Figure 2.3, the degree of curvature varies widely among liquids, with strongly bonded systems

typically displaying Arrhenius-like behavior and weakly interacting systems showing strongly non-Arrhenius responses. In Angell's classification scheme, glass-forming liquids are indexed by their *fragility* m, defined by

(2.3)
$$m \equiv [d \log \langle \tau \rangle / d (T_g/T)]_{T = T_g}$$

For example, one of the best known structural glass formers is silicon dioxide (SiO_2), which has a fragility of m = 20 due to nearly Arrhenius-like relaxation behavior arising from a three-dimensional network structure of strong covalent bonds. On the opposite end of the spectrum are liquids composed of weakly interacting molecules such as toluene (m = 107), which show much steeper temperature dependence in their relaxation times and correspondingly higher fragility values.

II. b. 2. Non-Debye Relaxation in Supercooled Liquids.

The second nearly universal feature of supercooled liquids near the glass transition is the appearance of increasing non-Debyeness in the α -relaxation as T_g is approached upon cooling from the melt.

The α -relaxation in supercooled liquids has been studied in the linear response regime using a wide variety of approaches [8] which are able to resolve the dynamical properties of the material near T_g in either the frequency domain or the time domain. The relaxation behavior of a material is characterized by a response function f(t) which describes the time domain response of the system to an external perturbing agent. The frequency domain response can be derived through Fourier transformation of f(t):

(2.4)
$$f(\omega) \sim F \{-df/dt\}$$

The simplest type of response function assumes that the perturbed system will regain its equilibrium configuration in an exponential manner characterized by a single relaxation time τ . This is the so-called Debye relaxation function, which is expressed in the time domain as

$$(2.5) f_{Debye}(t) \sim \exp[-(t/\tau)]$$

The frequency domain representation is obtained using eq. 2.4:

$$(2.6) \quad f_{Debye}(\omega) \sim \int\limits_{-\infty}^{\infty} e^{i\omega t} \Biggl[-\frac{d}{dt} \Bigl(f_{Debye}(t) \Bigr) \Biggr] dt$$

(2.7)
$$f_{Debye}(\omega) \sim \frac{1}{1-i\omega t}$$

However, the response of a glass forming liquid rarely obeys eq. 2.5, and instead displays a characteristic departure from Debye behavior in the form of a relaxation which is typically broadened relative to eq. 2.5. Figure 2.4 shows the actual imaginary part of the relaxation response of Ethanol (C_2H_5OH , $T_g=97$ K) as obtained from measurements of the complex dielectric constant $\varepsilon(\omega,T)=\varepsilon'+i\varepsilon''$ in a frequency-domain dielectric spectroscopy experiment (dielectric spectroscopy is outlined in detail in Chapter 4). The Debye form of the dielectric constant is given by the *Debye equations*:

(2.8)
$$\varepsilon' = \varepsilon_{\infty} + \frac{\varepsilon_0 - \varepsilon_{\infty}}{1 + \omega^2 \tau^2}$$

(2.9)
$$\varepsilon'' = \frac{\omega \tau \left(\varepsilon_0 - \varepsilon_{\infty}\right)}{1 + \omega^2 \tau^2}$$

To illustrate the departure from Debye-like behavior, the Debye response of eq. 2.9 is also plotted on Figure 2.4, along with Cole-Davidson (α =0.796) and KWW (β =0.850) fits to the data. The width of the ethanol relaxation is clearly broadened.

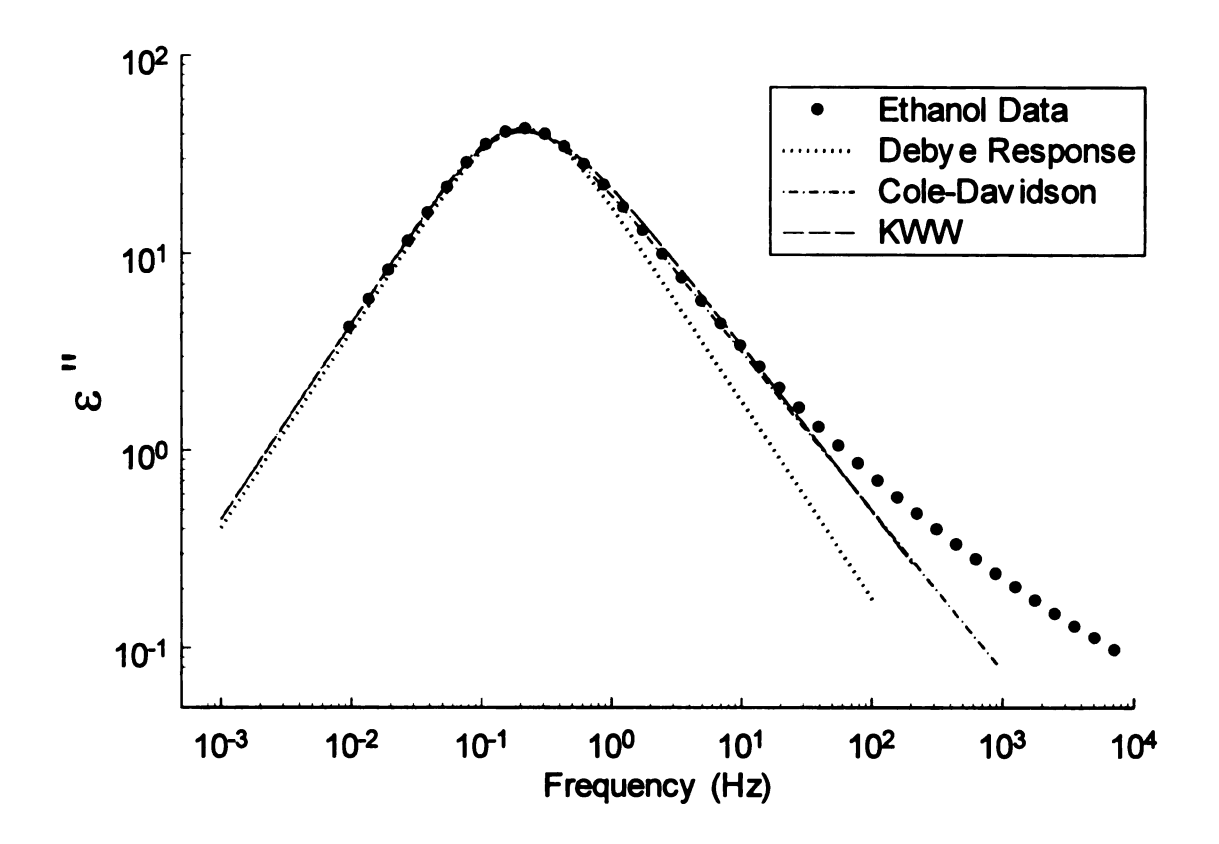


Figure 2.4. Imaginary part of the dielectric constant of supercooled ethanol at T=102 K. Fits to the Debye, Cole-Davidson ($\alpha=0.796$), and KWW ($\beta=0.850$) functions have been included for reference.

To account for the broadened shape, phenomenological fitting functions such as the Kohlraush-Williams-Watts (KWW) [9] and Cole-Davidson (CD) [10] forms have been applied with good success in the peak region of the relaxation. In the frequency domain, the KWW function is the Fourier-transform of a stretched exponential time domain function:

(2.10)
$$f_{kww}(t) \sim \exp[-(t/\tau)^{\beta}]$$

The stretching exponent β , which can vary between 0 and 1, provides a measure of the degree of departure from a Debye relaxation ($\beta = 1$). Furthermore, it can be shown [11] that β is related to width of the asymmetrically shaped imaginary part of the relaxation shown in Figure 2.4. More specifically, β can be related to the normalized width w, which is the full width of the relaxation at half maximum (W) in decades divided by the width of a Debye relaxation ($W_D = 1.14$ decades):

$$(2.11)$$
 $w = W / W_D$

(2.12)
$$(1 - \beta) = 1.047 (1 - w^{-1})$$

The Cole-Davidson (CD) function also gives an estimate of non-Debyeness, and is used extensively in frequency-domain dielectric spectroscopy studies:

(2.13)
$$\varepsilon(\omega) = \varepsilon_{\infty} + (\varepsilon_{0} - \varepsilon_{\infty})/(1 - i\omega/\omega_{p}^{CD})^{\alpha}$$

Here, the exponent α ranges between 0 and 1, providing a measure of the non-exponentiality of the relaxation. The CD form reduces to the Debye form for the case of $\alpha = 1$.

Bohmer et al. [12] have studied the degree to which the fragility is correlated with non-exponentiality of the relaxation process for a given material. By plotting the fragility of the material versus the stretching exponent β obtained at T_g, he suggests that a general correlation exists between the two which arises from the nature of the bonding mechanism present. "Fragile" liquids (high m values) typically show non-Arrhenius relaxation behavior and highly non-exponential relaxations, while "Strong" liquids (low m values) exhibit Arrhenius relaxation behavior and relaxation which is closer to exponential.

Richert [13] has suggested two possible explanations for the non-exponential nature of the relaxation process in supercooled liquids. The first approach assumes that the supercooled liquid consists of many individual heterogeneous regions each of which relax in a nearly exponential manner but with differing relaxation times. The non-exponential relaxation behavior of the material is then the result of averaging the distribution of exponential relaxations governing behavior in the individual sub-regions. The second approach assumes that the sub-regions of the liquid are all homogeneous and that the relaxation of each region is intrinsically non-exponential.

III. Overview of Experimental Studies of the Glass Transition.

Experimental study of the dynamical aspects of the glass transition in supercooled liquids has been carried out using a variety of methods over a very long period of time. The common goal of dynamical studies is to determine the response of a material in the presence of an external perturbing agent. Each technique probes the dynamical response on a characteristic timescale, and is sensitive to certain degrees of freedom such as molecular reorientation or vibration. Some techniques provide greater flexibility than others, and in many cases the results of independent methods can be combined to form more or less complete picture of the material behavior at various timescales.

There are several ways to categorize the methods that are used in studies of the glass transition. The approach that will be taken in this thesis will be to categorize experimental methods based upon the timescale which they are most successful in examining. To this end, we can divide the range of supercooled liquid behavior into three dynamical regimes: (1) slow processes such as those associated with molecular

reorientation and diffusion, (2) intermediate processes associated with intramolecular conformation, and (3) fast dynamics associated with phonon processes.

Slow dynamics (~10⁻³ seconds and longer) which are typically associated with the α -relaxation have been examined with a variety of methods including dielectric spectroscopy [14-17], specific heat spectroscopy [18,19], frequency-dependent shear modulus [20], and ultrasonics [21]. Dielectric spectroscopy (see Chapter 4) uses alternating electric fields to probe polarization processes in a material, and is capable of studying dynamical behavior over an extremely wide range of timescales ($10^{-11} - 10^6$ seconds). Specific heat spectroscopy is a relatively new technique that investigates the frequency-dependence of the specific heat in response to small temperature oscillations of the system about a point of equilibrium. Ultrasonic experiments typically measure density relaxation in response to acoustical stimuli.

The intermediate dynamical regime is more difficult to quantitatively define, but roughly corresponds to timescales of approximately $10^{-3} - 10^{-8}$ seconds. Probes that are effective in this range include dielectric spectroscopy and ultrasonics. This timescale is characteristic of β -relaxation processes that are typically easiest to observe at temperatures below T_g . Below T_g , the large response of the α -relaxation is suppressed (frozen out), leaving faster processes such as molecular side-group rotations in a more favorable position for observation.

The fast process regime occurs on a timescale that is shorter than approximately 10^{-9} seconds. Among the tools available to the experimenter are inelastic (Brillouin) light scattering ($10^{-9} - 10^{-12}$ sec), inelastic neutron scattering ($10^{-10} - 10^{-12}$ sec), and dielectric spectroscopy. The Mode-Coupling Theory (MCT) of viscous liquids (see section IV.c.)

has recently made predictions regarding the nature of fast relaxation processes above T_g , and many of these experimental techniques have focused on verifying these predictions. Examples of this include neutron scattering studies [22] of the so-called "Boson Peak", which is a collection of vibrational states giving rise to a distinct peak in the relaxation spectra of supercooled liquids in the 0.1 - 1 THz frequency range. The crossover from structural relaxation (α -process) to fast vibrational excitations have been studied by dielectric [23] and light scattering [24] experiments, and incoherent neutron scattering [25] has been used to study the crossover from Debye to non-Debye behavior in the α -relaxation.

One principal focus of recent studies is determination of the mean relaxation time $\tau(T)$ for various relaxation processes. Wu *et al.* [26] have recently compared the mean α -relaxation time as determined by various techniques including specific heat spectroscopy and dielectric spectroscopy carried out on the same material. It is a remarkable fact that while each technique probes a different property of the material, the measurements show the same qualitative behavior and in some cases the measured relaxation times are virtually identical.

The similarity of relaxation phenomena as measured by various techniques has prompted to some to search for "universalities" in the behavior of supercooled liquids near the glass transition. Dixon *et al.* [27] have proposed an empirical scaling form which appears to successfully collapse the dielectric spectroscopy data for a variety of simple liquids onto a single "master curve". Whether this scaling form suggests a deeper universality underlying the behavior of supercooled liquids remains an open question.

The scaling form and its inherent advantages and disadvantages will be discussed in more detail in Chapter 5.

IV. Theories of the Glass Transition in Supercooled Liquids.

IV. a. Introduction.

Theoretical study of the slowing dynamics of supercooled liquids approaching the glass transition has been a topic of intense study for many years. Early studies postulated the existence of a true phase transition at a temperature $T < T_g$ based on reasonable extrapolations of various thermodynamic quantities to temperatures below T_g. recently, attempts have been made using first-principle hydrodynamical arguments to characterize the behavior of liquids at temperatures well above Tg in hope of gaining a basic understanding of the processes involved in the initial slowing of the liquid. useful then, to attempt to classify theories of viscous slowdown and the glass transition into separate categories based upon the temperature range in which they are deemed most appropriate. Following an approach by Ediger et al. [28], theories of supercooled liquid behavior can be classified as one of two types: (1) Theories which postulate a lowtemperature phase transition as being responsible for the apparent divergence, at a temperature $T_0 < T_g$, of the viscosity and mean relaxation times as predicted by the VTF form (eq. 2.2), and (2) Theories which attempt to characterize the initial slowing of the high temperature liquid, resulting in the prediction of divergent behavior near a high temperature critical point T_c.

IV. b. Theories predicting low temperature phase transitions.

In 1948, Walter Kauzmann [3] first proposed that a thermodynamic phase transition might be responsible for the glass transition in supercooled liquids. The argument, generally referred to as the "Kauzmann Paradox", involves examination of the supercooled liquid entropy S as shown schematically in Fig. 2.5 for three cooling rates R_1, R_2 , and R_3 .

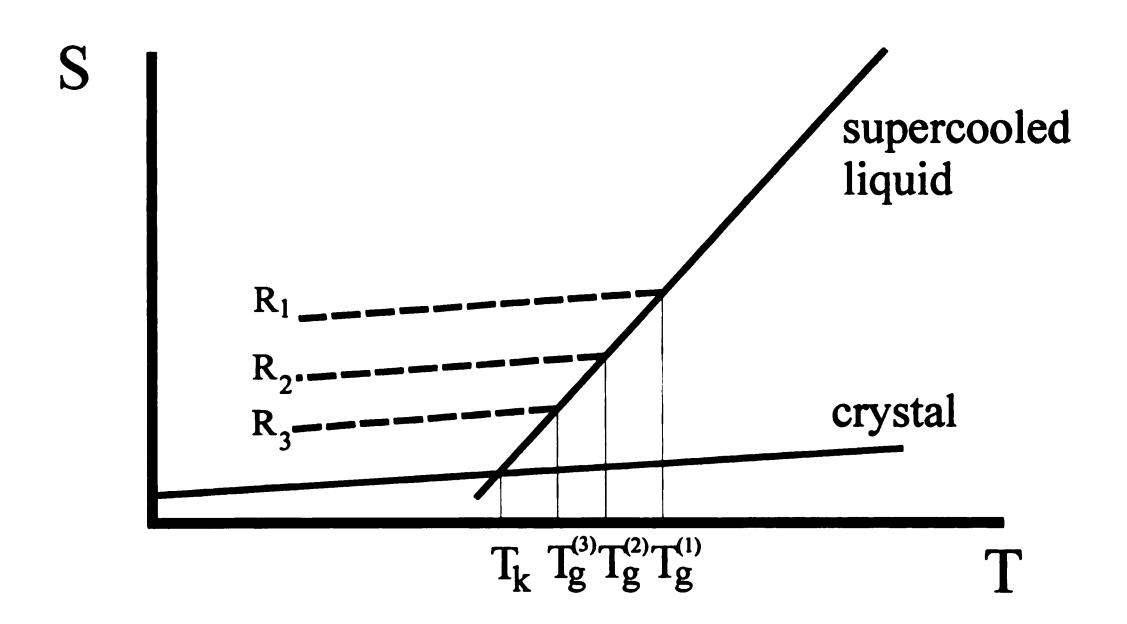


Figure 2.6. Graphical illustration of the Kauzmann Paradox.

The argument goes as follows: For a given rate of cooling R_1 , the laboratory glass transition will be seen to occur at a temperature $T_g^{(1)}$, at which point the specific heat

However, if a slower rate R_2 of cooling is used, the liquid has more time to equilibrate and the glass transition will occur at a temperature $T_g^{(2)}$ where $T_g^{(2)} < T_g^{(1)}$. Following this line of reasoning, one can imagine cooling slower and slower until eventually the entropy of the supercooled liquid becomes equal to the entropy of the low energy crystalline phase. The temperature T_K at which this occurs is called the Kauzmann Temperature and further extrapolation of the liquid entropy for an infinitely slow rate of cooling leads to the undesirable situation of negative liquid entropy at temperatures well above 0 K. Such a situation is a clear violation of the 3^{rd} law of thermodynamics, and has been termed the "Entropy Crisis" in the glass transition literature. Kauzmann proposed that a mechanism, such as a thermodynamic phase transition, must exist in the vicinity of T_K which would prevent the liquid from entering a regime where its entropy is less than that of the crystal.

Support was given to the phase transition idea from the predicted divergence of the relaxation times (or equivalently, the viscosity) by the VTF form (eq 2.2) at a temperature T_0 , which in many cases was striking similar to T_K . The Kauzmann Paradox and its implication of an impending entropy crisis in supercooled liquids fueled the efforts and imagination of theorists in the 1950's and 1960's. This time period was largely dominated by two prevalent theories of the glass transition: Free-Volume Theory, and Adam-Gibbs Theory.

Free-Volume Theory was first introduced by Cohen and Turnbull [29,30] in the late 1950's and later received a modified interpretation in terms of percolation theory [31,32]. In its simplest form, the theory imagines that an individual molecule moves

through a fluid comprised of other identical molecules. At high temperatures, the molecule is relatively free to move about, and interacts with other molecules through binary collision events. As the liquid temperature decreases and the density increases, each molecule becomes enclosed in a transient "cage" formed by neighboring molecules. In this scenario, the molecule undergoes many collision events with the molecules comprising the cage before finally escaping via diffusion. The free volume available to the molecule, designated by v_f , is defined to be the volume v_f of the transient cage minus the minimum physical volume v_f of the molecule:

$$(2.14) v_f = v - v_c$$

Diffusive displacement, or the ability of a molecule to escape the cage, depends on the formation of voids through statistical fluctuation of the free volume. It can be shown [30] that if the temperature dependence of the free volume is assumed proportional to $T - T_0$, then the viscosity of the liquid will assume a VTF form (eq. 2.2). As the temperature approaches T_0 , the glass transition will occur as the cage effect strengthens and the number of available escape routes from the cage becomes vanishingly small.

The free-volume approach is intuitively appealing, however many theoreticians viewed it with skepticism due to the rather imprecise definition of what exactly constituted the "free volume" for a molecule. In the early 1960's, Adam and Gibbs [33] sought to explain the glass transition phenomena using fundamental thermodynamic arguments, with a belief that the entropy of a system was the principal variable governing glass formation. They proposed a molecular theory of the glass transition based on the notion that the liquid could be divided into small subsystems called *cooperatively rearranging regions* (CRR's). The basic premise of the theory was that molecular

packing in viscous liquids was too restrictive for individual molecules to reorient without the cooperation of their neighbors. The relaxation response of a material to a perturbative stress would then consist of a cooperative movement, or rearrangement, of groups of molecules. An individual CRR was defined to be a subsystem of the sample containing z molecules, which could rearrange itself into another independent configuration if given a sufficient fluctuation in energy. The macroscopic system was considered to be an ensemble of N equivalent, non-interacting CRR's, with an isothermal-isobaric partition function given by

(2.15)
$$Z = \sum_{E,V} w(z, E, V) \exp(-E/kT) \exp(-PV/kT)$$

where w is the degeneracy of energy-level E and volume V of the subsystem. If the sum in eq. 2.15 is taken only over values of E and V that permit a transition, then the result will be Z', an expression for the partition function of rearrangeable subsystems. The Gibbs free energy can be then be defined in each case as

(2.16)
$$G = z\mu = -kT \ln Z$$

(2.17)
$$G' = z\mu' = -kT \ln Z'$$

where μ and μ' are chemical potentials. If it is assumed that n of the N subsystems are in states allowing a transition, then the cooperative transition probability $W_z(T)$ is given by

(2.18)
$$W_z(T) \propto \frac{n}{N} = \frac{Z'}{Z} = \exp[-(G' - G)/kT]$$

Substitution of 2.16 and 2.17 into 2.18 yields the transition probability of a cooperative region as a function of its size z:

(2.19)
$$W_z(T) = A \exp(-z\Delta\mu/kT)$$

Here $\Delta\mu=\mu'-\mu$ represents the potential energy hindering the cooperative rearrangement and A is a frequency factor whose dependence on T and z is assumed negligible in comparison to that encountered in the exponential. The average transition probability $\overline{W}(T)$ is determined by summing over all possible non-vanishing values of $W_z(T)$ corresponding to different values of z. Before the sum can be carried out however, it should be noted that there is a critical lower limit z^* to the size of cooperative regions that can contribute non-zero transition probabilities. For a given temperature, z^* is determined by the smallest cooperative region that contains two configurations: one in which the region resides before transition, and another into which it may move. The sum is then expressed as

(2.20)
$$\overline{W}(T) = \sum_{z=z}^{\infty} A \exp[-z\Delta\mu/kT]$$

The summation of this geometrical series is

(2.21)
$$\overline{W}(T) = \frac{A}{1 - \exp(-\Delta \mu / kT)} \exp\left(\frac{-z^* \Delta \mu}{kT}\right)$$

and for $\Delta\mu/kT >> 1$ the denominator is nearly 1 and essentially independent of temperature. Absorbing it into a new temperature independent prefactor \overline{A} gives

(2.22)
$$\overline{W}(T) = \overline{A} \exp \left(\frac{-z^* \Delta \mu}{kT} \right)$$

Based on configurational entropy arguments, it can be shown that the critical size z* can expressed as

$$(2.23) z' = \frac{N_A s_c}{S_c}$$

where N_A is Avogadro's number, s_c^* is the critical configurational entropy and S_c is the configurational entropy of the macroscopic system. N_A , $\Delta\mu$, k, and s_c^* can be absorbed into a new constant C and the average cooperative transition probability becomes

(2.24)
$$\overline{W}(T) = \overline{A} \exp\left(\frac{-C}{TS_c}\right)$$

The final step involves supplying a suitable expression for the configurational entropy S_c , which is the difference between the liquid and crystal entropy and depends on temperature. The temperature dependence of S_c can be determined by integration of the excess specific heat $\Delta C_p = C_p^{liquid} - C_p^{glass}$:

$$(2.25) S_c(T) = \int_{T_b}^{T} \frac{\Delta C_p}{T} dT$$

Providing a functional form for ΔC_p is difficult, but it has been shown [34] that the particularly simple form $\Delta C_p = \alpha/T$, where α is a material dependent constant, describes the behavior of many molecular liquids. Using this form, the integration in eq. 2.25 is straightforward and yields

$$(2.26) S_c(T) = \frac{\alpha(T - T_K)}{T_K T}$$

This result can be substituted into eq. 2.24, to yield the final form of the transition probability:

(2.27)
$$\overline{W}(T) = \overline{A} \exp \left(\frac{-CT_K}{\alpha (T - T_K)} \right)$$

The mean relaxation time for the system is defined by $\tau \equiv 1/\overline{W}(T)$, and inversion of eq. 2.27 leads to the VTF expression (eq. 2.2) with the identification that D = C/A, $T_K = T_0$, and $\tau_0 = 1/\overline{A}$:

(2.28)
$$\tau(T) = \tau_0 \exp\left(\frac{DT_0}{T - T_0}\right)$$

The emergence of the VTF expression represents the major success of the Adam-Gibbs theory. Based on the idea of cooperatively rearranging subsystems, the prediction of non-Arrhenius behavior of the relaxation time agrees well with the experimentally established fact that many liquids display deviations from thermally-activated behavior. However, the theory in its original form provides little explanation for the observed non-exponential shape of the relaxation as discussed previously in section II.b.2. Recently, claims have been made [35] that non-exponential behavior will result if the Adam-Gibbs approach is modified to include interactions between the CRR's.

IV. c. Theories predicting critical behavior at $T > T_g$.

Early work on the liquid-glass transition focused almost exclusively on the temperature region near T_g and placed little, if any, attention on liquid behavior at higher temperatures. However, within the last decade much theoretical (and experimental) study of the liquid-glass transition has shifted the focus toward the high-temperature regime T_g $< T < T_m$ and away from the traditional low-temperature regime near T_g . The reason for this shift in focus is primarily due to the advent of Mode-Coupling Theory (MCT), which is an outgrowth of hydrodynamical liquid theory developed by Leutheusser [36] and Bengtzelius *et al.* [37,38] in the mid-1980's.

The rearrangement of molecules in a supercooled liquid is directly related to fluctuations in the local density. MCT asserts that the detailed nature of these structural rearrangements is contained in the time-dependent density autocorrelation function, $F(\bar{q},t)$. This quantity describes the time-dependence of the relaxation of density fluctuations having wavevector \bar{q} . $F(\bar{q},t)$ is also known as the intermediate scattering function, and is expressed as follows:

(2.29)
$$F(\vec{q},t) = \frac{1}{N} \langle \delta \rho^{\bullet}(\vec{q},t) \, \delta \rho(\vec{q},0) \rangle$$

where the microscopic density in the liquid $\rho(\bar{q}, t)$ given by

(2.30)
$$\rho(\vec{q},t) = \sum_{j=1}^{N} \exp(i\vec{q} \cdot \vec{r}_{j}(t))$$

where N is the number of particles and $\vec{r}_j(t)$ denotes the position of particle j at time t. The use of the intermediate scattering function $F(\vec{q},t)$ as the starting point for determining the dynamical behavior of the material is also of great practical importance to experimentalists, as this quantity can be measured in neutron and light scattering experiments.

Assuming the liquid is isotropic in nature, the equations of motion for $F(\bar{q},t)$ can be written in a form resembling a damped harmonic oscillator:

(2.31)
$$\ddot{F}(q,t) + \Omega^{2}(q)F(q,t) + \int_{0}^{t} \left[M^{0}(q,t-t') + \Omega^{2}(q)m(q,t-t')\right] \dot{F}(q,t')dt' = 0$$

Here, $\Omega^2(q)$ is a microscopic frequency, $M^0(q, t-t')$ is a function that describes the short time dynamics of the system, and m(q, t-t') represents the dynamics on longer timescales. In the *idealized* [38] version of MCT, $M^0(q, t-t')$ is assumed to be sharply

peaked around t=0, and m(q, t-t') is assumed to be quadratic in the correlation functions $F(\vec{q},t)$. The compicated mode-coupling equations, whose solution gives the full time-dependence of the intermediate scattering function, emerge upon substituting these forms for $M^0(q,t-t')$ and m(q,t-t') into eq. 2.31.

Solution of the idealized mode-coupling equations leads to predictions for the dynamical behavior of supercooled liquids. One of the main predictions is that there exists a critical temperature T_c at which the diffusion constant D (or equivalently, the inverse of the α -relaxation time τ) vanishes as a power-law:

(2.32)
$$D \propto \tau^{-1} \propto (T - T_c)^{\gamma}$$
, $\gamma > 1.5$

The critical temperature T_c is predicted to lie in the region between T_g and T_m , and such behavior has been verified recently in the computer simulation of a binary Lennard-Jones system [39]. Experimental investigations of real systems [40] reveal the existence of power law behavior at high temperatures ($T_c > T_g$) but fail to follow the power law close to T_c .

The fact that the experimentally determined α -relaxation times fail to show the predicted divergence at T_c has prompted re-examination of the MCT and its assumptions. In the *extended* [41] version of MCT, an additional term is included in the definition of $M^0(q,t-t')$ so as to allow for activated "hopping" processes which are ignored in the idealized version of the theory. It is claimed that the addition of hopping processes restores ergodicity in the liquid and results in no divergence of τ near T_c .

The second notable feature of MCT is its prediction of distinct relaxation processes occurring on varying timescales within the liquid. As discussed earlier in this chapter, it is well known that distinct α - and β -relaxation processes exist in real liquids.

MCT has attracted a significant amount of attention in the glass literature due to its prediction of crossover behavior between the various relaxation regimes. Stimulated by this prediction, many current experimental efforts have focused on studying such crossover behavior [25].

V. Conclusions.

As described in this chapter, the phenomenology of supercooled liquids is now well developed. The three major theoretical approaches (Free-Volume, Adam-Gibbs, and MCT) have provided useful starting points for understanding the dynamics of supercooled liquids. However, no single theory has yet been able to capture all of the salient features of the glass transition.

At present, MCT appears to demand the most attention in the literature due to its success in qualitatively describing the high temperature behavior of liquids. However, because it is presently unable to account for the observed behavior of real liquids in the lower temperature regime (T < T_c) there is considerable disagreement regarding the ability of MCT to provide a fundamental theory of the glass transition. For the number of experimental studies confirming the predictions of MCT, there is an equal number producing results which appear inconsistent with the theory [28,42]. It is possible that future versions of MCT (e.g. revisions of the more complex *extended* version) will resolve these issues and provide a more quantitative description of the dynamics at low temperatures.

REFERENCES

- [1] D. R. Uhlmann, J. Non-Cryst. Solids 7, 337 (1972).
- [2] D. Turnbull, Contemp. Phys. 10, 473 (1969).
- [3] W. Kauzmann, Chem. Rev. 43, 219 (1948).
- [4] G. P. Johari, Ann. New York Acad. Sci. 279, 117 (1976).
- [5] G. P. Johari and M. Goldstein, J. Chem. Phys. 53, 2372 (1971).
- [6] H. Vogel, Phys. Z. 22, 645 (1961); G.S. Fulcher, J. Am. Ceram. Soc. 8, 339 (1925);
 G. Tamman and W. Hesse, Z. Anorg. Chem. 156, 245 (1926).
- [7] C. A. Angell, J. Non-Cryst. Solids 131-133, 13 (1991).
- [8] L. Wu, P. K. Dixon, and S. R. Nagel, J. Non-Cryst. Solids 131-133, 32 (1991).
- [9] G. Williams and D. C. Watts, Trans. Faraday Soc. 66, 80 (1970).
- [10] D.W. Davidson and R.H. Cole, J. Chem. Phys. 18, 1417 (1951).
- [11] P. K. Dixon, Phys. Rev. B 42, 8179 (1990).
- [12] R. Bohmer, K. L. Ngai, C. A. Angell, D. J. Plazek, J. Chem. Phys. 99, 4201 (1993).
- [13] R. J. Richert, J. Non-Cryst. Solids 172-174, 209 (1994).
- [14] M. Shablakh, R. M. Hill, and L. A. Dissado, Chem. Soc. Faraday Trans. 2 78, 625 (1982).
- [15] L. Wu, Phys. Rev. B 43, 9906 (1991).
- [16] M. A. Miller, M. J. Ruiz, F. J. Bermejo, and N. O. Birge, (accepted for publication in Phys. Rev. B 57, June 1, 1998).
- [17] D. L. Leslie-Pelecky and N. O. Birge, Phys. Rev. B 50, 13250 (1994).
- [18] N. O. Birge, Phys. Rev. B 34, 1631 (1986).
- [19] P. K. Dixon, Phys. Rev. B 42, 8179 (1990).
- [20] Y. H. Jeong, Phys. Rev. A 36, 766 (1986).
- [21] Y. H. Jeong, S. R. Nagel, and S. Bhattacharya, Phys. Rev. A 34, 602 (1986).

- [22] F. J. Bermejo, A. Criado, and J. L. Martinez, Phys. Lett. A 195, 236 (1994).
- [23] P. Lunkenheimer, A. Pimenov, M. Dressel, Yu. G. Goncharov, R. Bohmer, and A. Loidl, Phys. Rev. Lett. 77, 318 (1996).
- [24] H. Z. Cummins, G. Li, Y. H. Hwang, G. Q. Shen, W. M. Du, J. Hernandez, and N. J. Tao, Z. Phys. B 103, 501 (1997).
- [25] J. Colmenero, A. Arbe, and A. Alegria, Phys. Rev. Lett. 71, 2603 (1993).
- [26] L. Wu, P. K. Dixon, S. R. Nagel, B. D. Williams, and J. P. Carini, J. Non-Cryst. Solids 131-133, 32 (1991).
- [27] P. K. Dixon, L. Wu, S. R. Nagel, B. D. Williams, and J. P. Carini, Phys. Rev. Lett. 65, 1108 (1990).
- [28] M. D. Ediger, C. A. Angell, and S. R. Nagel, J. Phys. Chem. 100, 13200 (1996).
- [29] D. Turnbull and M. H. Cohen, J. Chem. Phys. 29, 1049 (1958).
- [30] D. Turnbull and M. H. Cohen, J. Chem. Phys. 31, 1164 (1959).
- [31] M. H. Cohen and G. S. Grest, Phys. Rev. B 20, 1077 (1979).
- [32] G. S. Grest and M. H. Cohen, Phys. Rev. B 21, 4113 (1980).
- [33] G. Adam and J. H. Gibbs, J. Chem. Phys. 43, 139 (1965).
- [34] C. A. Angell and W. Sichina, Ann. New York Acad. Sci. 279, 53 (1976).
- [35] K.L. Ngai, J. Non. Cryst. Solids 131-133, 80 (1991).
- [36] E. Leutheusser, Phys. Rev. A 29, 2765 (1984).
- [37] U. Bengtzelius, W. Gotze, and A. Sjolander, J. Phys. C 17, 5915 (1984).
- [38] W. Gotze and L. Sjogren, Rep. Prog. Phys. 55, 241 (1992).
- [39] W. Kob and H. C. Andersen, Phys. Rev. Lett. 73, 1376 (1994).
- [40] P. Taborek, R. N. Kleinman, and D. J. Bishop, Phys. Rev. B 34, 1835 (1986).
- [41] W. Gotze and L. Sjogren, J. Phys. C 21, 3407 (1988).
- [42] B. Kim and G. F. Mazenko, Phys. Rev. A 45, 2393 (1992).

Chapter 3

ORIENTATIONALLY-DISORDERED CRYSTALS

I. The Need for Model Glass Systems in Studies of the Glass Transition.

The difficulties involved in studying the glass transition in supercooled liquids were briefly remarked upon in Chapter 1, and can essentially be linked to the inherent complexity of the liquid state itself. In general, six degrees of freedom must be associated with each constituent molecule of the liquid: three translational degrees to locate the molecule with respect to some origin and three more to describe its orientation. The situation is further complicated when attempts are made to account for the often transient nature of interactions between the molecules. Thus, the need to treat both translational and rotational degrees of freedom constitutes a significant barrier for theoretical and computer-simulation studies of the glass transition. The result has been the formation of a large gap between theory/simulation and experiment. Computer simulations of the glass transition in systems containing perhaps several hundred particles over timescales of 10^{-10} to 10^{-12} seconds is clearly far from what is examined in real experiments. To emphasize this point, Angell [1] has recently classified various features of the glass transition according to the level of difficulty involved in their simulation by computer. Despite the rapid advances in calculation speed of today's modern computers, he has concluded that much of the interesting phenomena occurring in supercooled liquids will continue to remain beyond reach for the foreseeable future.

Recently, attempts have been made to simplify the situation by studying the properties of *model glass systems*, which are materials that retain the essential features of

the structural glass transition in fully-disordered liquids, yet are somehow structurally less complex. The primary requirement of a model glass is the existence of a glass transition (or glasslike) transition in an environment which is less complex than the liquid. One particular class of materials called Orientationally-Disordered Crystals (ODC's) possess unique structural properties that make them excellent candidates for model glasses.

II. History of ODC's.

In the early 1930's, Pauling [2] first proposed that some molecular crystals could display a metastable phase characterized by molecules having translational order and rotational disorder. Experimental verification of Pauling's theory occurred in 1938, when Timmermans [3] observed that the behavior of several molecular solids could be explained if it were assumed that the nearly-spherical molecules comprising the solid were executing essentially free rotations. Shortly thereafter, dielectric measurements by Smyth [4] showed that this unique phase of matter displayed static dielectric constant values slightly *higher* than those observed for comparable temperatures in the high-temperature liquid state. The large values of the static dielectric constant, which is a quantity sensitive to the rotational motion of molecules in the sample, suggested that the molecules in the rotationally-disordered phase were executing rotations in a nearly free manner – even more free than the rotation of molecules in the liquid state.

The selection of an appropriate name to characterize the material and its rotationally-disorderd phase has proven difficult and resulted in much confusion in the literature. Originally, the high degree of mechanical plasticity possessed by the phase resulted in the material being referred to as a "plastic crystal" [3]. This title has also been

used to refer to the phase itself, along with other descriptive names such as "orientationally-disordered crystal" and "rotator crystal". The currently accepted labeling scheme refers to the actual rotationally-disordered phase of the material as a "rotor phase crystal" and the material itself is classified as an "orientationally-disordered crystal".

The existence of glassy behavior in the supercooled rotator phases of many ODC's was discovered by Suga and Seki in the late 1960's. By performing a number of thermodynamic experiments [5-9] studying the heat capacity and enthalpy relaxation of orientationally-disordered crystals, the Suga group discovered that the rotator phase of many substances exhibited an orientational glass transition possessing the same thermodynamic signatures as the glass transition in fully-disordered liquids (e.g. anomalous behavior in the specific heat). The term "glassy crystal" was proposed to represent the supercooled rotator phase below T_g, however this name has given way to the present terminology of "orientational glass". The prototype materials studied by the Suga group will be discussed in greater detail in section IV of this chapter.

III. Structure and Dynamics of ODC's.

Upon supercooling from the high-temperature liquid phase, the occurrence of first-order crystallization processes may result in the formation of a phase that is metastable relative to the lowest energy crystalline state. This behavior is due to differences in the growth rate of crystallites in the metastable and lowest energy crystalline states, and is commonly known as Otswald's "Law of Stages" [10]. Put more generally, Otswald's Law states that the supercooled liquid will tend *not* to transform directly into the lowest energy crystalline phase, but rather into a phase that is next most stable to the liquid. The rotator phase of ODC's is precisely such a metastable state, and

is characterized by molecules that are translationally ordered and rotationally disordered. The crystal structure of the rotator phase is usually f.c.c. or b.c.c. due to packing constraints and energy arguments.

Most materials possessing rotator phases typically have molecular units which are globular or nearly spherical in shape. Figure 3.1 provides a two-dimensional representation of the actual three-dimensional character of a typical rotator phase crystal. In the absence of any applied fields, each molecule rigidly attaches itself to a lattice site, yet retains its rotational freedom. Similar to the liquid phase, the rotator phase can be supercooled to reveal a glass-like transition in the orientational degrees of freedom which is similar to the structural glass transition in supercooled liquids.

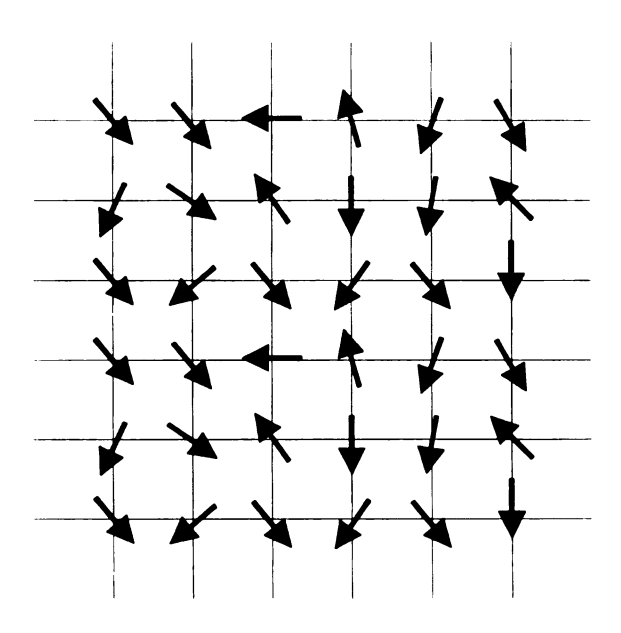


Figure 3.1. The translational order and rotational disorder of molecules in a typical rotator phase crystal.

IV. Example ODC's.

Suga's pioneering work on ODC's began with studies of cyclic alcohols [5], all of which are characterized by a main hydrocarbon ring supplemented by an OH radical. Rotator phases have been observed [6] in cycloheptanol (C₇H₁₃OH), cyclohexanol (C₆H₁₁OH), cyclopentanol (C₅H₉OH), and cyclooctanol (C₈H₁₅OH) to name a few. However, Suga first discovered glassy behavior in cyclohexanol, and thus cyclohexanol emerged as the prototypical model glass system before any of the other cyclic alcohols.

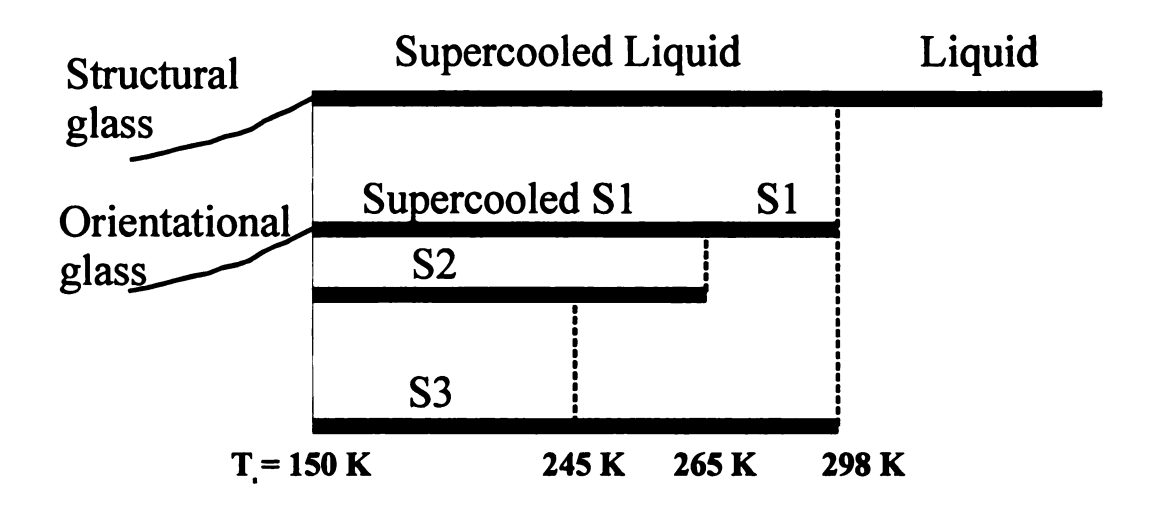


Figure 3.2. Schematic diagram of the phases of cyclohexanol.

Following the labeling scheme of Suga, Figure 3.2 provides a useful schematic diagram illustrating the behavior of cyclohexanol as its temperature is varied. Upon very slow cooling, the liquid undergoes a first-order transition at 298 K to S3, the stable crystalline phase. Moderate cooling rates (~ 10 K/min) will not result in transition to S3, but rather a transformation to S1 will occur. The S1 phase is a rotator phase (f.c.c.

structure, lattice constant a=8.6 angstroms) and is characterized by translational order and rotational disorder. S1 can then be supercooled to form an orientational glass at $T_g=150$ K. Due to its metastability, the supercooled S1 phase is susceptible to crystallization resulting in either S2 or S3, depending on the cooling rate of the experiment. Of course, the transition at 298 K can be avoided altogether through the use of high cooling rates (~20-30 K/min) resulting in the fully-disordered supercooled liquid. However, the supercooled liquid phase of cyclohexanol is rarely examined in experiments. In addition to the high cooling rates required for formation, the supercooled liquid demonstrates poor stability against crystallization [5].

The orientational glass transition in cyclohexanol occurs when the rotational ability of the cyclohexanol molecules vanishes. The result is a glass transition associated with the orientational degrees of freeedom that displays the same thermodynamic signatures as the structural glass transition in fully-disordered liquids. The similarity in behavior can be seen in a plot of the specific heat versus temperature in the supercooled S1 phase of cyclohexanol as shown in Figure 3.3. Here, the orientational glass transition at ~ 150 K involves a drop in the specific heat of approximately 20 J mol⁻¹ K⁻¹ corresponding to the freezing of rotational degrees of freedom. Below T_g , only vibrational mechanisms contribute to the specific heat, and the specific heat resembles that of a crystalline solid.

Despite its lengthy history, cyclohexanol is still of interest to experimentalists studying the glass transition. For example, Gangasharan and Murphy [11] have recently investigated the supercooled S1 relaxation phenomena using dielectric spectroscopy; NMR studies of the molecular motion have been carried out by Kuhns *et al.*[12], and

Mizukami et al. [13] have reported calorimetric evidence suggesting that supercooled S1 exhibits more than one type of α - and β -relaxation.

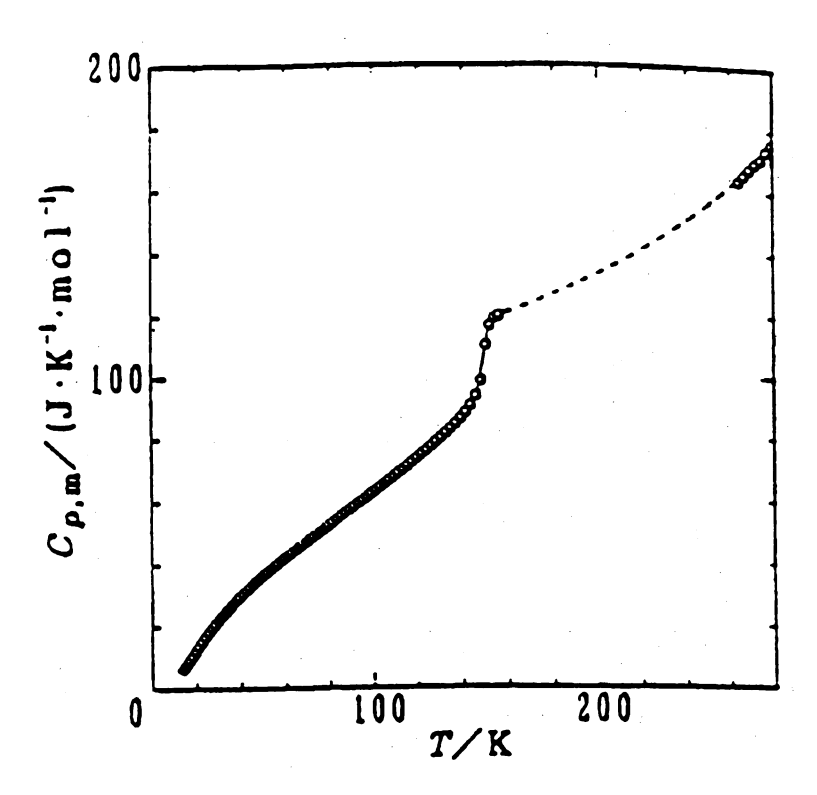


Figure 3.3. Experimental heat capacity of cyclohexanol in the supercooled S1 phase. The sudden drop in C_p at ~ 150 K is due to the orientational glass transition. (Data from: M. Mizukami *et al.*, Solid. St. Comm. 100, 83-88 (1996)).

Currently, the search for model glass systems has shifted away from cyclohexanol toward other materials. This is due in part to the fact that cyclohexanol is quite difficult to maintain in the supercooled S1 phase. Cyclo-octanol, on the other hand, has an additional two hydrocarbons which provide greater resistance to crystallization. Thus, because of its structural similarity to cyclohexanol and the additional stability provided by its rotator phase, cyclo-octanol has received considerable attention in the past 5 years.

Cyclo-octanol and its usefulness as a model glass system will be discussed in detail in Chapter 5.

Even more recent has been the confirmation (or "re-discovery") [14] of an experimentally accessible rotator phase in ethanol (C₂H₅OH). As will be greatly expanded upon in Chapter 6, ethanol can be readily prepared in both the supercooled liquid *and* rotator phases - a very desirable feature which invites comparison of the dynamical aspects of the glass transition in each phase.

V. Motivation.

The rotator phase of ODC's provides a unique environment in which to isolate and study the dynamical aspects of the glass transition without the additional complexity of translational disorder. It is the purpose of this thesis to experimentally investigate the properties of two ODC's in particular: cyclo-octanol and ethanol.

First, we wish to determine if certain universalities discovered in dynamical response of supercooled liquids also exist in the supercooled rotator phase of ODC's. This may help to determine which features of the glass transition are truly universal, and which are linked to the particular structural characteristics of a material. Previous low-frequency dielectric studies performed by our group on the rotator phase of cyclo-octanol [15] have indicated that the material possesses the same general features seen in structural glass forming liquids. Chapter 5 of this work extends the previous range of our dielectric measurements on cyclo-octanol to much higher frequencies in an attempt to provide a detailed description of the α -relaxation. Recent studies [16] of supercooled liquids have suggested that universal behavior exists in the high-frequency response of a material, and we wish to investigate if this holds for ODC's as well.

The second goal of this work is to provide a quantitative comparison of the dynamical aspects of the glass transition in two structurally dissimilar phases. A comparison of this type may provide critical insight as to what degrees of freedom are most relevant to the glass transition, and has never been possible before due to lack of an appropriate material. As discussed in end of section IV of this chapter, the intrinsic phase polymorphism of ethanol provides a perfect opportunity for such a comparison. Chapter 6 presents the comparison of the α -relaxation dynamics in the supercooled liquid and rotator phases of ethanol.

REFERENCES

- [1] C. A. Angell, Comp. Mat. Sci. 4, 285-291 (1995).
- [2] L. Pauling, Phys. Rev. 36, 430 (1930).
- [3] J. Timmermans, J. Chim. Phys. 35, 331 (1938).
- [4] C. P. Smyth, Trans. Faraday Soc. 42, 175 (1946).
- [5] K. Adachi, H. Suga and S. Seki, Bull. Chem. Soc. Japan 41, 1073-1087 (1968).
- [6] K. Adachi, H. Suga and S. Seki, Bull. Chem. Soc. Japan (Short Communications) 43, 1916 (1970).
- [7] H. Suga and S. Seki, J. Non. Cryst. Sol. 16, 171-194 (1974).
- [8] O. Haida, H. Suga, and S. Seki, J. Chem. Thermodynamics 9, 1133-1148 (1977).
- [9] H. Suga, Journal de Chimie physique 82, 275-282 (1985).
- [10] J. Sherwood, *The Plastically Crystalline State*, Chapter 1, John Wiley & Sons, New York (1979).
- [11] M. Gangasharan and G. Murphy, J. Chem. Phys. 99, 271 (1993).
- [12] P. L. Kuhns and M. S. Conradi, J. Chem. Phys. 80, 5851-5857 (1984).
- [13] M. Mizukami, H. Fujimori, and M. Oguni, Solid. St. Comm. 100, 83-88 (1996).
- [14] A. Srinivasan, F.J. Bermejo, A Andres, J. Dawidowski, J. Zuniga and A. Criado, Phys. Rev. B 53, 8172-8175 (1996).
- [15] D.L. Leslie-Pelecky and N.O. Birge, Phys. Rev. Lett. 72, 1232 (1994); Phys. Rev. B 50, 13250 (1994).
- [16] N. Menon and S.R. Nagel, Phys. Rev. Lett. 74, 1230 (1995).

Chapter 4

EXPERIMENTAL TECHNIQUES

I. Dielectric Spectroscopy.

One of the most useful and productive techniques available to the experimentalist interested in characterizing the orientational and translational motion of molecules in a polar material involves measurement of the material's dielectric properties. This technique is referred to as *dielectric spectroscopy*, and consists of measuring the frequency and temperature dependent response of an ensemble of dipolar molecules to an externally applied electric field of frequency f. The method provides an estimate of the time required for reorientation of the molecule, or the so-called *relaxation time*.

II. Review of Dielectric Theory.

II. a. Polarization Mechanisms in Dielectrics.

When a dielectric material is placed into an external electric field, such as that produced in the region separating parallel plates of a capacitor, a separation of charge occurs and the material becomes *polarized*. The resulting polarization is measured in terms of a dipole moment per unit volume, and depends strongly on the chemical makeup of the material. The macroscopic polarization in the material is actually a superposition of the effects of several microscopic polarization mechanisms occurring simultaneously on the molecular level. These microscopic polarization mechanisms can be divided into two general classes: *induced* polarization and *orientational* polarization.

Orientational polarization occurs when molecules with intrinsic electric dipole moments attempt to reorient themselves in the direction of an externally applied electric

field as shown in Fig. 4.1. Molecules having permanent dipole moments are termed polar molecules, and the material as a whole is designated a polar dielectric. In practice, this polarization mechanism is limited by thermal agitation of the molecules, which prohibits uniform alignment with the field.

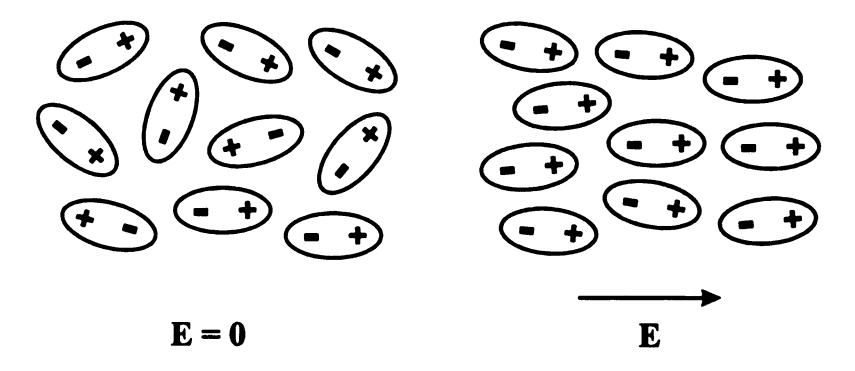


Figure. 4.1. Polar molecules in an external electric field.

Induced polarization occurs even in non-polar materials, and is a result of "stretching" the charge distribution of a given atom or molecule in such a manner so as to cause a physical separation of the centers of positive and negative charge. For example, in a typical atom with no external fields present, the location of the positively charged nucleus and center of the surrounding negatively charged electron cloud coincide, and thus no dipole moment exists. However, in the presence of an electric field, the positively charged nucleus is displaced relative to the surrounding electron cloud, resulting in an induced dipole moment. The size of the induced moment depends on the magnitude of the local electric field present as well as the atom or molecule's polarizability, α. The magnitude of the dipole moment induced in an individual atom or molecule by the local electric field can then be expressed as

$(4.1) \quad \mu = \alpha F$

where F is the local electric field present at the location of the molecule.

For N non-polar atoms in a volume V, the total polarization due to induced dipoles is obtained by summing the contributions of all dipoles over the volume of the sample.

The two classes of polarization mechanisms, orientational and induced, combine to give the final macroscopic polarization observed in the material. However, upon application of the external electric field, the contribution of each mechanism to the total polarization occurs at differing rates. The electronic and molecular polarization occurs rapidly (~10⁻¹² sec) because these processes only involve a shift of the equilibrium charge distribution. The orientational polarization occurs much more slowly, as interactions with other molecules hinder the rotation of individual dipoles as they attempt to align with the field. As a result, the total polarization in the material approaches a maximum only at very long times.

II. b. Behavior in Static Fields - Static Dielectric Constant.

In attempting to understand the general behavior of dielectrics when subjected to electric fields, a natural starting point is to consider their behavior in the presence of fields that do not vary with time. Such an approach introduces fundamental concepts and provides a natural stepping stone for the more advanced treatment involving time-varying fields.

Let us begin by considering a typical parallel plate capacitor assembly having opposite charges of magnitude σ on each plate, which give rise to a uniform electric field E in the region between the plates. When the region between the plates is devoid of

material and a vacuum exists, the magnitude of the electric field can be expressed in terms of the charge density on the plates. In the cgs system of units, this is given by

$$(4.2) E_{\text{vacuum}} = 4\pi\sigma$$

If a material with dielectric constant ε is subsequently inserted between the plates, the electric field decreases by a factor of the dielectric constant ε , and is given by

$$(4.3) E = \frac{4\pi\sigma}{\varepsilon}$$

The drop in field strength is due to the polarization mechanisms discussed in section II.a, which create a distribution of bound charge producing an electric field pointing in the opposite direction of the field produced by the free charge on the capacitor plates. To account for polarization in the dielectric, we introduce the electric displacement D, which is defined in terms of the free charge density as

(4.4)
$$D = 4\pi\sigma$$

and is related to electric field E and polarization P by the relation

$$(4.5) \quad D = \varepsilon E = E + 4\pi P$$

Rearrangement of terms leads to an expression for the dielectric constant in terms of the electric field and polarization present in the dielectric:

$$(4.6) \quad \varepsilon - 1 = \frac{4\pi P}{E}$$

To determine ε for a particular material, an accurate expression must be provided for the polarization P. To obtain this, we must first have knowledge of the local electric field F that each molecule experiences, which in general is not the same as the macroscopic field E. The difference is due to dipole-dipole interactions that modify the local environment and cannot be neglected. One way of deriving an expression for the

local field is to consider a microscopic spherical region surrounding the molecule whose overall size is large compared to the molecular dimensions but small compared to the size of the sample. In this picture, the interactions of dipoles with one another can be calculated, and Lorentz showed [1] that for a cubic lattice of polarizable atoms the dipoles inside the spherical region produce zero electric field. The local field inside the sphere is then due to contributions from all sources external to the spherical region. Using techniques from electrostatics (see refs. 2,3), the result for the local field F experienced by an individual dipole can be expressed as

$$(4.7) F = \frac{(\varepsilon + 2)E}{3}$$

As discussed earlier, the total dipole moment of a molecule consists of both intrinsic and induced portions. The induced portion of the moment can be described in terms of the molecular polarizability α and local field F. The resulting contribution, P_1 , to the macroscopic polarization P for N molecules in a volume V is then given by

$$(4.8) P_1 = \frac{N\alpha F}{V}$$

For non-polar substances $P = P_1$, and this result can be directly substituted into Eq. 4.6 to give the Clausius-Mossoti relation for the static dielectric constant:

$$(4.9) \quad \frac{(\varepsilon - 1)}{(\varepsilon + 2)} = \frac{4\pi N\alpha}{3V}$$

The Clausius-Mossoti equation is a satisfactory description of the behavior of the dielectric constant in non-polar gases and very dilute liquids, but cannot be applied to the case of polar liquids. In many liquids and polycrystalline solids, the effect of orientational polarization far exceeds polarization induced by distortion of the charge

distribution, and must be accounted for in any theory attempting to provide an accurate description of the behavior.

In the absence of any applied fields, individual dipoles are randomly oriented and no net polarization exists in the material. Application of a field causes the dipoles to rotate in an attempt to align with the field. The examination of a system of rigid dipoles under the influence of an external electric field was first carried out by Debye [4], who began with an expression for the polarization due to permanent dipoles in the material:

$$(4.10) P_2 = \frac{N}{V} \mu \langle \cos \theta \rangle$$

Here, $\langle \cos \theta \rangle$ is the mean value of the cosine of the angle of inclination of a dipole with respect to the external field. Debye then assumed that the individual moments would distribute themselves about the field direction based on Boltzmann statistics, and integrating over all possible directions gives

(4.11)
$$\langle \cos \theta \rangle = \coth \left(\frac{\mu F}{kT} \right) - \frac{kT}{\mu F} = L \left(\frac{\mu F}{kT} \right)$$

where $L(\mu F/kT)$ is the Langevin function originally used to calculate the mean magnetic moment of a gas consisting of particles with permanent magnetic dipoles. For $\mu F/kT$ << 1, corresponding to local fields that are not too strong, the value of the function approximates to $\mu F/3kT$, and substitution of this result into eq. 4-10 gives:

$$(4.12) P_2 \approx \frac{N\mu^2 F}{3kTV}$$

To obtain the Debye expression for the dielectric constant in a material where both induced and orientational polarization is accounted for, we combine the effects of

induced and orientational mechanisms to obtain the total polarization and substitute the result into Eq. 4.6. The result for the dielectric constant is given by:

$$(4.13) \qquad \frac{\varepsilon - 1}{\varepsilon + 2} = \frac{4\pi N}{3V} \left(\alpha + \frac{\mu^2}{3kT} \right)$$

This expression is in good agreement with the measured dielectric constant of many gases and dilute liquids, but fails to provide reasonable results in the case of dense liquids. In fact, a major shortcoming of the equation is the prediction of ferroelectric behavior in dense liquids when the temperature falls below a certain critical value.

The failure of the Debye equation is due to the fact that the Lorentz local field does not accurately describe the interaction of dipoles when the density is high, and thus the expression for the local field at each molecule is incorrect. Onsager [5] produced a dramatically improved theory of dielectric polarization by considering a different approach to calculating the dipolar interactions and arrived at a more accurate expression for the local field F. His treatment represented the molecule as a point dipole of moment m in a spherical cavity of radius $a = \left(\frac{3V}{4\pi N}\right)^{1/3}$. The local field F within the cavity now consisted of two parts G and R, the first of which is the field produced in the empty cavity by the external applied field,

$$(4.14) \qquad G = \left(\frac{3\varepsilon}{2\varepsilon + 1}\right) E$$

and the second part being a reaction field generated in the cavity from the polarization induced by the dipole:

$$(4.15) \qquad R = \frac{2(\varepsilon - 1)}{(2\varepsilon + 1)a^3} \text{ m}$$

The dipole moment m consists of both an induced part and a permanent part, given by

(4.16) $m = \mu + \alpha F$

The local field is now obtained by F = G + R, and an approach similar to that used by Debye gives the final expression for the Onsager formula. A detailed derivation of the Onsager equation can be found in a number of references, including Frolich [3] and Smyth [4]. The final result is as follows, where ε_{∞} is the contribution of fast electronic polarization processes, μ is the molecular dipole moment, and $N_0 = N/V$:

(4.17)
$$\frac{\left(\varepsilon - \varepsilon_{\infty}\right)\left(2\varepsilon + \varepsilon_{\infty}\right)}{\varepsilon\left(\varepsilon_{\infty} + 2\right)^{2}} = \frac{4\pi N_{0}\mu^{2}}{9kT}$$

The Onsager expression is superior to the Debye form, and provides sufficient agreement with the experimentally determined static dielectric constants of many non-hydrogren bonded dipolar liquids. Unfortunately, even eq. 4.17 fails for hydrogen bonded liquids such as water and ethanol because the formation of a hydrogen bond between molecules changes the local environment so as to be inconsistent with Onsager's expression for the local field. The inadequacy eq. 4.17 can be illustrated numerically for the case of ethanol (C_2H_5OH). Because solution of eq. 4.17 is simplest for the dipole moment μ , we can substitute the known values for ϵ , ϵ_{∞} , and N_0 at room temperature (298 K) and compare the result with the actual measured dipole moment. In Debye units (1 D = 10^{-18} esu-cm), the Onsager expression applied to ethanol at 298 K (ϵ = 24.3, ϵ_{∞} = 1.85, and N_0 = 1.0572e+22 m⁻³) leads to a dipole moment of μ = 2.96 D. This is considerably larger than the experimentally measured moment of 1.67 D [6].

Thus, the failure of the Onsager expression has led to more sophisticated developments such as that by Kirkwood [7] which attempt to describe the intermolecular interactions in greater detail.

II. c. Time-Varying Electric Fields - The Complex Dielectric Constant

The application of time varying electric fields gives rise to dielectric dispersion and loss that is not present in the case of static fields. Dispersion and loss can be qualitatively understood by considering the reaction of an individual molecule to an external electric field that varies with time. When the frequency of the field is very low, even bulky molecules interacting strongly with their neighbors are able to stay in phase with the field, and the measured dielectric constant will yield values close to that of the static dielectric constant. On the other hand, if the frequency of the field is very high, then the period of the field is much shorter than the time required for a molecule to complete rotation and the molecules cannot reorient themselves quickly enough to align with field. Orientational polarization does not contribute to the total polarization in the dielectric at high frequencies and only induced polarization mechanisms contribute. The resulting value of the dielectric constant, ε_{∞} , is often referred to as the "optical" dielectric constant. Finally, there exists a band of intermediate frequencies where the dipolar response is measurable but lags behind the external electric field. This characteristic phase lag gives rise to energy dissipation in the dielectric, and to account for it a complex dielectric constant, $\epsilon^* = \epsilon' + i\epsilon''$, is introduced. The real part ϵ' represents the dielectric constant discussed in the previous section, and ε'' is called the loss. The real and imaginary parts are related through mutual transformation relations called the Kramers-Kronig relations [8].

To provide a quantitative description of the behavior in time-varying fields, an accurate description of the time-dependent polarization P(t) in the material must be specified. The simplest description that quantitatively displays the phenomena of dispersion and loss was first examined by Debye [4]. In his theory, he assumed that the total polarization (P) in the material consisted of a sum of induced (P₁) and orientational (P₂) effects:

$$(4.18) P = P_1 + P_2$$

Furthermore, he assumed that the orientational contribution P_2 would approach its equilibrium value in an exponential fashion given by

(4.19)
$$dP_2/dt = (P - P_1 - P_2) / \tau$$

(4.20)
$$P_2 = (P - P_1) [1 - \exp(-t / \tau)]$$

where τ is designated to be the macroscopic *relaxation time* in the dielectric describing the decay of the polarization upon removal of the external field. A pictorial representation of the response of the orientational and electronic polarization to an electric field turned on at t = 0 can be seen in Figure 4.2.

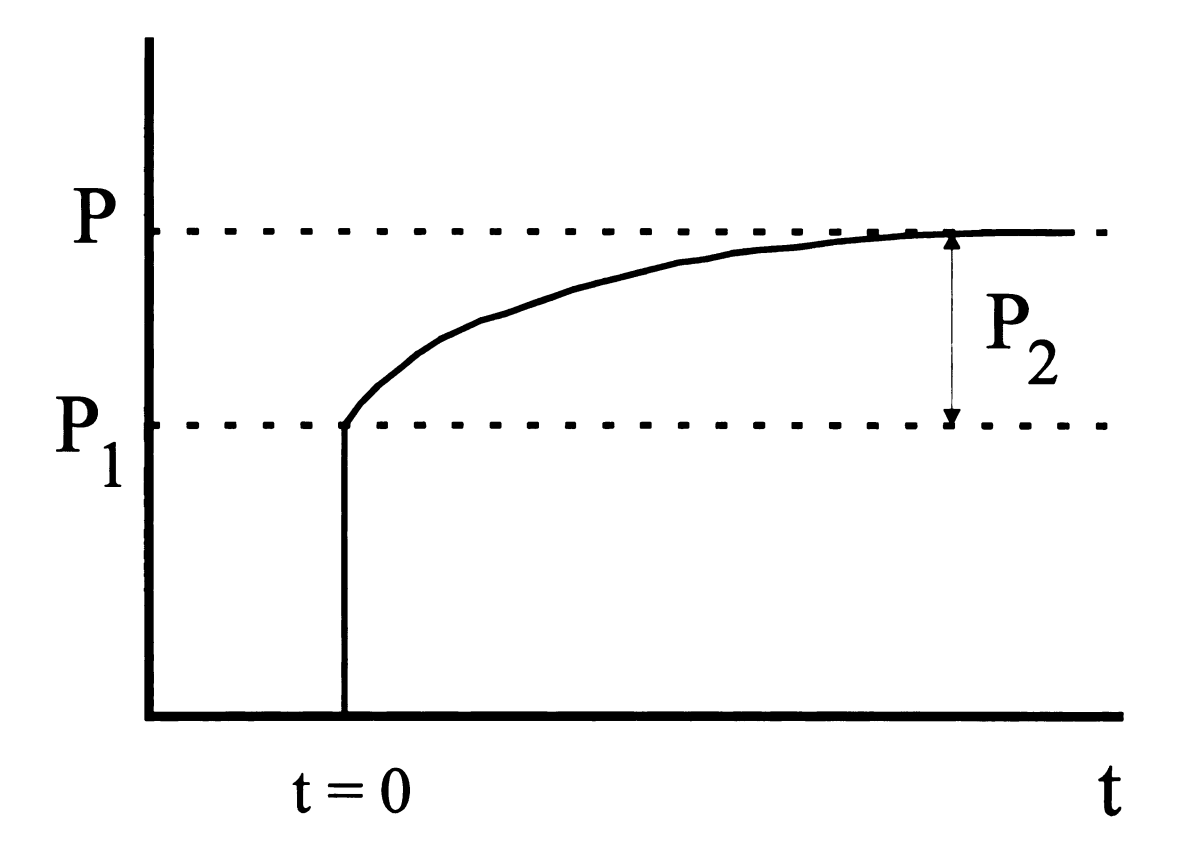


Figure 4.2. The response of induced and orientational polarization mechanisms to a constant electric field turned on at t = 0.

Recall from the previous section that the equilibrium polarization P can be expressed in terms of the static dielectric constant (which we will explicitly refer to as ε_s) and the induced polarization P_1 can be expressed in terms of the optical dielectric constant ε_{∞} :

(4.21)
$$(\epsilon_s - 1) = 4\pi P / E$$

(4.22)
$$(\varepsilon_{\infty} - 1) = 4\pi P_1 / E$$

Subtracting 4.22 from 4.21 gives

$$(4.23) P - P_1 = (\varepsilon_s - \varepsilon_\infty)E / 4\pi$$

The time-varying electric field E can be written as a complex quantity, where ω is the angular frequency of the oscillation:

(4.24)
$$E(t) = E_0 \exp(i\omega t)$$

The above equations for $P - P_1$ and E can then be substituted into (4.19) to give the differential equation for the orientational polarization contribution:

(4.25)
$$dP_2 / dt = (\varepsilon_s - \varepsilon_\infty) E_0 \exp(i\omega t)/4\pi - P_2 / \tau$$

The solution of (4.25) shows that the ratio P_2 / E is a complex quantity, indicating that the orientational polarization is out of phase with the driving field:

$$(4.26) P2(t) = (\varepsilon_s - \varepsilon_\infty)E(t) / [4\pi (1 - i\omega\tau)]$$

The total polarization in the dielectric is then given as

$$(4.27) P(t) = P_1 + P_2(t) = 4\pi [(\varepsilon_{\infty} - 1) + (\varepsilon_{s} - \varepsilon_{\infty})/(1 + i\omega\tau)] E(t)$$

The dielectric susceptibility, χ_e , can be obtained using the general relation $P = \chi_{\epsilon} E$, and it can be seen that χ_e is complex:

(4.28)
$$\chi_e = 4\pi [(\epsilon_{\infty} - 1) + (\epsilon_s - \epsilon_{\infty})/(1 + i\omega\tau)]$$

The final expression for the dielectric constant in alternating fields can be obtained using the relationship between ϵ and χ_e :

$$(4.29) \quad \varepsilon = 1 + 4\pi \gamma_e$$

(4.30)
$$\varepsilon = \varepsilon_{\infty} + (\varepsilon_{s} - \varepsilon_{\infty}) / (1 + i\omega \tau)$$

Separation of (4.30) into real and imaginary parts and introducing $\varepsilon = \varepsilon' + i\varepsilon''$ gives the Debye equations for the dielectric constant and loss:

(4.31)
$$\varepsilon' = \varepsilon_{\infty} + (\varepsilon_{s} - \varepsilon_{\infty}) / (1 + \omega^{2} \tau^{2})$$

(4.32)
$$\varepsilon'' = (\varepsilon_s - \varepsilon_{\infty})\omega\tau / (1 + \omega^2\tau^2)$$

The frequency response of a dielectric obeying the Debye equations (4.31) and (4.32) is shown in Fig. 4.3 for the case $\varepsilon_0 = 10$, $\varepsilon_\infty = 2.0$, and $\tau = 1.0$.

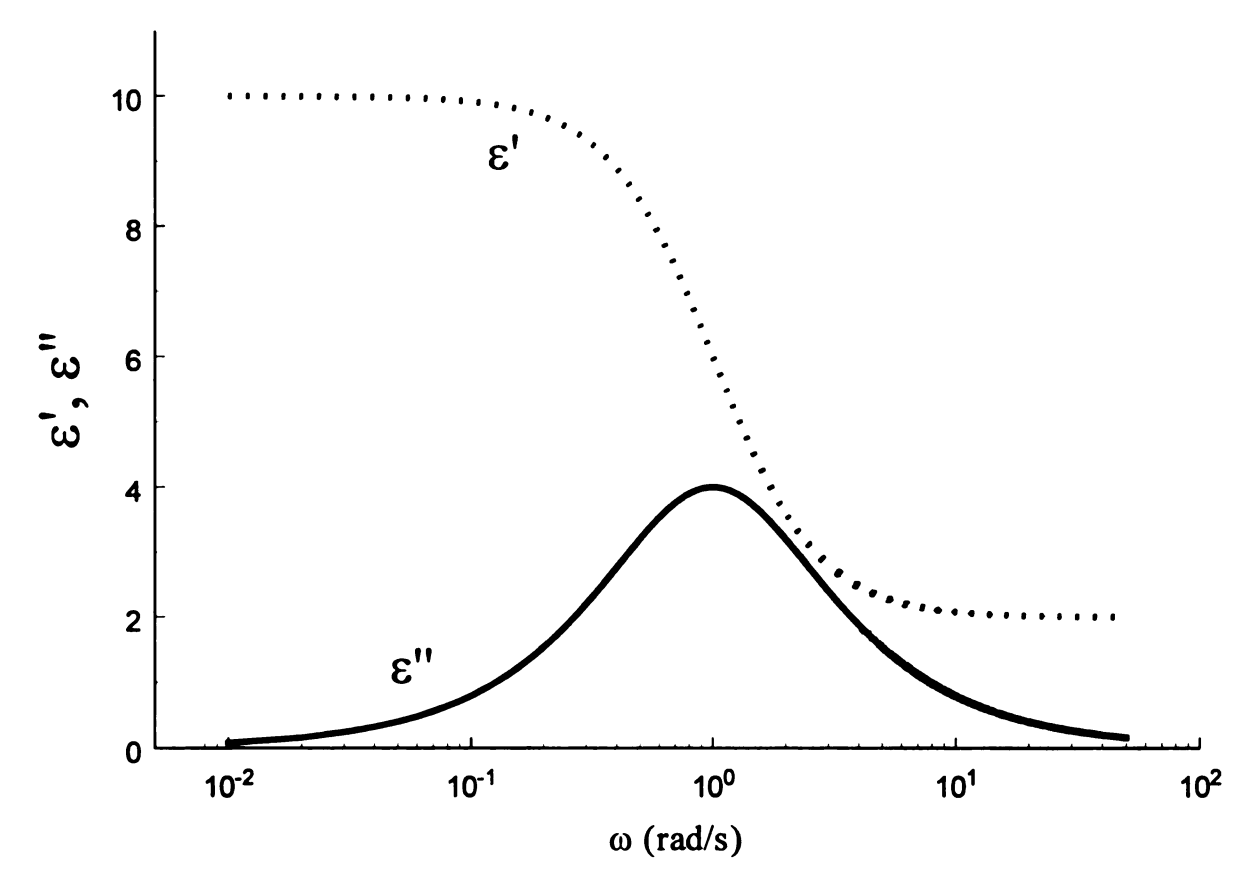


Figure 4.3. Frequency response of a dielectric obeying the Debye equations. This example assumes $\varepsilon_0 = 10$, $\varepsilon_\infty = 2.0$, and $\tau = 1.0$.

An expression for the macroscopic relaxation time τ can be determined by maximizing eq. 4.32 with respect to ω , the result being given as

(4.33)
$$\tau = 1/\omega_{peak}$$

where ω_{peak} is the angular frequency locating the maximum of ϵ'' . Thus, measurement of a material's dielectric response under the influence of a time-varying electric field provides an estimate of the mean relaxation time.

The Debye equations provide a useful way of understanding the behavior of dielectrics in time varying fields and assume that the orientational polarization process is

governed by a single relaxation time τ . However, as discussed earlier in Chapter 2, the measured dielectric response of most supercooled liquids is typically non-Debye in nature, showing a relaxation spectrum that is broadened relative to what is expected from the Debye theory.

III. Dielectric Measurement System.

III a. Goals of Dielectric Spectroscopy.

The primary goal of dielectric spectroscopy is to accurately measure the complex dielectric constant, $\varepsilon = \varepsilon' + i\varepsilon''$, as a function of temperature and applied electric field frequency. The most practical method of generating an external electric field in a material involves driving a capacitor containing the material with a voltage that varies harmonically in time. Using this method an electric field is generated in the region between the capacitor plates and a current flows through the sample, in this case a polar liquid. For a given temperature and frequency, the impedance of the sample can be determined by measuring the voltage across, and current through the sample. As will be discussed in the next two sections, knowledge of the sample impedance at a particular temperature and frequency allows determination of $\varepsilon = \varepsilon' + i\varepsilon''$.

The frequency range of the measurement dictates the type of measurement technique used. Fortunately, study of the alpha relaxation in supercooled liquids does not require the use of extremely high frequency techniques (> 10 MHz). For this study, lockin amplifier techniques were utilized for frequencies in the range 1 mHz to 10 kHz, and an impedance analyzer was employed for higher frequencies in the range 1kHz to 10MHz. These techniques will be discussed in the following sections.

III. b. The Dielectric Sample Cell

The sample cell used for the dielectric measurements was a glass-sealed coaxial capacitor similar in design to that used by Adachi, *et al.* [9]. Shown in Figure 4.4, the capacitor consists of stainless steel inner and outer conductors separated by two ceramic Macor spacers.

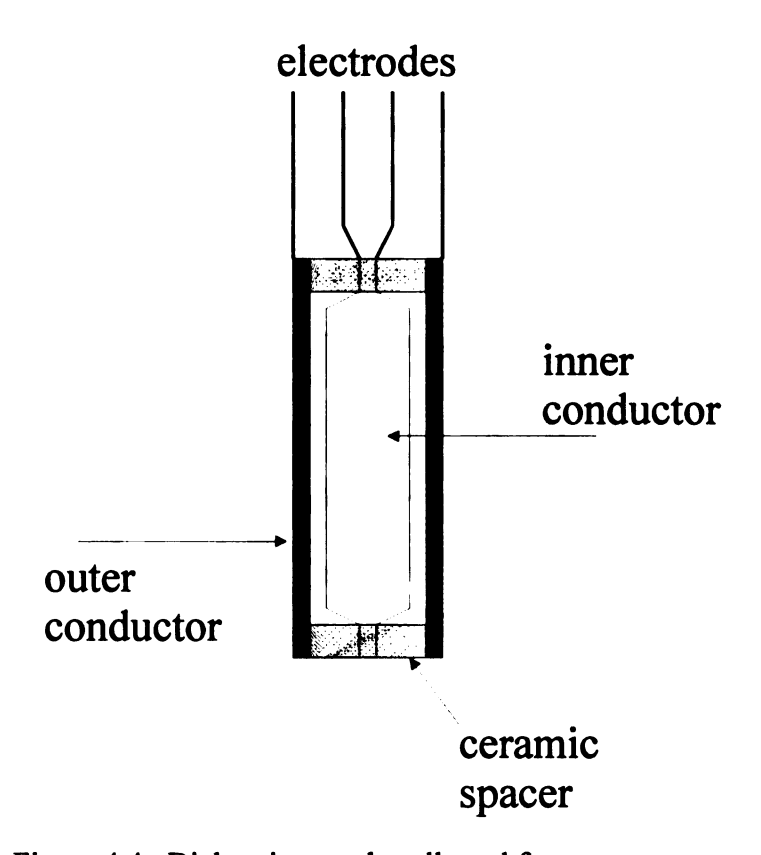


Figure 4.4. Dielectric sample cell used for measurements.

The gap between inner and outer conductors was 2.54e-4 meters, resulting in a nominal empty cell capacitance of $C_0 = 49.7 pF$. The four electrodes at the top of the capacitor were fashioned from 0.030-inch diameter tungsten rods. The material choice of tungsten was necessary for glass-to-metal bonding, and the largest possible diameter was chosen

so as to minimize lead inductance as well as provide increased surface area during glass bonding process.

The entire capacitor assembly was then encased in a form-fitting envelope of Pyrex glass using facilities and personnel at the Scientific Glassblowing Laboratory located in the Chemistry building at MSU. Pyrex was chosen over other materials due to its resiliency to thermal cycling stresses over temperatures ranging from liquid Helium (4K) to room (300K), as well as other factors such as availability and cost.

III. c. Low Frequency Measurement Circuit

In the range 1mHz to 10kHz, the real (ϵ ') and imaginary (ϵ '') parts of the dielectric constant were measured using a Stanford SR850 Dual Phase Lock-in Amplifier in conjunction with a Stanford SR570 Current-to-Voltage Amplifier as shown in Figure 4.5.

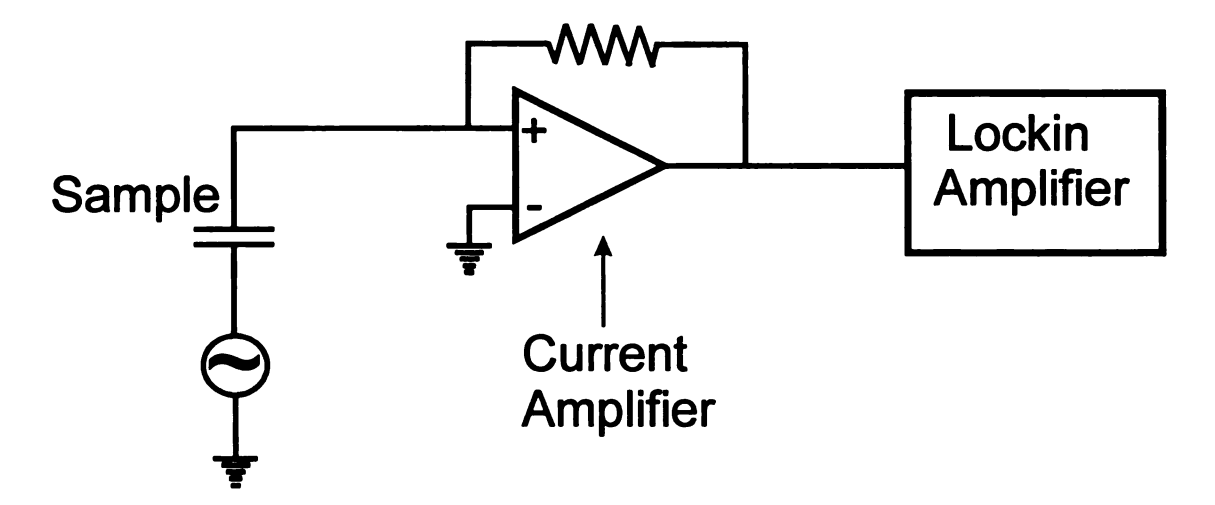


Figure 4.5. Circuit used for low-frequency (1mHz – 10kHz) measurements.

There are several reasons why this measurement circuit was chosen over a more traditional ratio-transformer bridge, which was available for use in the form of a General

Radio 1616 Precision Capacitance Bridge. First, the lockin-amplifier setup allows for measurement at much lower frequencies (~ 1mHz) than the capacitance bridge (~10 Hz). This allowed for a more complete determination of the peak region of the α -relaxation. The experiment is also a high impedance measurement, since the capacitance of the full cell is typically in the range 10⁻¹⁰-10⁻¹² pF and measurement frequencies extend to the The virtual ground configuration of the current amplifier eliminates mHz realm. charging of the parasitic capacitance between the sample and the current amplifier, allowing a 2-terminal measurement instead of the typical 4-terminal configuration. In this scheme, the internal oscillator of the SR850 sinusoidally drives the capacitor containing the sample liquid. Because real dielectrics exhibit loss, the current in the sample has two components: 1) a component which is in-phase with the driving voltage and related to energy dissipation in the dielectric, and 2) a component which is 90° outof-phase with the driving voltage related to the molecules ability to remain in phase with the external electric field. This behavior can be accounted for by introducing a complex dielectric constant $\epsilon^* = \epsilon' + i\epsilon''$ into the standard current-voltage relationship for a capacitor containing a dielectric:

$$(4.34) I = iV_0 \omega \epsilon^{\bullet} C_0$$

Here, V_0 is the magnitude of the applied voltage, $\omega = 2\pi f$, and C_0 is the capacitance of the cell when empty. The SR570 Current-to-Voltage amplifier transforms the current into a complex voltage that can be measured by the lock-in amplifier, where β is the gain of the current amplifier:

(4.35)
$$V_{out} = V_x + iV_y = \beta I = \beta i V_0 \omega \epsilon^* C_0$$

Substituting the expression for the complex dielectric constant and solving for ϵ' and ϵ'' gives

$$(4.36) \quad \epsilon' = \frac{V_y}{\beta \omega V_0 C_0}$$

$$(4.37) \quad \epsilon'' = \frac{V_x}{\beta \omega V_0 C_0}$$

III. d. High-Frequency Measurement Circuit

For frequencies ranging from 1 kHz to 10 MHz, a Hewlett-Packard 4192A Impedance Analyzer was used in a standard four-terminal pair configuration to measure the capacitance C and conductance G of the sample as shown in Figure 4.6. The four terminal pair arrangement avoids measurement of the sample voltage and current using the same electrical leads, and is essential for minimization of the parasitic capacitance and inductance which occurs in the measurement circuitry at frequencies above 1 MHz.

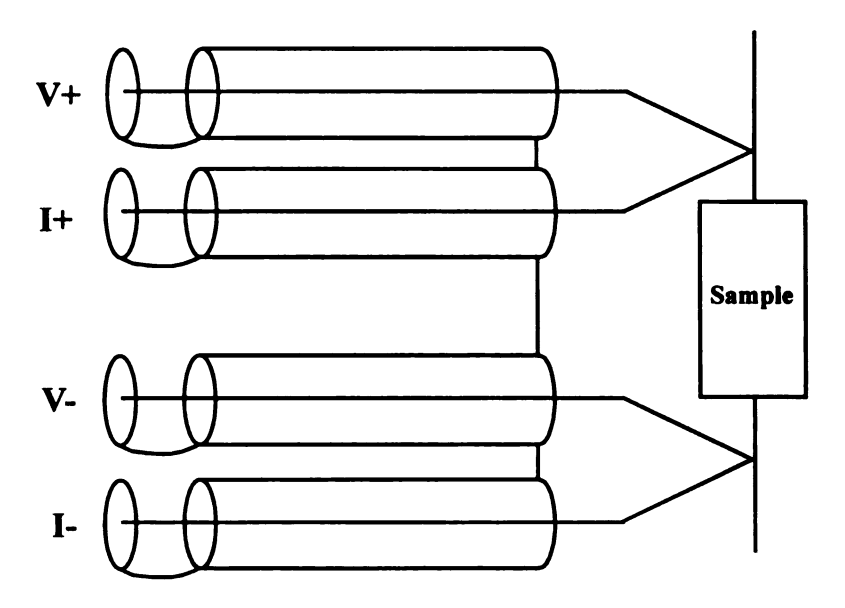


Figure 4.6. Schematic of Four-Terminal-Pair Measurement.

Among its many features, the HP4192A provides the experimenter with the ability to auto-correct for phase shifts (in the measurement of impedance) that occur in the four coaxial cables connecting the sample to the instrument. The correction assumes an individual cable length of exactly 1m, and custom cables were fashioned to allow implementation of this feature.

The HP4192A operates by first determining the sample impedance from measurements of the voltage and current using an autobalancing bridge technique [10]. Next, the instrument determines C and G by modeling the sample as either a parallel or series combination of capacitance and resistance. The model to be used is selected by the experimenter using a selector switch on the instrument's front panel. In this study the parallel model was chosen to be the most accurate representation of the sample. It should be noted, however, that either choice is acceptable since measurements were not seen to vary substantially between the two types of models.

The final step involves determination of ϵ' and ϵ'' based on C and G. The relationship between the various quantities is given as follows, where C_0 is the capacitance of the cell when empty and $\omega = 2\pi f$:

$$(4.38) \quad \varepsilon' = \frac{C}{C_0}$$

$$(4.39) \quad \varepsilon'' = \frac{G}{\omega C_0}$$

The process of determining ε' and ε'' using 4.38 and 4.39 is actually more complex that it appears. The measurements of C and G usually need to be corrected for errors which are introduced by lead inductance and non-standard coaxial cable lengths. These corrections are nontrivial, and are crucial in obtaining accurate measurements. The

interested reader is referred to Appendix A for a summary of empirical and theoretical attempts to understand data corrections for the dielectric experiments.

III. e. Cryostat and Temperature Control

In order to provide a controlled environment for measurement, the capacitor containing the sample was suspended inside a nested cryocan arrangement. The use of a high thermal conductivity copper can nested inside a brass can provided the thermal isolation necessary to achieve sample cell temperature stability to within 0.05 K of the desired target temperature.

The cryocan arrangement was then attached to an insert consisting of two hollow stainless steel tubes. The tubes provided a conduit for electrical connections and allowed introduction of helium exchange gas between the cryocans for temperature control. The entire assembly was then immersed in a dewar capable of holding either liquid nitrogen or helium as dictated by the requirements of the experiment.

Temperature control was achieved through the use of helically wrapped heater wires on both the sample cell and copper cyrocan. The cell heater consisted of approximately six feet of enameled high-resistivity wire (Thermo-Alumel, 23 Ω /ft) giving a total resistance of 140 Ω . The copper can heater was considerably more robust, and consisted of 10 feet of enameled Nichrome wire (50 Ω /ft) for a total resistance of 500 Ω . The cell and copper can heaters were controlled using programmable power supplies (Kepco model 150-ATE for copper can heater, MSU E-Shop 0-60V for sample cell) in conjunction with a proportional-integral-derivative (PID) algorithm of our own design.

Measurement of temperature was carried out using platinum (Pt) resistance thermometers (RTD's). Cell temperature was determined by measuring the resistance of

an Omega model F3105 attached to the glass envelope at the cell's midpoint. Similarly, the copper can temperature was determined using an Omega model F100 embedded in the upper lid of the can. A homemade (MSU E-shop) conductance bridge provided resistance measurements for the sample cell RTD, and a Keithley 196 Digital Multimeter was used to read the copper can RTD.

IV. Sample Fabrication Methods.

The materials examined in this study consisted of hydrogen-bonded liquids, and due to their tendency to absorb water considerable attention was given to obtaining samples of high purity. Two techniques were used for sample preparation: 1) Fractional Vacuum Distillation, and 2) Nitrogen Atmosphere Loading. Both methods involved filling the capacitor cell in a controlled environment free from impurities.

IV. a. Fractional Vacuum Distillation.

The technique of Fractional Vacuum Distillation (FVD) yields samples of very high purity and is illustrated in Figure 4.7. The system consists of five major components including solvent bottle, cold trap, sample cell, roughing pump, and diffusion pump. The liquid to be purified is first independently vapor loaded into a solvent bottle containing a small amount of desiccant material (CaH₂) which aids the process of water removal. The solvent bottle and sample cell are then attached using 9mm Fischer-Porter valves to a cold trap submerged in a liquid nitrogen bath. The function of the cold trap is to freeze out impurities such as pump oil that may be introduced from the pumping station. The contents of the solvent bottle are then frozen using liquid nitrogen and a vacuum of approximately 10⁻⁶ Torr is produced in all regions using the diffusion pump backed by the roughing pump. Because CaH₂ reacts with hydrogen bonded liquids to produce H₂

gas, it is often necessary to subsequently thaw the solvent bottle and repeat the entire process. This is referred to as a "Freeze-Pump-Thaw" cycle, and is repeated several times until no measurable quantity of gas is drawn from the solvent bottle.

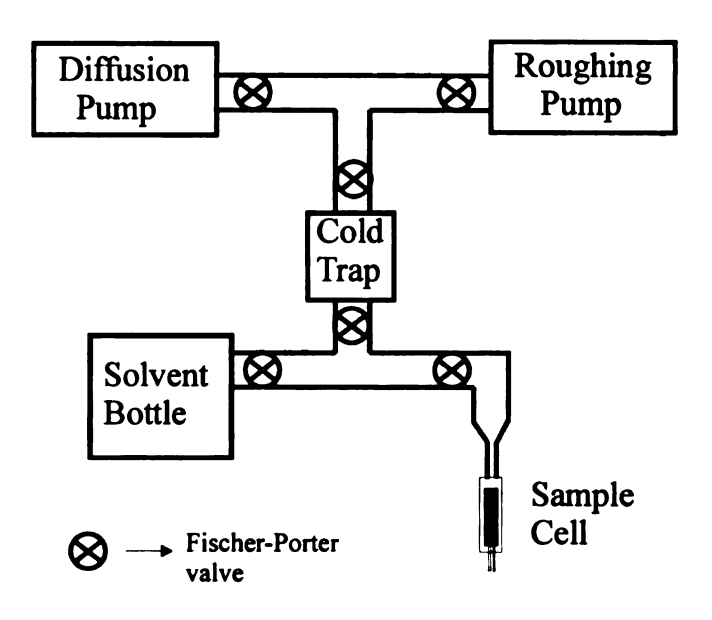


Figure 4.7. Fractional Distillation System.

When a sufficient vacuum exists, the solvent bottle/cold trap/sample cell is sealed off from the pumping apparatus by means of a FP valve on the cold trap. The liquid in the solvent bottle is then vaporized by gently heating a bath of warm water surrounding the bottle. Simultaneous cooling of the sample cell with liquid nitrogen forces the vapor travel through the connecting tubing and condense in the cell. This process continues until the sample cell is filled to a level deemed appropriate by the experimenter, at which point the vapor transfer is stopped by closing the FP valve located above the sample cell.

The final step is to freeze the contents of the sample cell, pump off any excess gas that may be present, and transport the cell to the MSU Chemistry Glassblowing Laboratory for subsequent sealing using a natural gas torch.

IV. b. Nitrogen Atmosphere Loading.

When conditions do not dictate the controlled precision of FVD, a less complex and much less time consuming method may be used to load the sample cell called Nitrogen Atmosphere Loading. Using this technique the unopened bottle of sample liquid, an independent transfer container, and sample cell are initially placed inside a standard polyethylene glove bag (Aldrich AtmosBagTM). The bag is then sealed with 2" duct tape and purged several times with nitrogen gas so as to remove any water vapor that may be present prior to initiating the filling process. The bag is then inflated with nitrogen so as to obtain a comfortable working space, and the sample cell filled with liquid by hand. The valve at the top of the sample cell is then closed, and the cell is removed from the bag and attached to the portable pumping station used for FVD. The contents of the sample cell are then frozen, and the remaining nitrogen gas pumped off. Finally, the cell is transported to MSU Chemistry Glassblowing Laboratory for sealing.

REFERENCES

- [1] J.D. Jackson, *Classical Electrodynamics*, John Wiley & Sons, New York, 1975, pp152-155.
- [2] P. Debye, *Polar Molecules*, Chemical Catalog, New York, 1929.
- [3] H. Frohlich, *Theory of Dielectrics*, Oxford University Press, 1949.
- [4] C.P. Smyth, *Dielectric Behavior and Structure*, McGraw-Hill Book Company, Inc., New York, Chapter 1, 1955.
- [5] L. Onsager, J. Am. Chem. Soc. 58, 1486 (1936).
- [6] CRC Handbook of Chemistry and Physics, CRC Press Inc., Boca Raton, Florida, 1988, p. E-59.
- [7] C.P. Smyth, *Dielectric Behavior and Structure*, McGraw-Hill Book Company, Inc., New York, 1955, pp. 28-34.
- [8] J.D. Jackson, *Classical Electrodynamics*, John Wiley & Sons, New York, 1975, p. 311.
- [9] K. Adachi, H. Suga, and S. Seki, Bull. Chem. Soc. Jpn. 41, 1073 (1968).
- [10] M. Honda, *The Impedance Measurement Handbook*, Section 2-3, Yokogawa-Hewlett-Packard LTD, 1989.

Chapter 5

DIELECTRIC STUDIES OF CYCLO-OCTANOL

I. Motivation.

The dielectric studies of cyclo-octanol represent the first effort of the Birge group to construct a phenomenological approach toward understanding the glass transition. By studying the glass transition in a material which is structurally less complex than a fully-disordered supercooled liquid, we hoped to identify which aspects of the glass transition are most "universal" and which depend on the detailed structural nature of a material. The intrinsic translational periodicity and rotational disorder characteristic of the rotator phase in orientationally-disordered crystals provides an ideal environment for such studies.

The sections that follow present dielectric spectroscopy measurements performed on cyclo-octanol covering ten decades in frequency. Due to the necessity for two independent experimental techniques, the dielectric measurements naturally divide into two overlapping studies: a low-frequency set which covers the range 1 mHz to 10 kHz, and a high-frequency set which extends the measurements to 10 MHz.

II. Dielectric Measurement of Cyclo-Octanol.

II. a. Experimental Notes.

The sample material for the low and high frequency studies consisted of cyclo-octanol (C₈H₁₅OH) purchased from Aldrich Chemical Company, Milwaukee, WI. The original purity of the stock cyclo-octanol was given as 99.5%, but additional efforts were made to ensure a clean sample through vacuum distillation (see Chapter 4, section IV.a).

The distilled sample was then introduced to the coaxial capacitor cell and sealed under vacuum using facilities at the MSU Chemistry Scientific Glassblowing laboratory. The sealed sample cell was then attached to the cryostat and measurement electronics.

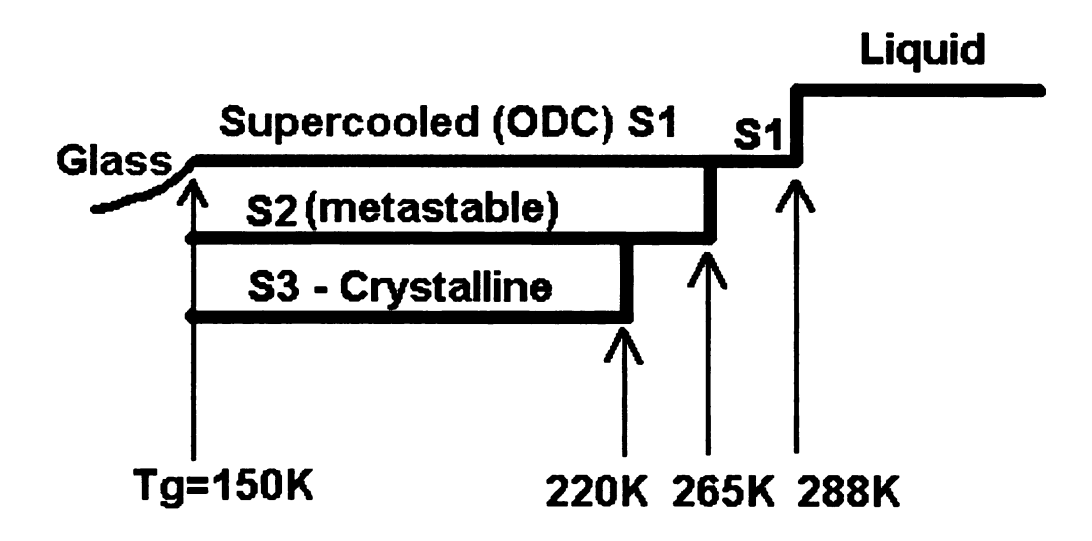


Figure 5.1. Schematic diagram illustrating the various phases of cyclo-octanol.

The phase diagram for cyclo-octanol has been previously studied [1,2] using using dielectric measurements, and a schematic diagram is shown in Figure 5.1. On cooling from the high temperature liquid, the sample will undergo a transition to the orientationally-disordered S1 phase at 288 K. The S1 phase has f.c.c. structure with a lattice constant of 9.56 Angstroms. Slow cooling in the S1 phase will result in transition at 265 K to the S2 phase, which is also orientationally-disordered but has a dielectric response which is negligible compared to that of S1. The transition at 265 K can be bypassed through the use of moderate cooling rates of 5-10 K/min, resulting in the supercooled S1 phase and eventually the orientational glass transition at $T_g = 147$ K.

Virtually all of the dielectric measurements presented in this chapter were obtained from the supercooled S1 phase. It should also be noted that transition to the stable crystalline phase S3 occurs below 220 K. Time-dependent transitions to lower energy configurations can also occur in the region 220 – 265 K if cooling rates are not sufficiently high.

II. b. Summary of Low-Frequency (1mHz – 10kHz) Measurements.

The initial dielectric experiments on cyclo-octanol were carried out by Leslie-Pelecky and Birge [3] in 1991-1994 here at Michigan State University. The work investigated the α-relaxation dynamics of cyclo-octanol in the low-frequency regime over a temperature range of 166 - 205 K. This section will provide a short review of the low-frequency results, as they are important in establishing the motivation for extension of the dielectric studies to higher frequencies.

Using an established cooling protocol discussed elsewhere [3], Leslie-Pelecky and Birge measured the complex dielectric constant $\varepsilon^* = \varepsilon' + i\varepsilon''$ of the supercooled S1 phase over a frequency range 1 mHz - 10 kHz for temperatures 166 - 205 K. The measured dielectric response is shown in Figure 5.2, where the solid lines passing through the data are fits to the KWW function described previously in Chapter 2. Other empirical fitting forms such as Cole-Davidson [4] were also tried, but neither provided better fits to the data. For frequencies approximately 2-3 decades and higher above the main peak in ε'' , empirical fitting of the relaxation data with the KWW and others fail to provide an accurate representation of the data [5]. However, the KWW can be used in the main peak region to extract parameters such as the mean relaxation time ($\tau \sim 1/f_{peak}$) and degree of non-Debyeness (via the KWW stretching exponent β and eq. 2.10). Figures 5.3 (a) and

(b) show the temperature dependence of the width of the relaxation relative to a Debye process (β =1) and the mean relaxation time τ . These two graphs indicate that the dynamical response of cyclo-octanol displays the same two nearly universal features found in structural glass forming liquids: 1) Rapidly increasing relaxation time for molecular motion as the temperature is decreased, and 2) increasingly non-Debye relaxation behavior as the glass transition is approached.

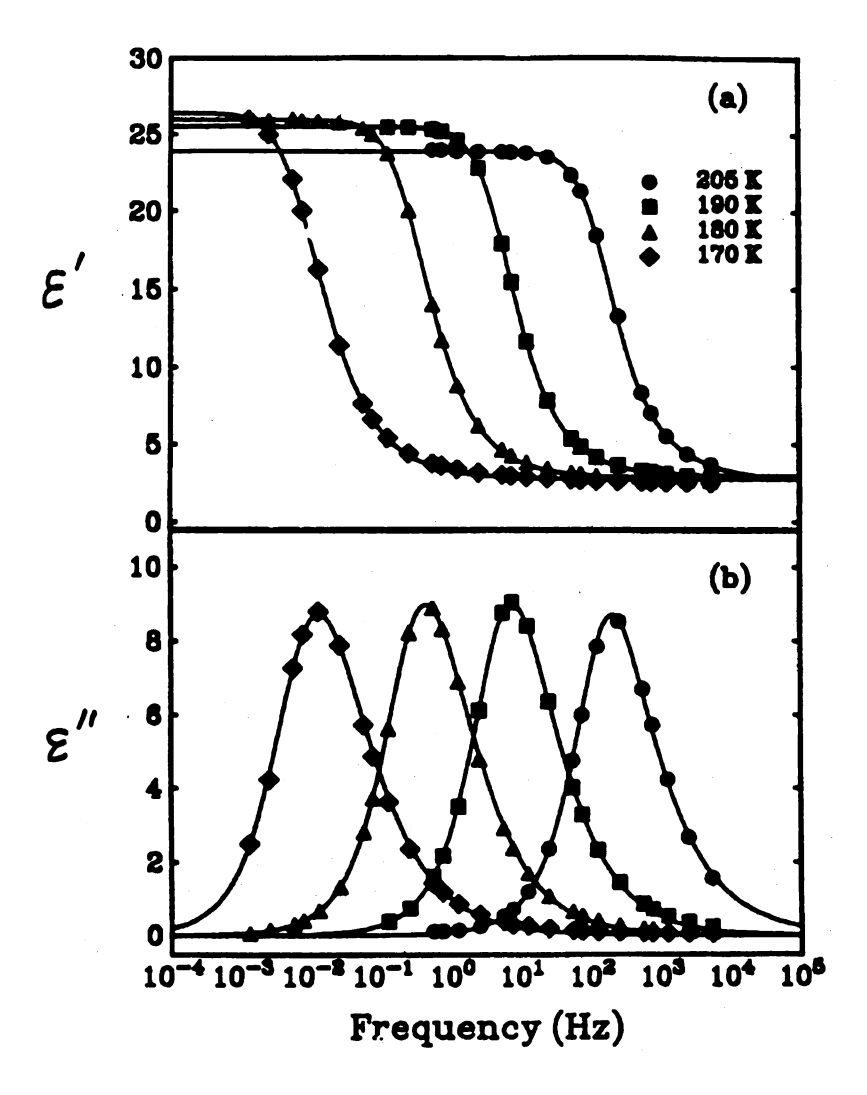
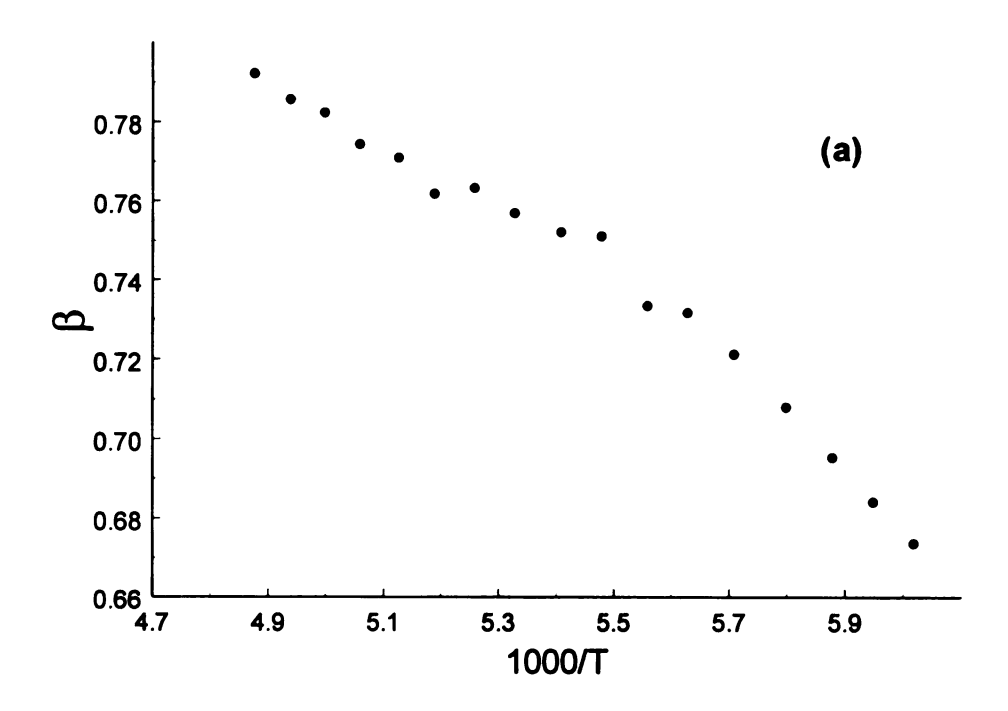


Figure 5.2. a) ε' and b) ε'' for the supercooled S1 phase of cyclo-octanol as measured by Leslie-Pelecky *et al.* in the low-frequency regime.



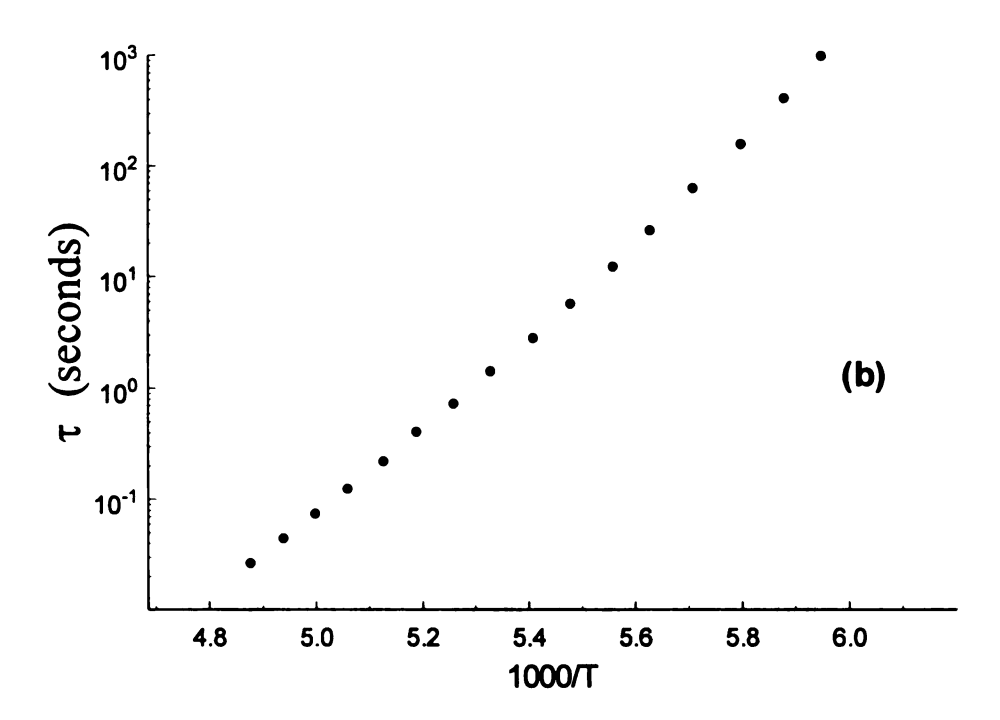


Figure 5.3. Temperature dependence of parameters extracted from the KWW fitting of Figure 5.2 data. (a) "streching exponent", β , and (b) mean relaxation time τ .

The search for universalities in the relaxation behavior of cyclo-octanol continued with scaling of the dielectric data [3] using an empirical form proposed by Dixon *et al.*[5]. Despite the rather complex look of the scaling form, it has been successful in collapsing the dielectric data for a wide variety of glass forming materials onto a single "master" curve. The results of the scaling for cyclo-octanol can be seen in Figure 5.4, and it appears that the data scale in accordance with that of structural glasses for all regions *except* in the high frequency wing where small deviations appear.

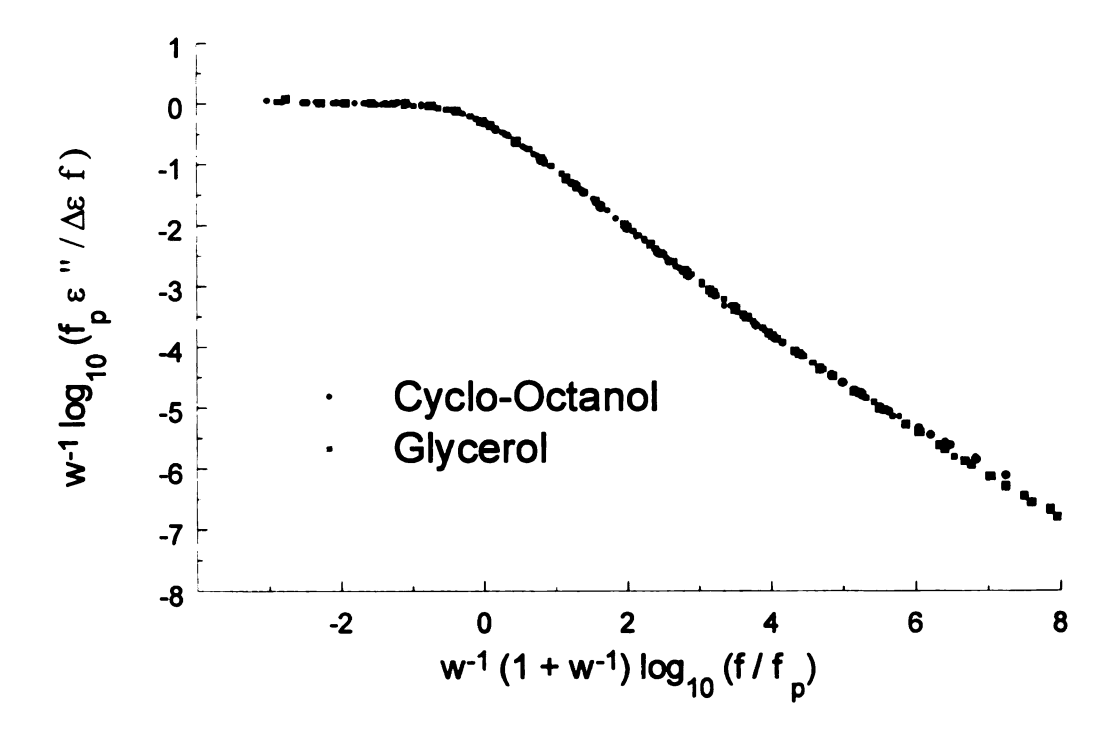


Figure 5.4. Scaling of the dielectric data using a form given by Dixon *et al*. Cyclo-octanol begins to show slight deviations from structural glass formers (e.g. glycerol) at high frequencies.

It was originally thought that this discrepancy might be related to fact that the measuring apparatus was optimized for low frequencies, and that data at the high end of the measurement range might be less reliable.

The decision to extend the dielectric measurements was based on the need to obtain a more detailed picture of the shape of the relaxation at higher frequencies. Additional measurements in the higher frequency regime would conclusively determine if the discrepancy observed on the scaling plot was a real feature of the data. This was important to know because some people have assumed that the scaling form and its resulting "master" curve is a universal feature of glass forming liquids, despite recent arguments to the contrary [7]. Based on the validity of the scaling form, predictions have been made of divergent behavior in the static dielectric constant at low temperature [8]. Thus, accurate knowledge of the high frequency behavior of a material is of great importance.

II. c. High-Frequency (1kHz – 10 MHz) Measurements.

For a long time, dielectric studies of glass forming liquids focused their attention on studying the low frequency (kHz region) dynamical response of the alpha relaxation. The availability and ease of low frequency measurement techniques in conjunction with the fact that one could learn a great deal from such studies meant that few experiments targeted the high frequency response of a material. However, recent interest in the high-frequency regime coupled with advances in dielectric spectroscopy have produced studies [9] probing the dynamics of glass formers at frequencies well into the high GHz regime. These experimental techniques have provided a wealth of new data regarding the high frequency response of supercooled liquids near the glass transition. While our

experimental setup cannot achieve such extremely high frequencies, its 10 MHz range still provides enough flexibility to allow examination of the dynamics several decades above the peak of the alpha relaxation.

The high frequency tail of the α-relaxation in supercooled liquids is known to obey a shallow power-law that extends for many decades in frequency above the main peak [5]. In an attempt to determine the form of the expected power-law behavior of cyclo-octanol at high frequencies, the dielectric measurements were extended to 10 MHz using the high frequency measurement circuitry described in Chapter 2, section III.d.

Figure 5.5 shows the results of the high frequency measurements combined with the low frequency measurements of Leslie-Pelecky and Birge, and the data sets agree well in the overlap frequency range. It can be clearly seen that the high frequency response of cyclo-octanol is most definitely not like a power law, but rather the data display a characteristic "shoulder" at all temperatures investigated. This feature is due to an additional relaxation process, or β -relaxation, which overlaps the primary α -relaxation.

Secondary relaxation processes such as the β -relaxation in Figure 5.5 typically occur in the temperature region below T_g where the α -relaxation is frozen out. The origin of β -processes have been studied extensively by Johari [9] and Johari and Goldstein [10], and quite often can be associated with a molecule's ability to overcome internal energy barriers and convert itself into different structural configurations. The appearance of β -relaxations at temperatures above T_g is not as common, but several cases have been documented in the literature. Examples of liquids displaying high temperature β -relaxations include chlorobenzene-decalin and toluene-pyridine [9] (shown in Figure

5.6) and benzyl chloride-toluene [11]. With regards to the latter study, the secondary relaxation process was explicitly identified as a rotation of the CH₂Cl subgroup.

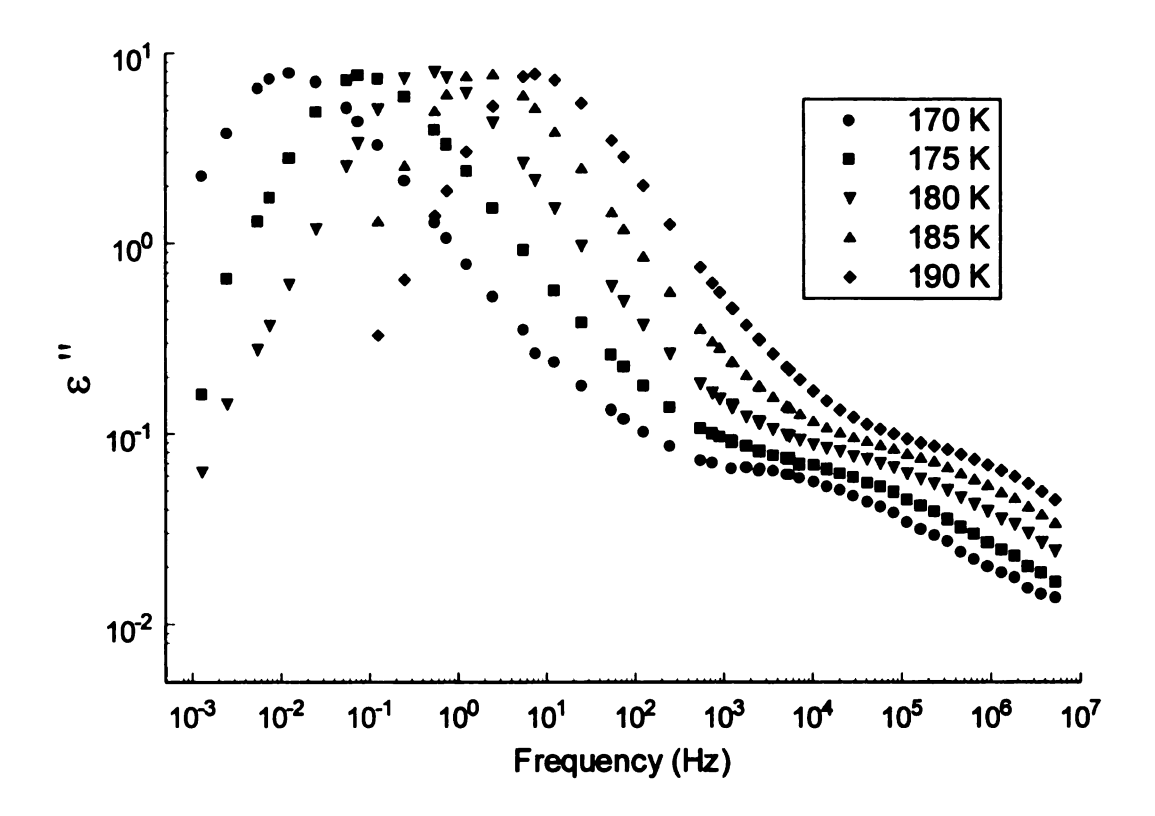


Figure 5.5. The imaginary part of dielectric response of cyclo-octanol covering a frequency range of ten decades. The appears of the high temperature β-relaxation is readily apparent at high frequencies.

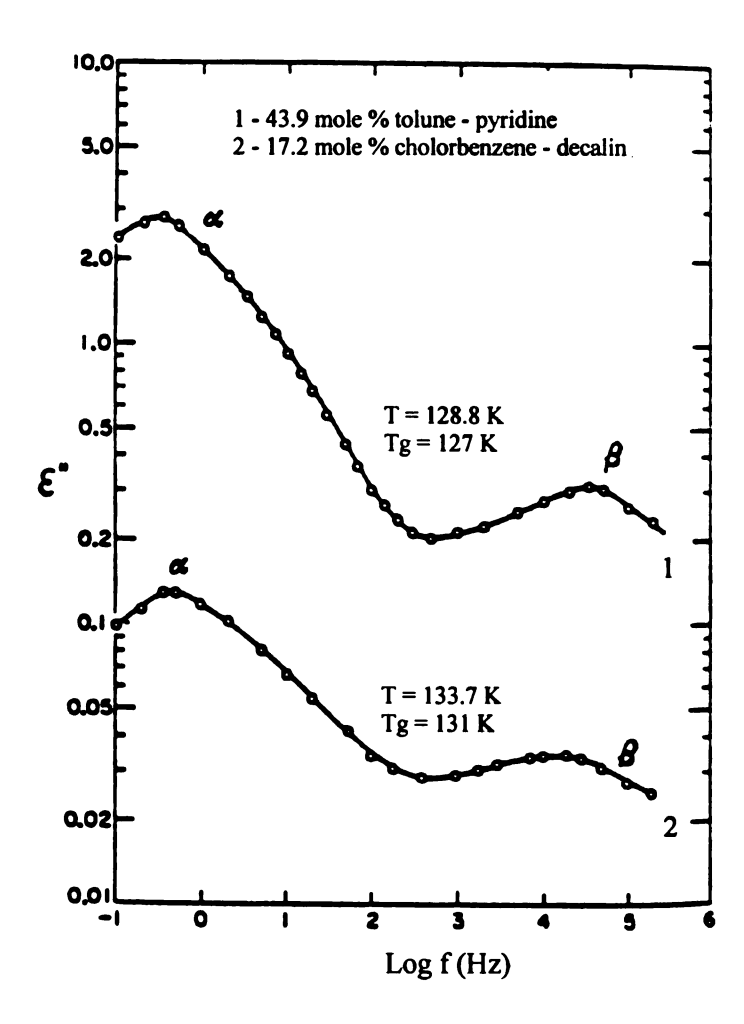


Figure 5.6. Some additional examples of high-temperature β relaxation processes similar to those observed in cyclo-octanol. (Data from: G. P. Johari, J. Chem. Phys. **58**, 1776 (1973)).

Interest in identifying the source of the high temperature β -relaxation in cyclooctanol is not limited solely to the Birge group at MSU. Concurrent with our high frequency measurements, Brand [12] produced an independent study of the fast dynamics in cyclo-octanol covering an extremely wide frequency range (10^{-6} - 10^{12} Hz). As can be seen in Figures 5.7 to 5.9, Brand found evidence for *two* secondary processes (labeled β and γ) both exhibiting thermally activated dynamics (i.e. Arrhenius behavior in the

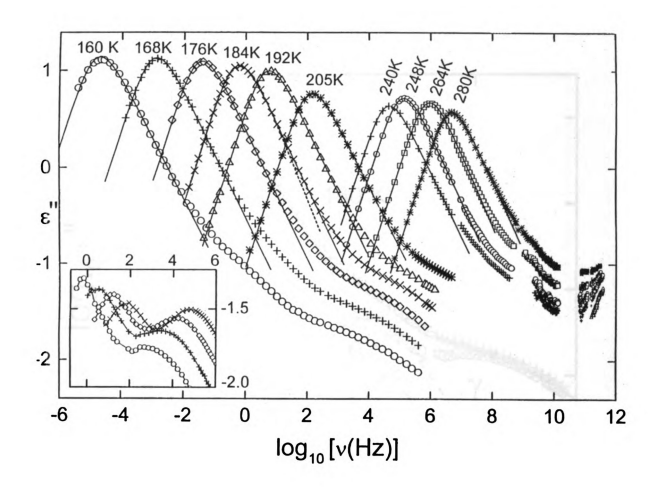


Figure 5.7. The dielectric loss (ε") curves for cyclo-octanol as obtained by R. Brand. The inset to the figure contains dielectric measurements of the stable crystalline phase S3 at the four lowest temperatures shown on the main plot. (Data from: R. P. Brand et al., Phys. Rev. B 56, 5713 (1997)).

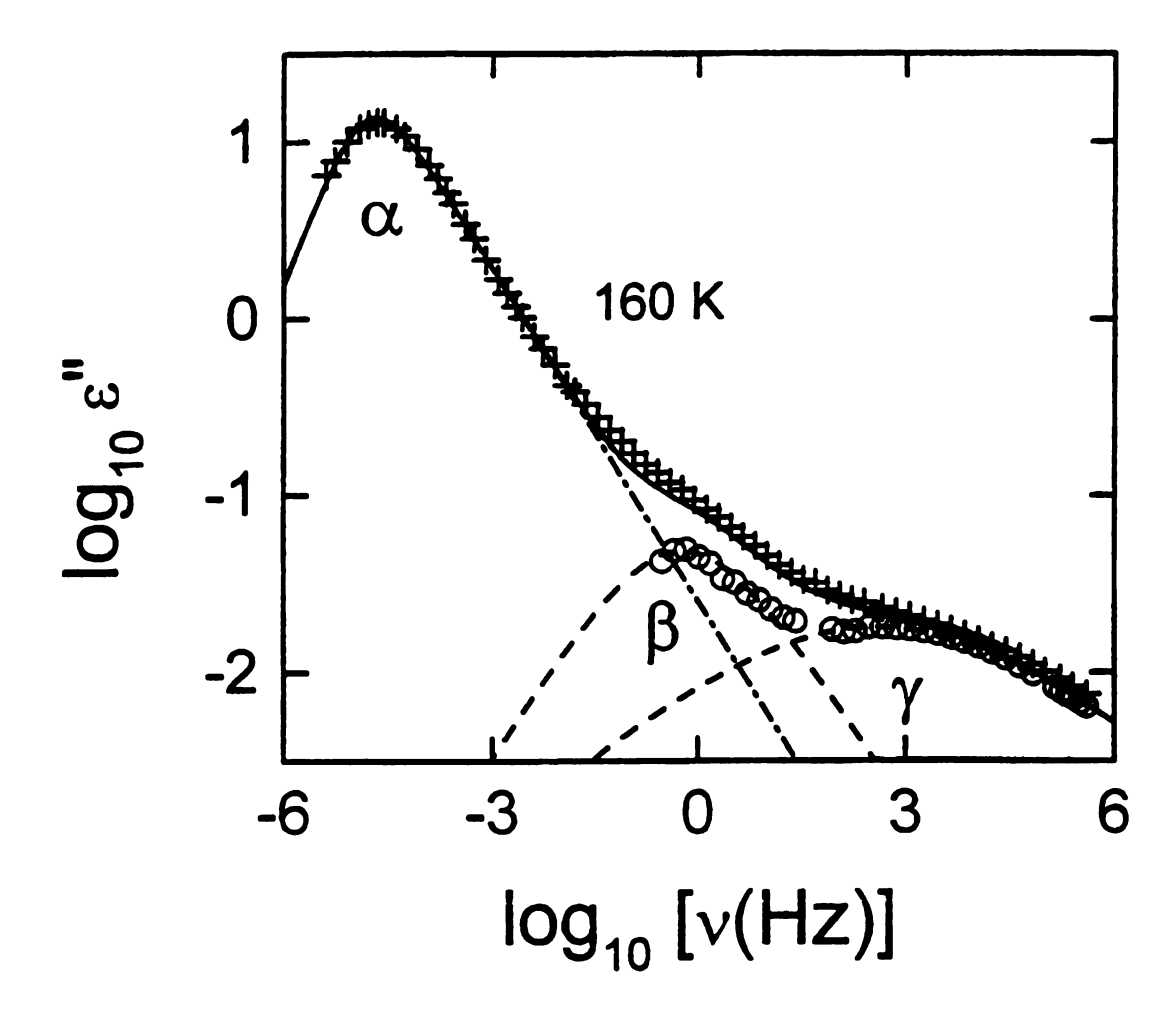


Figure 5.8. The dielectric loss (ϵ ") at a temperature of 160 K as obtained by R. Brand. In contrast to our measurements, Brand identifies three separate processes labeled as α , β , and γ . (Data from: R. P. Brand *et al.*, Phys. Rev. B **56**, 5713 (1997)).

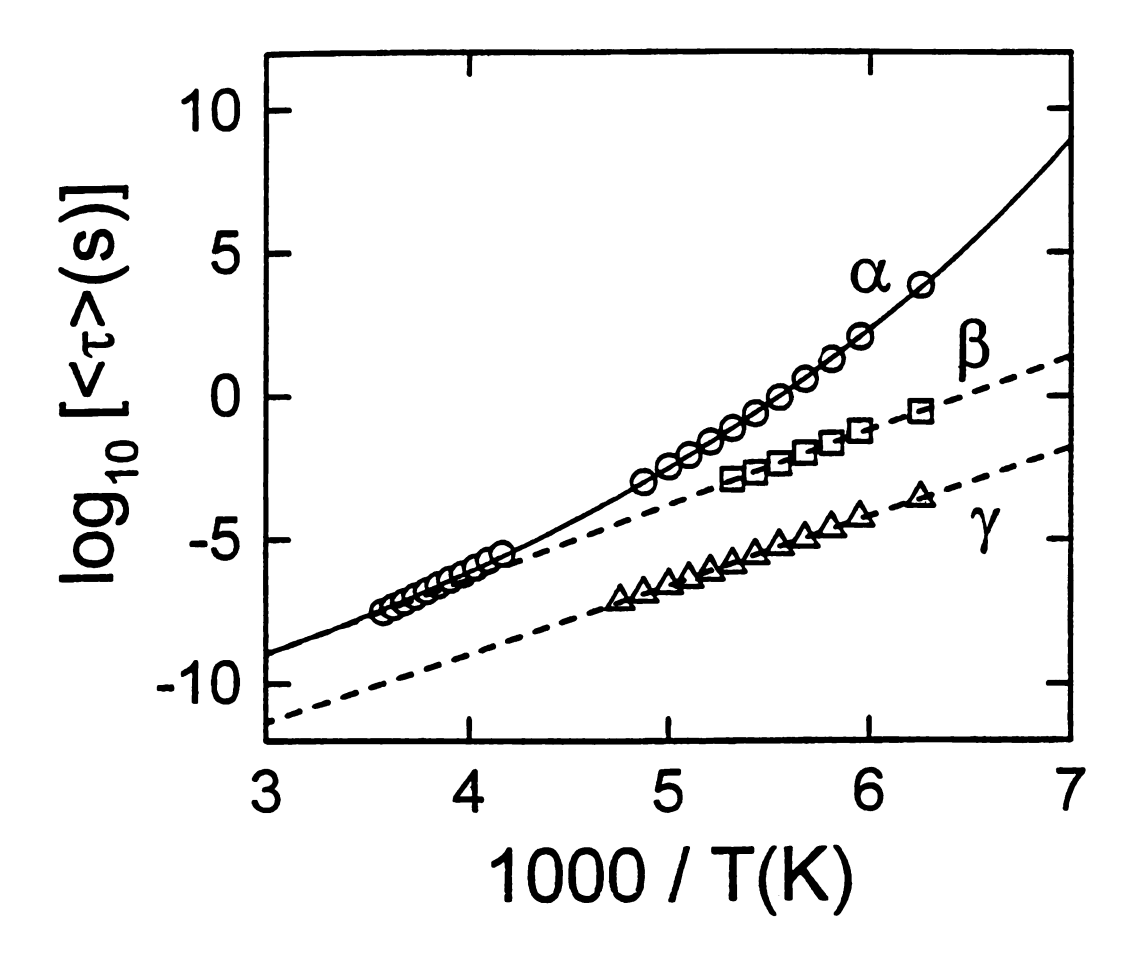


Figure 5.9. Plot of the mean relaxation times for the α , β , and γ processes shown in Figure 5.7. Similar to the results of Leslie-Pelecky *et al.* [3], the behavior of the α -process was found to be non-Arrhenius. The β and γ processes exhibit thermally activated (Arrhenius) behavior. (Data from: R. P. Brand *et al.*, Phys. Rev. B **56**, 5713 (1997)).

temperature-dependence of their relaxation times). Comparison of Figure 5.5 with Figure 5.7 shows that our labeled β -process appears to correspond well with Brand's γ -relaxation. For example, comparison of our 175 K data to Brand's 176 K set shows an inflection point corresponding to the first noticeable contribution of the secondary process at approximately 10^3 Hz. The β -process in Brand's study becomes increasingly obscured by the large α -response at higher temperatures and is simply not visible in our data.

Given our data for the supercooled S1 phase, it is very difficult to quantitatively determine the temperature dependence of the secondary relaxation processes. The optimal situation would be to subtract the α -response away leaving only the response of secondary processes. The difficulty with this approach lies in the fact that none of the empirical fitting functions (Cole-Davidson, KWW, etc.) accurately describe the α -relaxation at frequencies higher than a few decades above the main peak. Because of the power-law nature of the α -relaxation at higher frequencies, the subtraction process using empirical fitting forms will not effectively remove the α -response at high frequencies. The remaining response would not only contain the secondary processes, but also a contribution from the α -relaxation as well.

Brand's determination of the temperature-dependence of the secondary processes avoided the aforementioned problems by noting that both of the secondary relaxation processes were also present in the stable crystalline (S3) phase. The α -relaxation is not present in the ordered S3 phase, thus making it possible to accurately extract the temperature dependence of the secondary relaxations using a Cole-Cole [13] fitting

function. The solid line passing through the data of Figure 5.8 shows the result of adding together the Cole-Davidson fit of the main peak plus the Cole-Cole fits of the secondary processes β and γ . The resulting line agrees remarkably well with the actual data except in the region ~ 0.1 - 1 Hz, where as expected, the Cole-Davidson has underestimated the α -response.

Specific identification of the source of the β -relaxation (as labeled in our study) is not clear-cut for cyclo-octanol. However, because the response is also observed in the stable crystal, it is most likely associated with the intrinsic flexibility of the 8-member carbon ring. Based on structural considerations, it has been suggested [14] that the main ring undergoes a continuous deformation resulting in multiple molecular conformations contributing to the appearance of the β -relaxation. A detailed NMR study, such as that of Kuhns *et al.* [15] for cyclohexanol, would no doubt prove useful in further study of the molecular motion in cyclo-octanol.

III. Discussion of Results.

The primary success of the dielectric studies of cyclo-octanol was establishing the fact that the orientational glass transition in ODC's displayed the same characteristic signatures of the structural glass transition in fully-disordered liquids: 1) an increasing width of the relaxation as the temperature is lowered, and 2) faster-than-Arrhenius behavior in the relaxation time as the temperature is lowered. However, extension of the dielectric data to higher frequencies revealed the presence of a beta relaxation that overlapped the tail of the primary alpha relaxation, preventing a more detailed study of its shape. The origin of the beta relaxation is somewhat unclear, but is attributed to the conformational ability of the 8-member carbon ring. Thus, it is clear that while cyclo-

octanol is a good model glass, the additional structural complexity of the molecule suggests that it is not an *ideal* model glass.

REFERENCES

- [1] M. Shablakh, L. Dissado, R. Hill, J. Chem. Soc. Faraday Trans. 79, 369 (1983).
- [2] H. Forsman and O. Andresson, J. Non-Cryst. Solids 131-133, 1145 (1991).
- [3] D.L. Leslie-Pelecky and N.O. Birge, Phys. Rev. Lett. **72**, 1232 (1994); Phys. Rev. B **50**, 13250 (1994).
- [4] D.W. Davidson and R.H. Cole, J. Chem. Phys. 18, 1417 (1951).
- [5] P. K. Dixon, L. Wu., S. R. Nagel, B. D. Williams, and J. P. Carini, Phys. Rev. Lett. 65, 1108 (1990).
- [7] It has been suggested that the log-log form of the scaling tends to suppress detail in the dielectric data thus small features of the data become "washed out" after scaling.
- [8] N. Menon and S. R. Nagel, Phys. Rev. Lett. 74, 1230 (1995).
- [9] G. P. Johari, J. Chem. Phys. 58, 1766 (1973).
- [10] G.P. Johari and M. Goldstein, J. Chem. Phys. 53, 2372 (1971).
- [11] L. Wu, Phys. Rev. B 43, 9906 (1991).
- [12] R. Brand, P. Lunkenheimer, and A. Loidl, Phys. Rev. B 56, 5713-5716 (1997).
- [13] K. S. Cole and R. H. Cole, J. Chem. Phys. 9, 341 (1941).
- [14] Private communication with M.F. Thorpe, Michigan State University.
- [15] P. L. Kuhns and M. S. Conradi, J. Chem. Phys. 80, 5851 (1984).

Chapter 6

DIELECTRIC STUDIES OF ETHANOL

I. Motivation.

The inherent complexity of cyclo-octanol and its overlapping relaxation processes indicated that the search for an ideal model glass system should focus on structurally simple materials. It has been known for two decades [1] that ethanol (C₂H₅OH) exhibits interesting phase polymorphism, and appears to be quite unique in that it can be made to assume a variety of phases simply by varying the temperature in a controlled manner. Figure 6.1 shows the various phases of ethanol that can be produced upon cooling from the high temperature liquid.

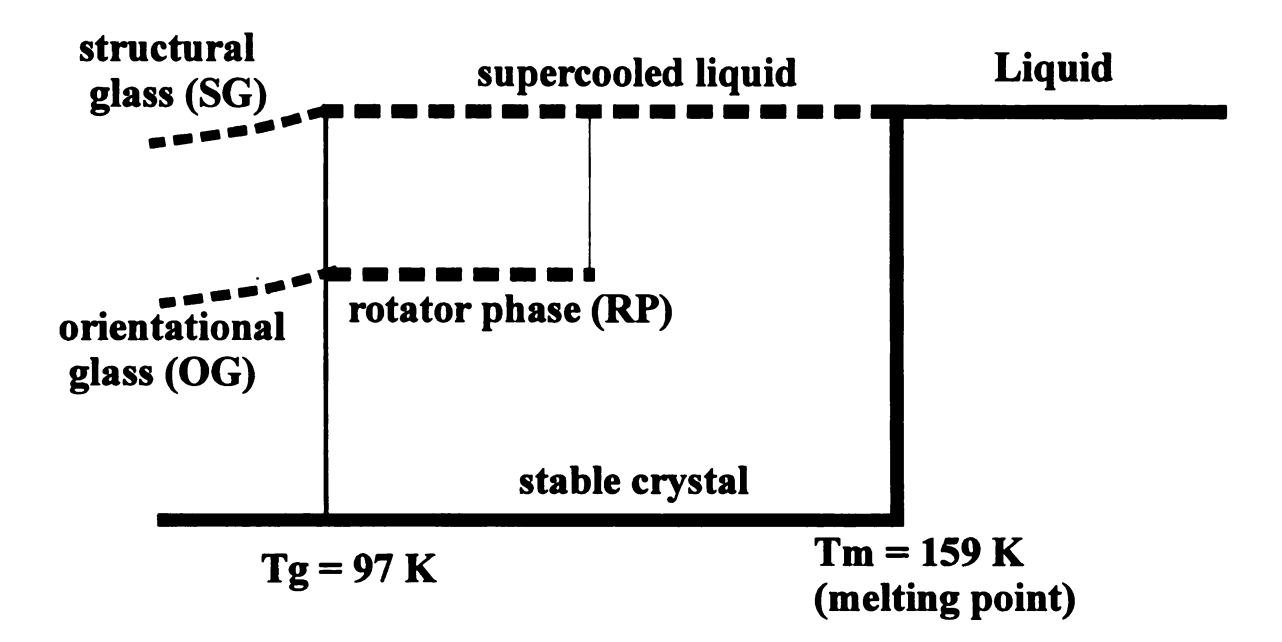


Figure 6.1. The various phases of ethanol.

The fully-disordered liquid phase transforms into a structural glass (SG) upon rapid cooling at a rate not less than 6 K/min. The orientationally-disordered crystalline phase transforms from a rotator phase (RP) to an orientational glass (OG) upon cooling at a moderate rate. Finally, the stable, orientationally-ordered crystal (monoclinic, lattice constant 5.377 angstroms [2]), is produced either by very slow cooling of the liquid or by annealing the RP or supercooled liquid. Recent X-ray, neutron diffraction and Raman spectroscopic [2,3] studies have confirmed the existence of an orientational glasslike transition in the RP crystal at nearly the same temperature (T_g = 97 K) observed for the supercooled liquid-to-structural glass transition. The close similarity of high-frequency dynamical behavior in the orientational glass and structural glass phases has been established by neutron time-of-flight spectroscopy and low-temperature specific heat measurements [4]. These properties, combined with the fact that the RP crystal can be readily prepared from the structural glass suggest that ethanol provides a unique opportunity to investigate and compare the relaxation dynamics of both phases near their respective glass transitions. Such a comparison may help to clarify the role of translational and rotational degrees of freedom in the dynamical response of a material approaching the glass transition.

II. Dielectric Measurement of Ethanol.

II. a. Experimental Notes.

Sample material for the dielectric study consisted of 200 proof, dehydrated ethyl alcohol (ethanol) as obtained from the Quantum Chemical Company of Tuscola, Illinois.

Transfer of ethanol from the sealed factory bottle to the capacitor cell was carried out using the nitrogen atmosphere loading method described in Chapter 4, section IV.b.

Because the goal of the experiment was to measure the complex dielectric constant ($\varepsilon = \varepsilon' + i\varepsilon''$) of the supercooled liquid and rotator crystal phases near their respective glass transitions, a rigid experimental cooling protocol was established which yielded reproducible results between runs. The protocol allowed production and measurement of all phases seen in Fig. 6.1 within a single experimental cooldown. This protocol can be summarized as follows. Rapid cooling of the liquid at a rate greater than 6 K/min bypasses crystallization at $T_M = 159$ K [5], and allows entry into the supercooled-liquid regime. Continuing to cool at the prescribed rate leads to the structural glass transition at $T_g = 97$ K. The RP crystal (body-centered cubic, lattice constant a = 5.37 angstroms [2]) is then formed by warming and annealing in the temperature range 102 K to 110 K. The exact temperature and annealing time required for conversion to the RP crystal depends on the warming rate, as well as the initial cooling rate into the glassy state [1].

The dielectric response of the RP crystal and SCL phases were investigated over frequency range of 1mHz to 10 MHz, utilizing both the low-frequency and high-frequency measurement techniques described in Chapter 4, sections III.c and III.d.

II. b. Dielectric Response of the SCL and RP Crystal Phases.

Figures 6.2 (a) and 6.2 (b) show the real (ϵ ') and imaginary (ϵ ") parts of the dielectric constant for the supercooled liquid as a function of frequency for temperatures of 96, 98, and 100 K. Figures 6.3 (a) and 6.3 (b) show the corresponding data taken in the RP crystal at temperatures of 96, 98, 100, 102, 104, 106, 108, and 110 K. Although the glass transition temperature is usually quoted as T_g =97 K, it should be emphasized that all the data were taken in the metastable equilibrium SCL and RP, respectively. The

data at 96 K, in particular, were observed not to change over more than an hour, indicating that no structural relaxation was taking place. Obtaining data over a broad temperature range in the SCL phase was hindered by the fact that time dependent transitions to the RP crystal occur above 102 K. Thus, in order to broaden the range of liquid phase data, additional measurements were made in the temperature range 164 K to 181 K. Figure 6.4 (a) and 6.4 (b) show the high-temperature liquid phase data, where the contribution of dc conductivity to the response at low frequencies is readily apparent.

The solid lines passing through the data in Figures 6.2-6.4 are fits to the Cole-Davidson fitting form [6] given by

(6.1)
$$\varepsilon(\omega) = \varepsilon_{\infty} + (\varepsilon_{0} - \varepsilon_{\infty})/(1 - i\omega/\omega_{p}^{CD})^{\alpha}$$

where $\omega=2\pi f$. It is well known that fitting relaxation data with empirical forms such as the Cole-Davidson or Kohlraush-Williams-Watts (KWW) function [7] does not accurately describe the relaxation at all frequencies. In particular, at frequencies higher than two decades or so above the peak, the data typically obey a shallow power-law dependence extending to very high frequency [8,9]. (The high frequency behavior and detailed examination of the shape of the dielectric relaxation will be examined in the next section). Nevertheless, the Cole-Davidson form can be used in the main peak region to provide estimates of parameters characterizing the dynamical response such as the mean relaxation time ($\tau \approx 1/\omega_p^{CD}$), and α , the degree of departure from a Debye-governed relaxation process ($\alpha=1$). The Cole-Davidson fit parameters as obtained for the RP crystal and SCL are summarized in numerical form in tables 6.1 and 6.2, respectively.

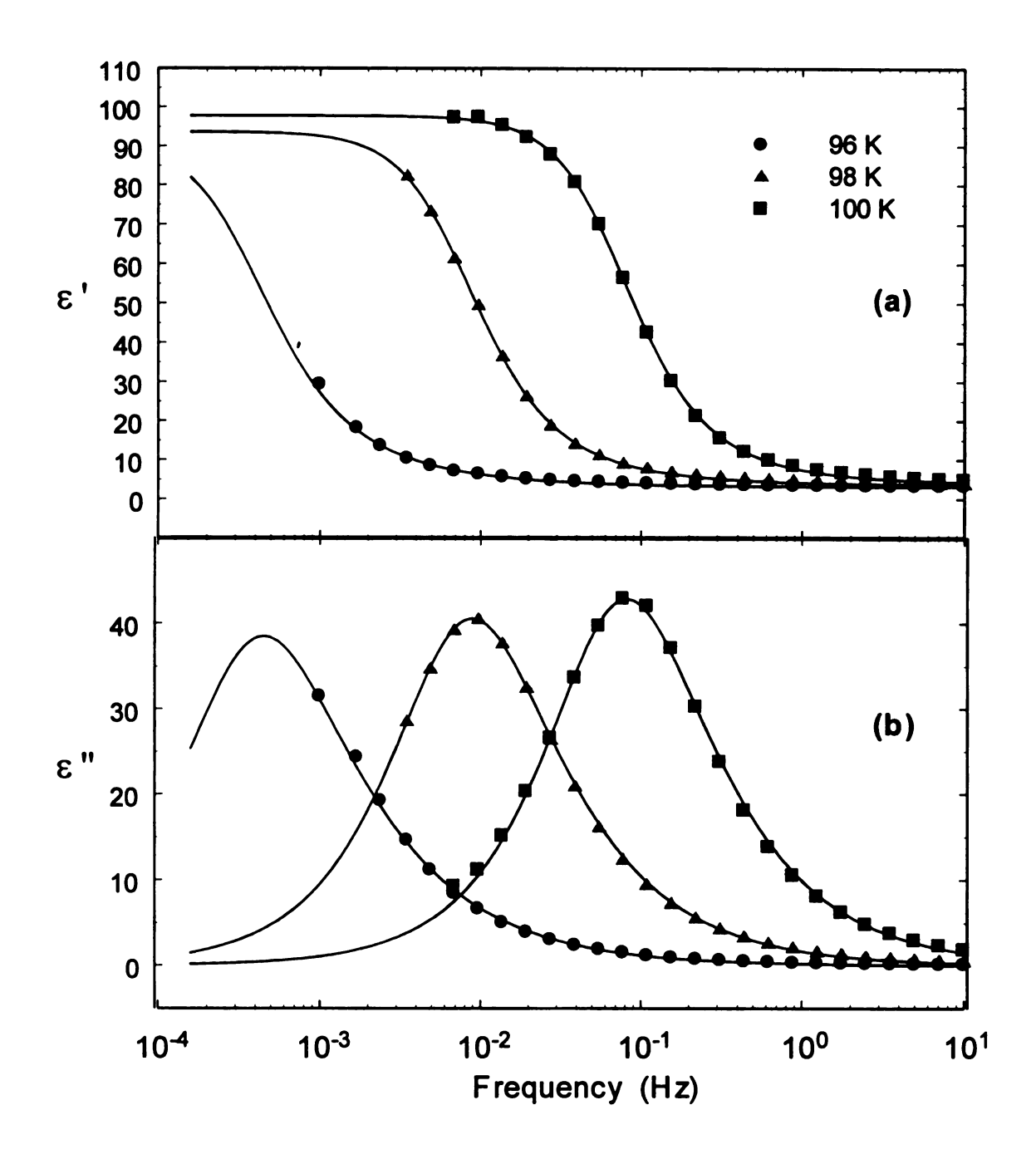


Figure 6.2. (a) ε' and (b) ε'' versus frequency for temperatures of 96, 98, and 100 K in the supercooled liquid phase of ethanol. Solid lines are fits to the Cole-Davidson function.

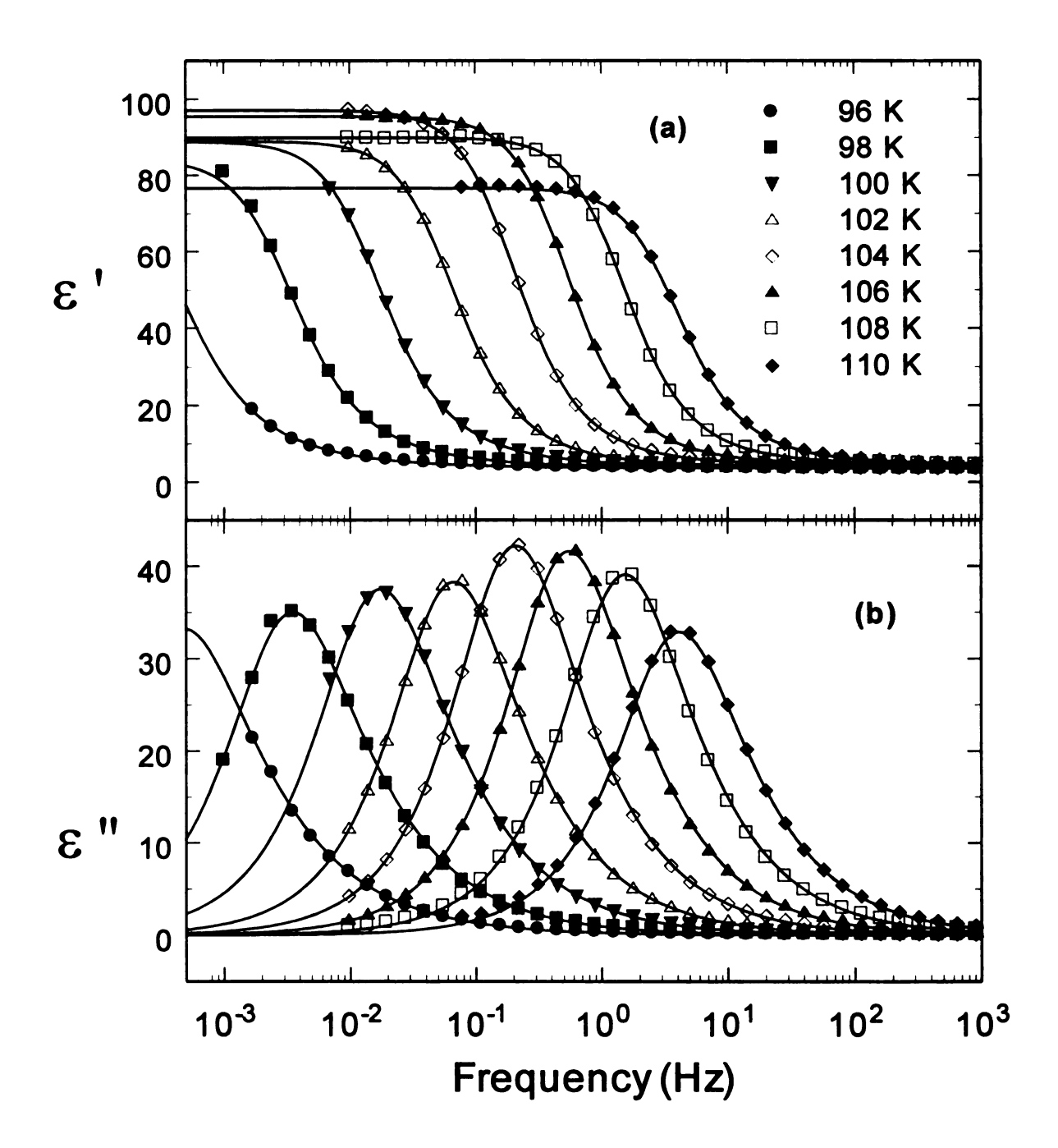


Figure 6.3. (a) ε' and (b) ε'' versus frequency for temperatures of 96, 98, 100, 102, 104, 106, 108, and 110 K in the RP crystal phase of ethanol. Solid lines are fits to the Cole-Davidson function.

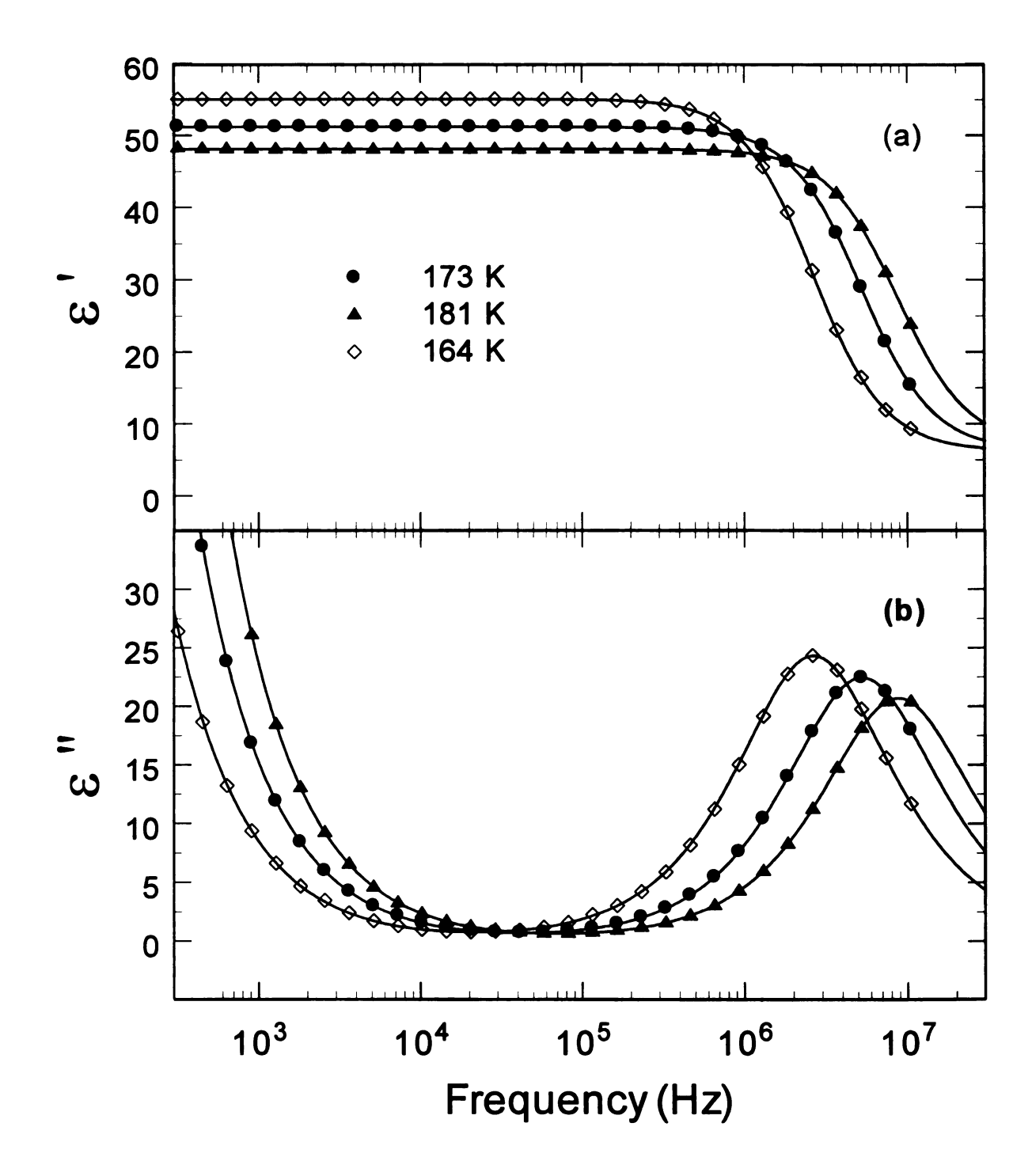


Figure 6.4. (a) ϵ' and (b) ϵ'' versus frequency for temperatures of 164, 173, and 181 K in the high temperature liquid phase of ethanol. Solid lines are fits to the Cole-Davidson function plus a term of the form $4\pi\sigma_{dc}/\omega$ in ϵ'' due to dc conductivity.

T(K)	τ (sec)	α	ϵ_{∞}	ε ₀ - ε _∞
96	424.1	0.710	3.60	78.1
98	58.6	0.744	3.77	82.0
100	12.1	0.760	3.86	85.2
102	3.0	0.796	3.85	85.1
104	0.95	0.811	4.21	92.9
106	0.35	0.821	4.34	91.1
108	0.13	0.822	4.44	85.5
110	0.05	0.815	4.53	72.2

Table 6.1. Cole-Davidson fitting parameters for the RP crystal phase of ethanol in the temperature range $96-110~\rm{K}$.

T(K)	τ (sec)	α	€∞	€0 - €∞	σ (sec ⁻¹)
96	347.2	0.776	3.22	80.2	
98	21.76	0.790	3.60	91.0	
100	2.27	0.819	3.88	94.0	
164	6.05e-8	0.987	6.16	48.9	676
169	4.18e-8	0.986	6.07	46.9	931
173	3.04e-8	0.998	6.28	44.9	1210
177	2.29e-8	1.000	6.47	43.2	1520
181	1.90e-8	0.925	5.37	42.7	1886

Table 6.2. Cole-Davidson fitting parameters for the SCL (96-100 K) and high-temperature liquid (164-181 K).

Figure 6.5 shows the temperature dependence of the width parameter, α , for both the SCL and RP crystal. Both phases display a characteristic feature common to many glass-forming materials, namely a decrease of α with temperature indicating deviation from idealized Debye behavior [10].

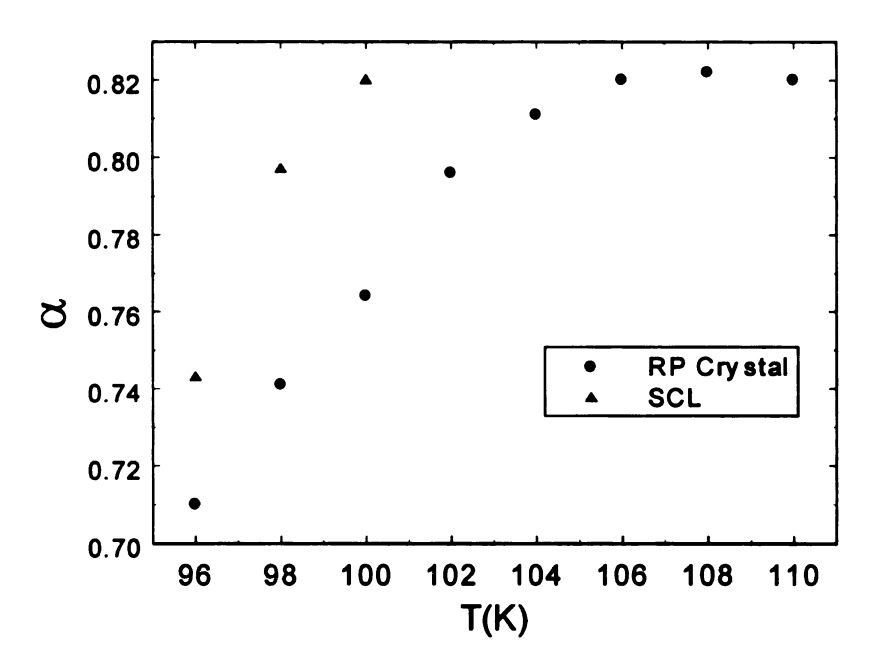


Figure 6.5. Plot of the Cole-Davidson width exponent, α , versus temperature for the SCL and RP crystal phases of ethanol.

Figures 6.2 and 6.3 show that the rotational contribution to the static dielectric constant, $\epsilon_0 - \epsilon_\infty$, is similar in the two phases, indicating that the molecules undergo complete rotation in the SCL as they do in the RP crystal. Figure 6.6 plots the static dielectric constant versus temperature, and reveals a surprising feature of the data. In both the SCL and RP, there is a marked decrease in $\epsilon_0 - \epsilon_\infty$ at low temperature which is not typically seen in the response of polar liquids. This type of behavior can usually explained by partial crystallization of the sample during cooling, which results in a

reduction of the total number of molecules capable of rotations. However, the observed decrease in Figure 6.6 can not be due to partial crystallization of the sample during the measurement because the data in Figure 6.2 were taken on warming from the SG, and the data in Figure 6.3 were verified to be reproducible on warming from the OG.

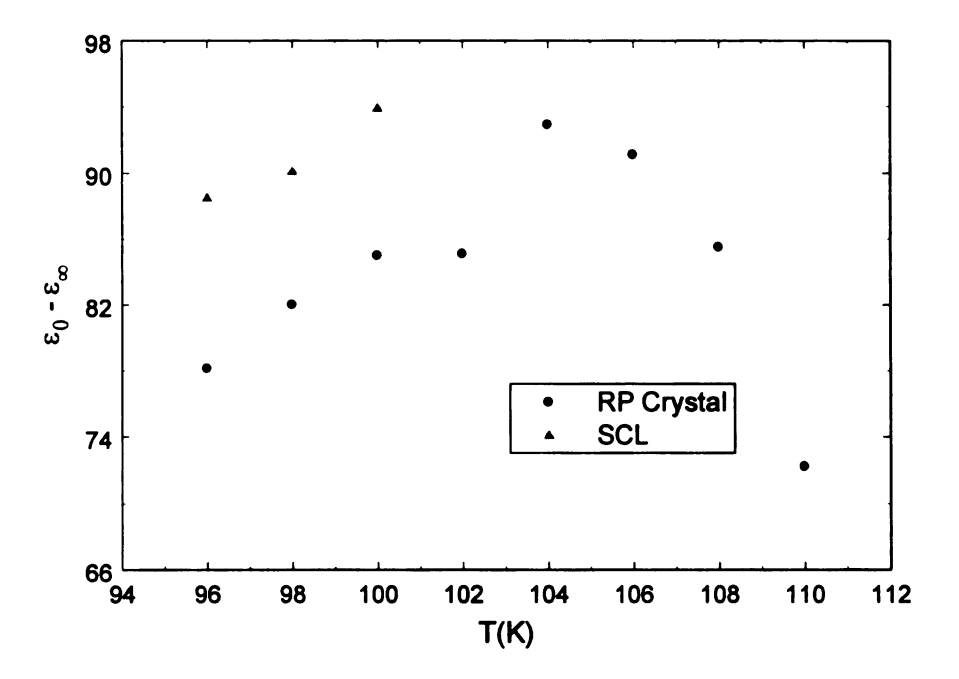


Figure 6.6. Plot of $\varepsilon_0 - \varepsilon_\infty$ versus temperature. The observed decrease in ε_0 - ε_∞ at low temperatures is not due to partial crystallization of the sample.

In particular, the only known crystalline phases of ethanol are the rotator phase we are studying and the stable crystal, which has a very small dielectric response. Thus, progressive transformation to the stable crystal is not consistent with the data.

Figure 6.7 shows the temperature dependence of the mean relaxation time in both the RP crystal and SCL phases. The mean relaxation time can be determined by $\tau \sim 1/\omega_p^{CD}$, where ω_p^{CD} locates the peak of ϵ'' . The solid lines are fits to the Vogel-Tamman-Fulcher equation [11] given by

(6.2)
$$\tau = \tau_0 \exp(A/(T-T_0))$$

Here, τ_0 is an attempt time and T_0 is the Vogel temperature at which the relaxation time diverges. Results of the VTF fitting for each phase are listed in table 6.3.

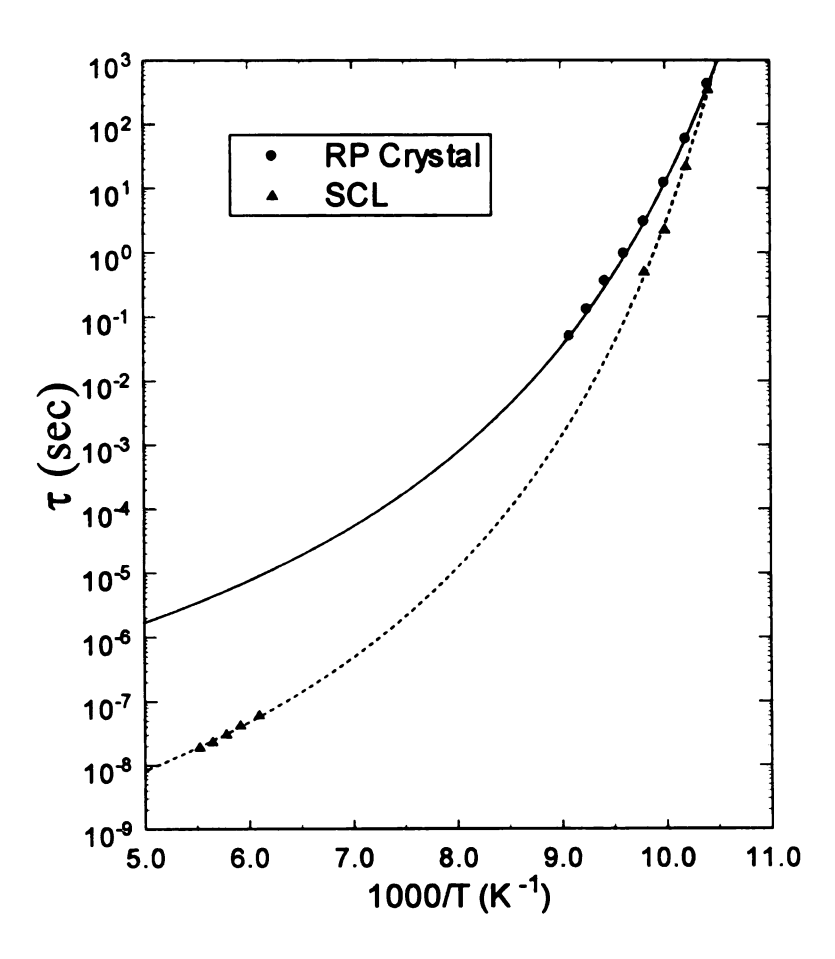


Figure 6.7. Temperature dependence of the mean relaxation time for the liquid (above T_m), supercooled liquid, and rotator crystal phases of ethanol.

Parameter	A	T _o	το
SCL	596	75.6	6.8e-11
RP crystal	529	73.5	2.6e-8

Table 6.3. VTF fit parameters of the mean relaxation time in the RP crystal and SCL phases of ethanol.

Examination of Figure 6.7 shows that the mean relaxation times in the two phases are nearly equal at T=96 K, and display a temperature-dependent shift toward a longer average relaxation time in the RP crystal phase relative to the SCL with increasing temperature. This manifests itself experimentally as a pronounced shift of the RP crystal relaxation peak toward lower frequency relative to the relaxation peak in the SCL at the same temperature. From a practical point of view, this behavior provides a useful method of determining if the sample has completely converted itself from the SCL to the RP crystal: for a given temperature simply perform successive measurements of the dielectric constant until the peak in ϵ " ceases to move to lower frequency.

The behavior of the relaxation times can be explained by considering the degrees of freedom available to the material in passing through the glass transition in each phase. The $OG \rightarrow RP$ transition involves the liberation of purely rotational degrees of freedom, while the $SG \rightarrow SCL$ transition involves liberation of both rotational and translational degrees of freedom. As the temperature increases above 96 K, the additional translational freedom present in the SCL provides the constituent molecules with a less restrictive local environment, leading to increasingly shorter relaxation times in the SCL relative to the RP crystal for a given temperature. Recent specific heat measurements

[1,12] performed on both the SCL and RP crystal near their respective glass transitions support this argument: the OG \rightarrow RP crystal transition involves an increase of about 22 $Jmol^{-1}K^{-1}$ and the SG \rightarrow SCL transition involves an increase in the specific heat of approximately 31 $Jmol^{-1}K^{-1}$. Presumably the extra 9 $Jmol^{-1}K^{-1}$ in the SCL specific heat not present in the RP crystal correspond to translational degrees of freedom. These results suggest that the rotational degrees of freedom are the dominant contributor to structural relaxation processes near the glass transition in both the RP crystal and SCL, and that flow processes such as mass diffusion associated with translational degrees of freedom in the SCL contribute to a lesser extent.

III. Detailed Study of the Shape of the Alpha Relaxation in Ethanol

III. a. Motivation.

The dielectric measurements of ethanol indicate that the material does not exhibit overlapping relaxation processes such as those observed in the behavior of cyclo-octanol. The α -relaxation appears to be "clean" out to the highest measurement frequencies of our experiment, and suggests that a detailed examination of the entire shape of the α -relaxation is possible. As was alluded to briefly near the end of Chapter 5, section II.b, the high-frequency behavior of supercooled liquids is known to obey a shallow power law. Based upon extrapolation and analysis of the "master" curve obtained from the Dixon scaling form, Menon *et al.* [13] have proposed that the high frequency power law behavior of a material will be described by

(6.3)
$$\epsilon''(f) \propto f^{-\sigma}$$
, $\sigma = 0.72 (1 + w^{-1}) - 1$

where w is the full width at half max (W) of the relaxation in decades normalized by the width of a Debye relaxation process ($W_D = 1.14$ decades):

(6.4)
$$w = \frac{W}{W_D} = \frac{W}{1.14}$$

The Dixon scaling form and Eq. 6.3 suggest that specific power law behavior will result for a given relaxation width, and we would like to determine if this holds true for the case of ethanol.

III. b. Determination of High-Frequency Power Law Behavior.

To extract the power law characterizing material behavior at high frequency, the data must be fit in an appropriate manner. The Cole-Davidson form, which was used to successfully in section II.b to characterize the low-frequency behavior in the peak region of the α-relaxation, cannot adequately represent the data at high frequencies. However, after publication [14] of our low-frequency results, we constructed an improved fitting function which can fit our full range of experimental data and appears to be quite superior to fitting with the single Cole-Davidson. The fitting form utilizes *two* Cole-Davidson functions having the same mean relaxation time but differing in their amplitudes and widths. The Cole-Davidson with the larger amplitude and smaller width fits the peak region, while the broader, lower amplitude CD is used to extract information about the high-frequency power law σ. The mathematical form of the fitting function is then taken to be:

(6.5)
$$\varepsilon(\omega) = \varepsilon_{\infty} + \frac{\Delta \varepsilon_{1}}{(1 - i\omega\tau)^{\alpha}} + \frac{\Delta \varepsilon_{2}}{(1 - i\omega\tau)^{\sigma}}$$
, $\omega = 2\pi f$

The assignment of uncertainties to the data is difficult for a dielectric experiment because most of the uncertainty is due to systematic rather than statistical error. For the fits, we have assumed that the uncertainty for each data point consists of a constant and proportional term. The constant term (typically 0.005) reflects the base accuracy and

noise level of the instruments. The proportional term (\sim .02) accounts for the possibility of relative errors on different gain settings as well as the fact that no empirical model can accurately represent the data over the entire frequency range. With regards to the latter, fitting without the proportional term will over-weight the measurements in the peak region of ϵ'' (where the dielectric response is the largest) at the expense of the data in the tail region where the response is much smaller.

The results of the double CD fitting for the RP crystal and SCL can be seen numerically (tables 6.4 and 6.5) and graphically (figures 6.8 through 6.11) on the pages that follow. In each of the figures, ϵ'' has been plotted on a logarithmic scale to emphasize the fit to the data in the high frequency power law regime where $\epsilon'' << \epsilon''_{peak}$. Fits using the single CD form have also been included to illustrate the improvement provided by the double CD form.

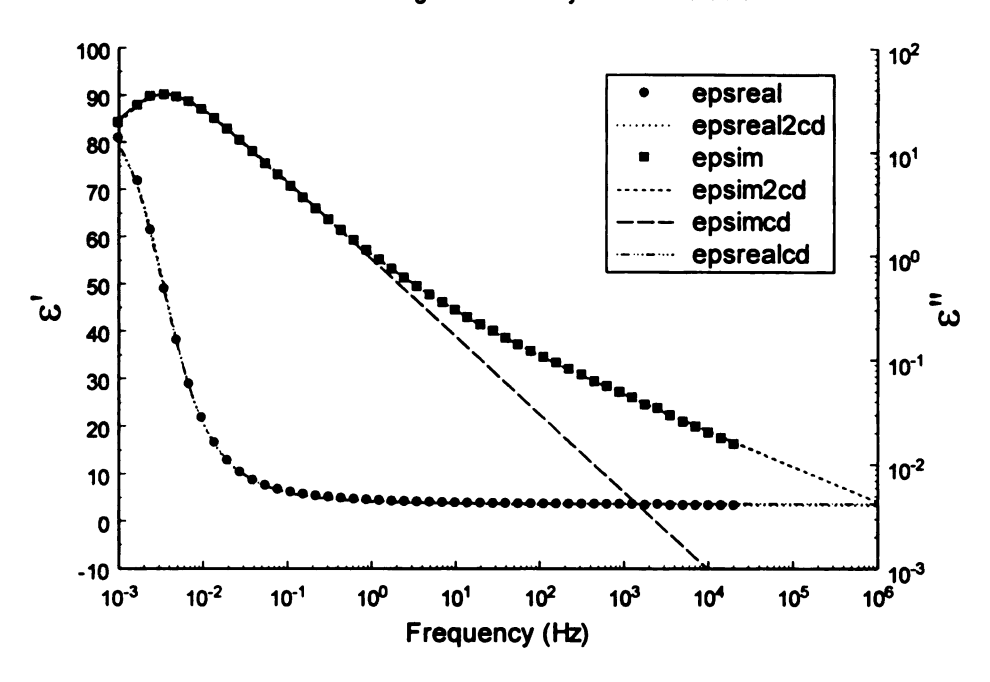
T(K)	Δε ₁	α	ϵ_{∞}	τ	Δε2	σ
98	74.3	.835	3.42	50.70	6.3	0.336
100	78.5	.853	3.48	10.27	6.7	0.346
102	78.3	.880	3.43	2.63	7.2	0.364
104	85.8	.889	3.60	0.85	7.6	0.359
106	82.7	.910	3.63	0.32	9.1	0.386

Table 6.4. Parameters obtained in the double CD fitting of the RP crystal phase of ethanol.

T(K)	Δει	α	€∞	τ	$\Delta \epsilon_2$	σ
98	81.1	0.879	3.31	20.34	9.3	0.419
100	79.9	0.932	3.43	2.21	15.5	0.472

Table 6.5. Parameters obtained in the double CD fitting of the SCL phase of ethanol.

CD and 2CD Fitting of 98K RP Crystal Dielectric Data



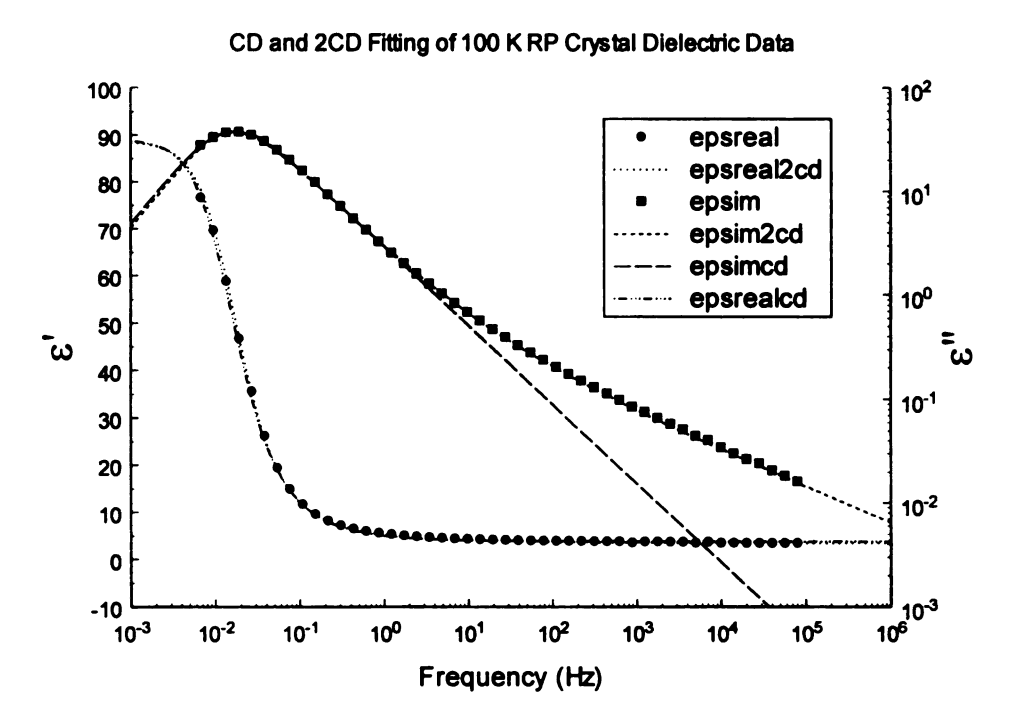
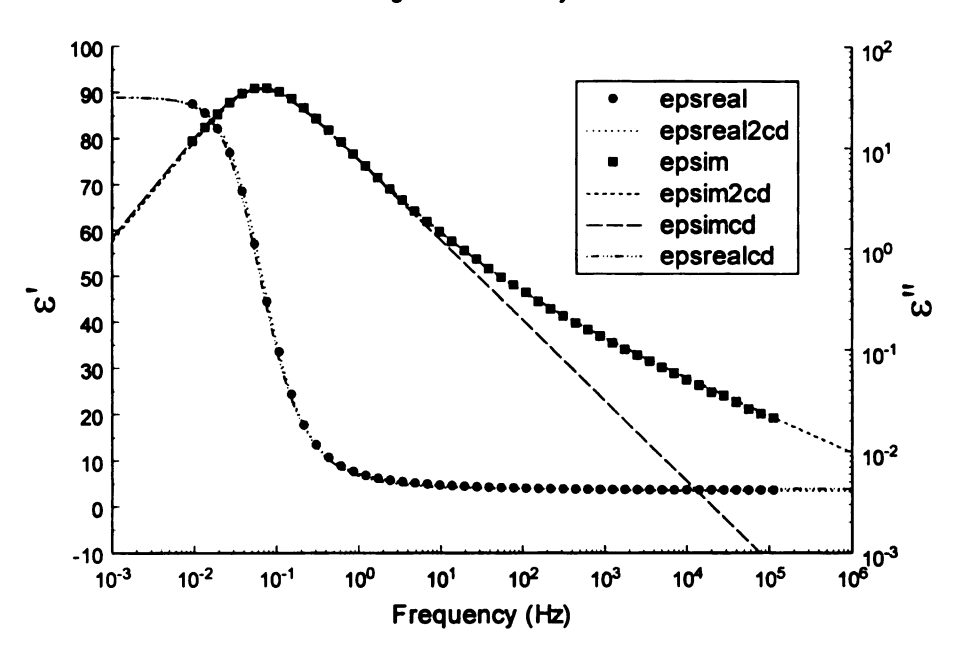


Figure 6.8. Double CD fitting of 98 K (top) and 100 K (bottom) RP crystal ethanol. Single CD fit is included for reference.

CD and 2CD Fitting of 102 K RP Crystal Dielectric Data



CD and 2CD Fitting of 104 K Rotator Crystal Dielectric Data

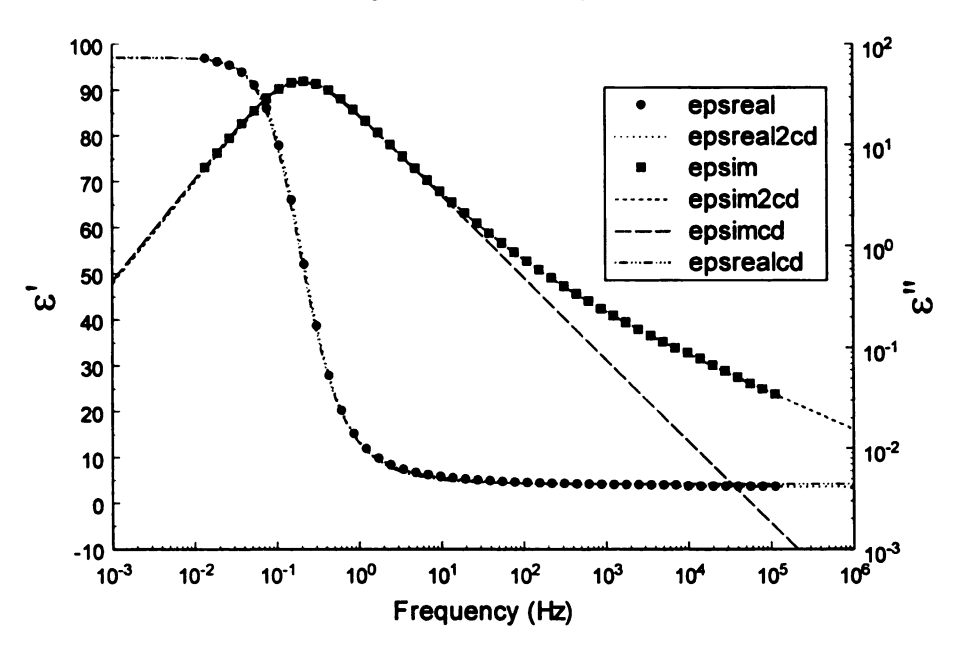
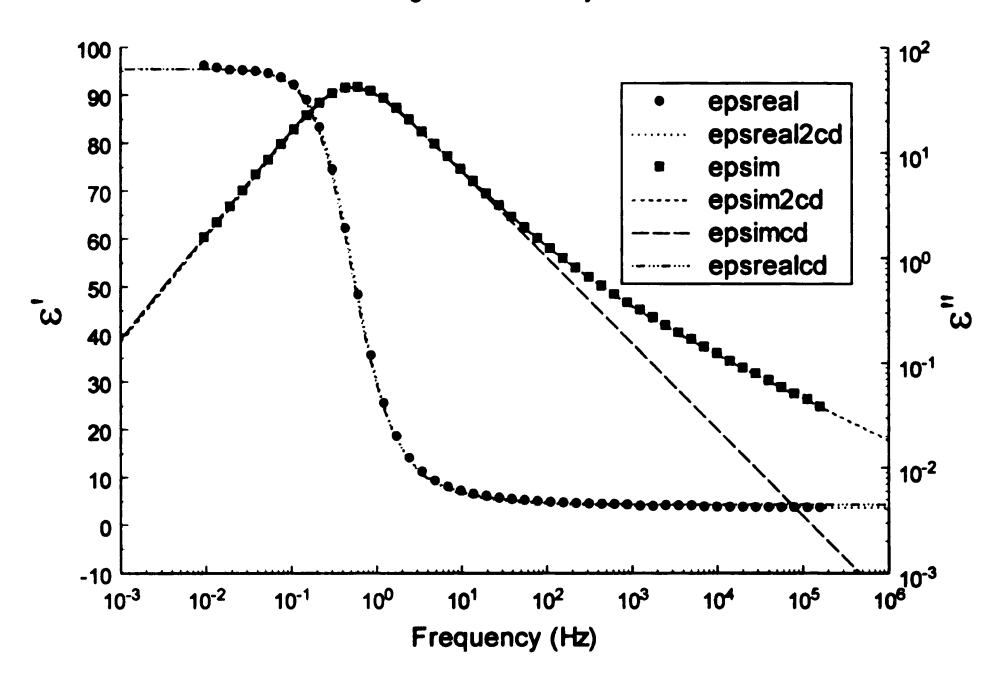


Figure 6.9. Double CD fitting of 102 K (top) and 104 K (bottom) RP crystal data. Fits to the single CD form are included for reference.

CD and 2CD Fitting of 106 K RP Crystal Dielectric Data



CD and 2CD Fitting of 98 K SCL Dielectric Data

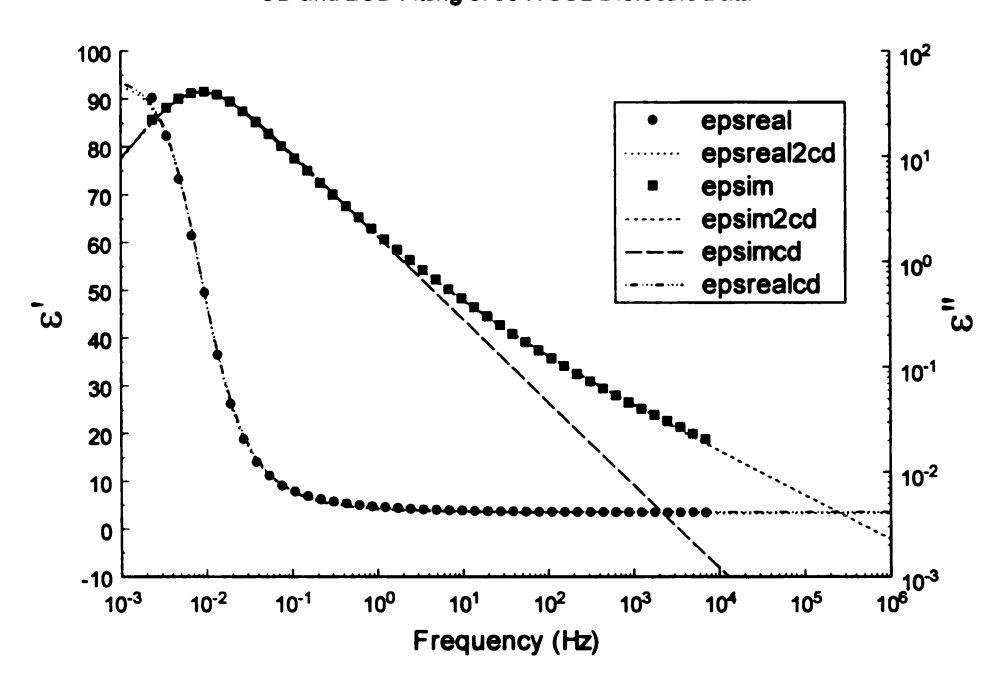


Figure 6.10. Double CD fitting of 106 K RP (top) and 98 K SCL (bottom). Fits to the single CD form are included for reference.

CD and 2CD Fitting of 100 K SCL Dielectric Data

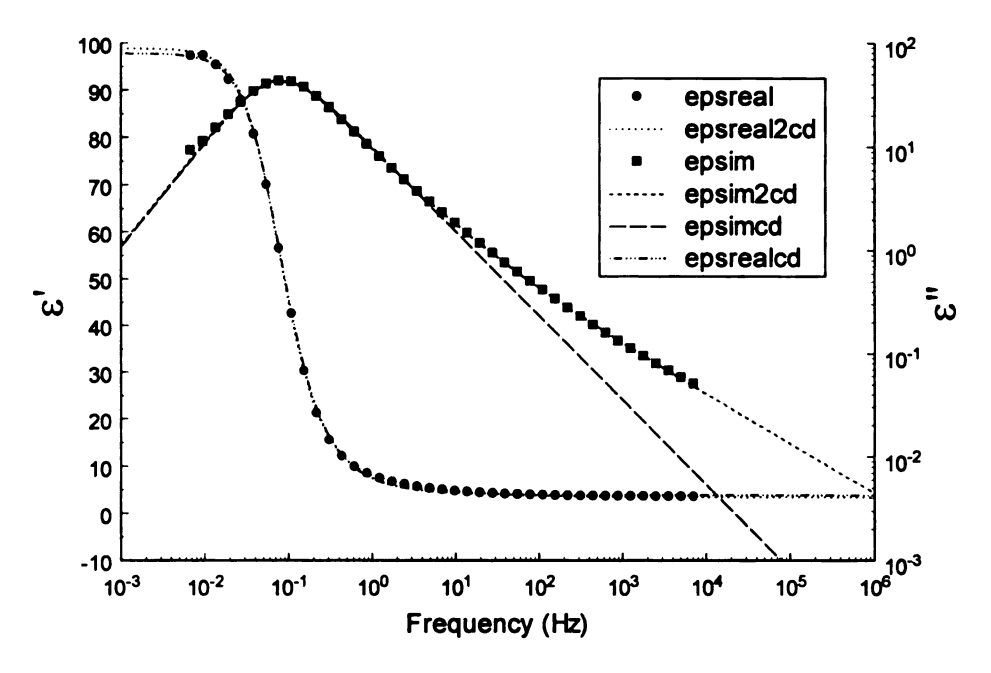


Figure 6.11. Double CD fitting of 100 K SCL data. Fits to the single CD form are included for reference.

The measured values of the high frequency power law were then be compared with the expectations of eq. 6.3 for both the RP crystal and SCL data. To obtain the expected values of σ from scaling, the normalized width (w) of the relaxation at each temperature had to be determined. To do this, the full width at half maximum (W) of the relaxation for a given temperature was determined by hand using the double CD fits to the ε'' data, and then normalized by the width of a Debye relaxation (1.14 decades) to give the relative width w. The measured relative widths w, along with the expected and measured values of the high frequency power law σ are summarized in tables 6.6 and 6.7 for the RP crystal and SCL, respectively. We observe that the the measured power laws

for the RP crystal are in fairly good agreement with the expectations from scaling, however the power law for the SCL appears to be slightly steeper than expected.

T(K)	W(decades)	W	O _{measured}	σ _{scaling}
98	1.262	1.107	0.336	0.371
100	1.248	1.095	0.346	0.377
102	1.233	1.082	0.364	0.386
104	1.227	1.076	0.359	0.389
106	1.219	1.069	0.386	0.393

Table 6.6. Measured relaxation widths and comparison of scaling-predicted and actual high-frequency power laws for the RP crystal phase of ethanol.

T(K)	W(decades)	W	o measured	♂ scaling
98	1.238	1.086	0.419	0.383
100	1.223	1.073	0.472	0.391

Table 6.7. Measured relaxation widths and comparison of scaling-inferred and actual high-frequency power laws for the SCL phase of ethanol.

III. c. Dixon Scaling of Ethanol Dielectric Data.

The α -relaxation data for both the RP crystal and SCL phases of ethanol were scaled using Dixon's formalism, which was introduced earlier in Chapter 5, section II.b. The results of the scaling for the RP crystal and SCL phases are shown in Figure 6.12. As can be seen from the figure, the RP crystal data appear to scale in accordance with that of true structural glasses (in order to avoid clutter on the scaling plot we have represented the so-called "master curve" using data from glycerol) while the SCL data show deviations at the higher frequencies. This behavior is consistent with the results of the power law comparsion carried out in the previous section, where it was shown that the measured high-frequency power law for the RP crystal was in agreement with the prediction of eq. 6.3. The steeper slope of the SCL power law manifests itself as the observed deviation on the scaling plot.

It is not clear why the RP crystal scales in accordance with structural glasses while the SCL appears to show deviations. In fact, this result is perhaps opposite to what might have been expected. However, because of the limited amount of SCL data available (due to the temperature range over which the phase is stable for measurement), we caution against a hasty dismissal of the scaling form's implied universality in the dielectric response of glass forming liquids.

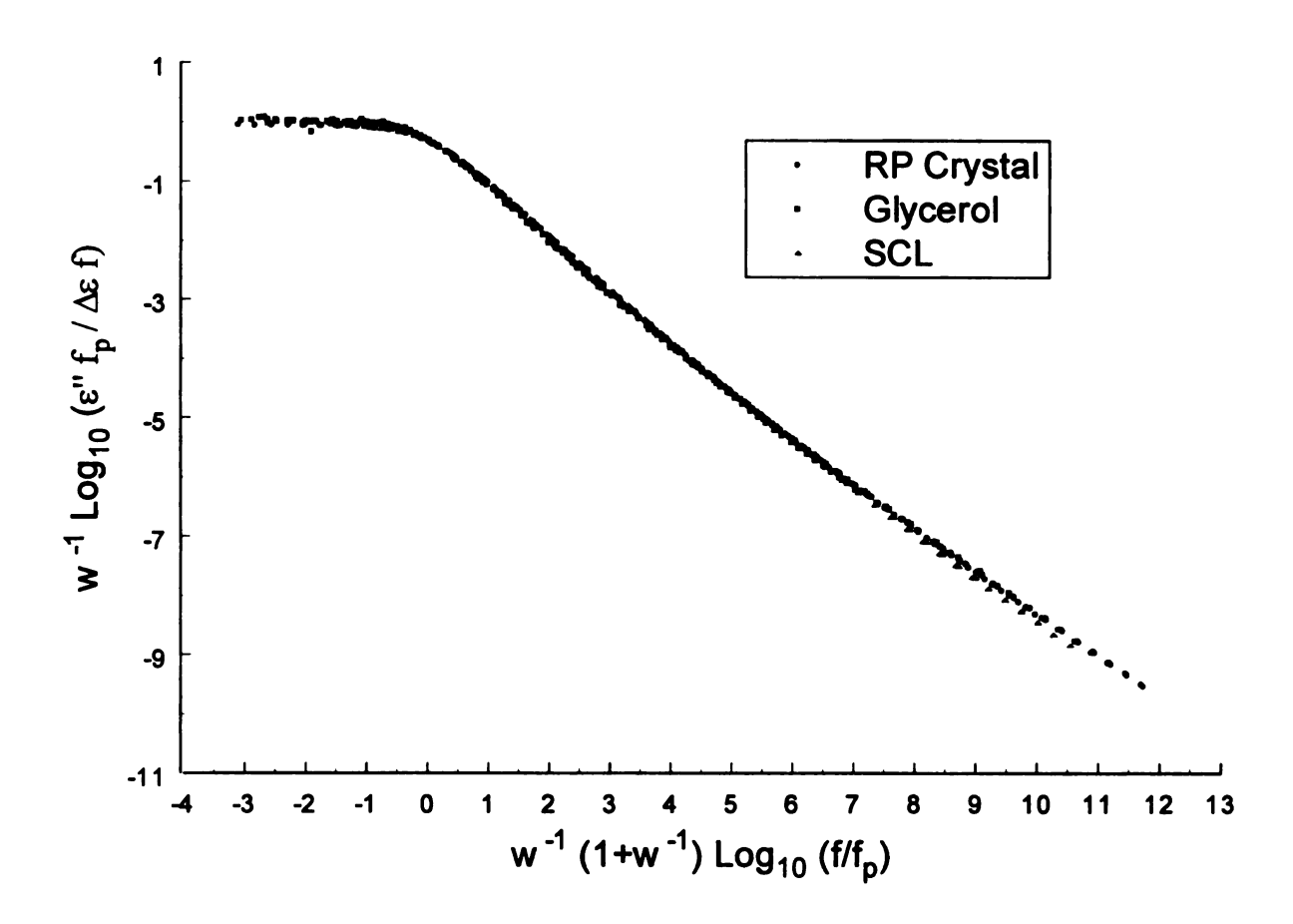


Figure 6.12. Dixon scaling of the RP crystal and SCL ethanol dielectric data.

The RP crystal scales in accordance with structural glasses
(represented here by glycerol) while the SCL shows systematic deviations at high frequencies.

REFERENCES

- [1] O. Haida, H. Suga, and S. Seki, J. Chem. Thermodyn. 9, 1133 (1977).
- [2] A. Srinivasan, F.J. Bermejo, A. de Andres, J. Dawidowski, J. Zuniga, and A. Criado, Phys. Rev. B 53, 8172 (1996).
- [3] R. Fayos, F.J. Bermejo, J. Dawidowski, H.E. Fischer, and M.A. Gonzalez, Phys. Rev. Lett. 77, 3823 (1996).
- [4] M.A. Ramos, S. Vieira, F.J. Bermejo, J. Dawidowski, H.E. Fischer, H. Schober, M.A. Gonzalez, C.K. Loong, and D.L. Price, Phys. Rev. Lett. 78, 82 (1997).
- [5] A typographical error in ref. 1 giving T_m as 169 K has been propagated in some papers, e.g. refs. 6 and 7.
- [6] D.W. Davidson and R.H. Cole, J. Chem. Phys. 18, 1417 (1951).
- [7] G. Williams and D. C. Watts, Trans. Faraday Soc. 66, 80 (1970).
- [8] P.K. Dixon, L. Wu, S.R. Nagel, B.D. Williams, and J.P. Carini, Phys. Rev. Lett. 65, 1108 (1990).
- [9] R. Brand, P. Lunkenheimer, and A. Loidl, Phys. Rev. B 56, 5713-5716 (1997).
- [10] M.D. Ediger, C.A. Angell, and S.R. Nagel, J. Phys. Chem. **100**, 13200-13212 (1996).
- [11] H. Vogel, Phys. Z. 22, 645 (1961); G.S. Fulcher, J. Am. Ceram. Soc. 8, 339 (1925);G. Tamman and W. Hesse, Z. Anorg. Chem. 156, 245 (1926).
- [12] F.J. Bermejo, A. Criado, R. Fayos, R. Fernandez-Perea, H. E. Fischer, E. Suard, A. Guelylah and J. Zuniga, Phys. Rev. B 56, 11536 (1997); F.J. Bermejo, H.E. Fischer, M.A. Ramos, A. de Andres, J. Davidowski, and R. Fayos in Complex Behaviour of Glassy Systems, M. Rubi et al.. (Eds.) Springer Lecture Notes in Physics, Springer Verlag, Berlin 1997, p. 44.
- [13] N. Menon and S. R. Nagel, Phys. Rev. Lett. 74, 1230 (1995).
- [14] M. A. Miller, M. J. Ruiz, F. J. Bermejo, and N. O. Birge, (accepted for publication in Phys. Rev. B 57, June 1, (1998)).

Chapter 7

NONLINEAR DIELECTRIC MEASUREMENT

I. Motivation and Background.

As described in Chapter 2, the relaxation behavior of many supercooled liquids is described quite accurately by the VTF form. The apparent divergence of the VTF equation (eq. 2.2) at a temperature T_0 has prompted a lengthy debate as to whether or not the glass transition is due to a thermodynamic phase transition. To date, no simulation [1] or experimental [2,3] study has observed evidence for such a transition, suggesting that the glass transition is simply the result of kinetic slowing of the liquid. This in fact may be true, however the possibility exists that the reason experimental studies have failed to observe a phase transition is because they are simply unable to get close enough to T_0 .

The idea to measure the *nonlinear* dielectric susceptibility in glass forming materials has its root in the field of spin glass systems [4], which are random spin systems with competing ferromagnetic and antiferromagnetic interactions. Prominent examples of spin glasses include AgMn and CuMn. In these systems, the random placement of the ions provides disorder, and the presence of the RKKY [5] interaction gives rise to both ferromagnetic and antiferromagnetic interactions. Because of the slow dynamics near the spin glass transition, research on spin glasses was plagued by many of the same problems faced by studies of the liquid-glass transition. However, a major breakthrough occurred when it was shown that the nonlinear magnetic susceptibility of

AgMn increased rapidly near the transition [6,7]. The equation of state for the system can be expanded in terms of the magnetic field:

(7.1)
$$M_H = \chi_0 - \chi_{NL}H^2 + O(H^4)$$

Here, M is the magnetization, H is the magnetic field, χ_0 is the linear magnetic susceptibility and χ_{NL} is the nonlinear magnetic susceptibility. The nonlinear susceptibility, which is related to the correlation length in a random system, is observed to diverge at a critical temperature T_f :

$$(7.2) \qquad \chi_{NL} = \left[\frac{T - T_f}{T_f} \right]^{-\gamma}$$

Because of its sensitivity to a growing correlation length in the material, a diverging nonlinear susceptibility is a characteristic signature of a second-order phase transition.

We are interested in carrying out a similar experiment for glass forming materials near the glass transition. The idea is to measure the nonlinear dielectric constant for a properly chosen material to determine if a similar divergence can be observed. For dielectrics, the nonlinear dielectric constant is defined by

(7.2)
$$D_E = \varepsilon^* - \varepsilon_{NL} E^2 + O(E^4)$$

where D is the electric displacement, E is the electric field, ε^* is the linear dielectric constant and ε_{NL} is the nonlinear dielectric constant. If a diverging nonlinear dielectric constant is observed, it may provide a conclusive answer to the elusive phase transition question. The absence of such a divergence in a carefully chosen material would also be meaningful, as it would raise fundamental questions regarding the ability of experiments to ever observe behavior consistent with a phase transition near T_0 .

II. Nonlinear Measurement Circuit.

Attempting a measurement of this sort is difficult because the nonlinear dielectric constant is much smaller in magnitude than the linear dielectric constant. By applying a large sinusoidal electric field of frequency f to a capacitor containing the sample, one can measure the response of the system at f as well as higher harmonics 3f, 5f, etc. The lowest order nonlinear signal occurs at 3f, and corresponds to ε_{NL} . However, because the nonlinear signal is much smaller in magnitude than the linear signal, a measurement scheme must be devised which can subtract the large linear response from the signal. The circuit we plan to use to measure the nonlinear dielectric constant is shown in Figure 7.1.

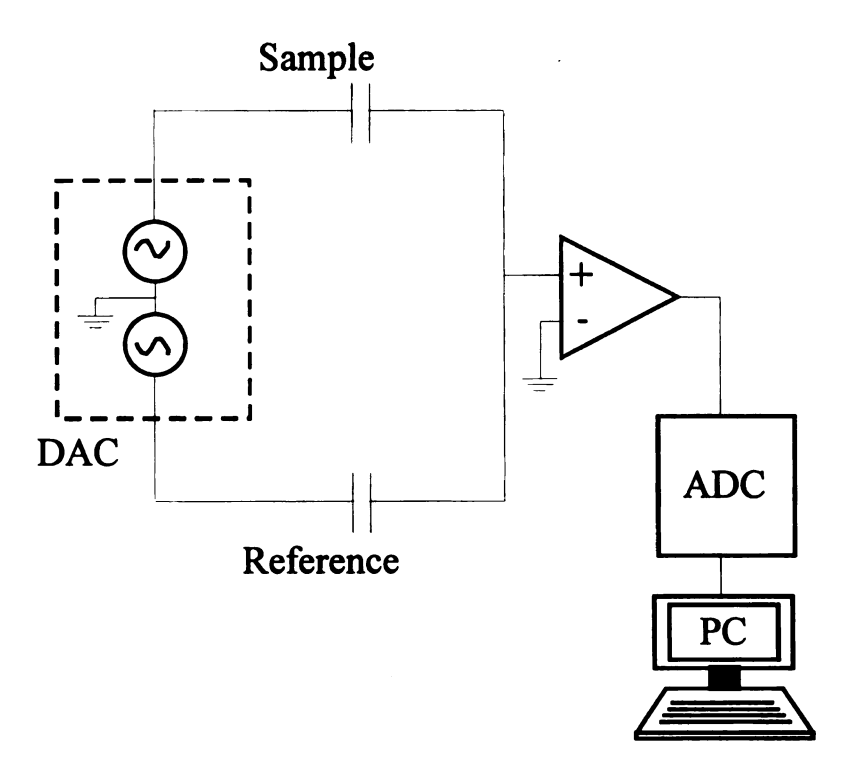


Figure 7.1. Circuit for nonlinear measurement.

Subtraction of the linear dielectric response is accomplished by a driving a reference capacitor nearly 180 degrees out of phase with respect to the capacitor containing the sample. Both the sample and reference capacitor are driven by a 2-channel IOTech digital-analog converter (DAC) which can perform the required phase shifting digitally. The output signal from the current-to-voltage amplifier is then read by a IOTech analog-to-digital converter (ADC) that is synchronized to the DAC. Information about the response of the system at the driving frequency and higher harmonics is obtained by fast-Fourier transformation (FFT) of the data using a personal computer.

III. Present Status of Experimental Work.

To minimize the noise level present in the measurement, synchronization of the DAC output and ADC sampling is crucial. To accomplish this, we trigger the ADC sampling using an appropriate division of the DAC's internal clock signal. To set the ADC sampling rate, we divide the DAC's internal 100 kHz clock signal using a programmable divide-by-N counter (Harris model CD4059AE, 24 pin DIP) and supply the resulting signal to the external trigger of the ACD. To verify that this method produces a low-background environment, we have performed extensive stimulus-response testing of the DAC and ADC. In general the synchronization between the instruments appears good, but we have encountered additional sidebands in the frequency response which are of undetermined origin. The sidebands appear unresponsive to filtering, and must be eradicated before the measurement can be proceed further. Once the desired low-noise background is achieved, we are confident that the measurement can be performed.

REFERENCES

- [1] R. M. Ernst, S. R. Nagel, and G. S. Grest, Phys. Rev. B 43, 8070 (1991).
- [2] L. Wu, Phys. Rev. B 43, 9906 (1991).
- [3] P. K. Dixon, S. R. Nagel, and D. Weitz, J. Chem. Phys. 94, 6924 (1991).
- [4] K. Binder and A. P. Young, Rev. Mod. Phys. 58, 801 (1986).
- [5] M. A. Ruderman and C. Kittel, Phys. Rev. 96, 99 (1954).
- [6] P. Monod and H. Bouchiat, J. Phys. (Paris) Lett. 43, L45 (1986).
- [7] L. P. Levy, Phys. Rev. B 33, 4963 (1988).

Chapter 8

SUMMARY AND FUTURE DIRECTIONS

In this work we have used dielectric spectroscopy to study the glass transition in the orientationally-disordered crystals cyclo-octanol and ethanol. In general, we find that the orientational glass transition in each material displays the same two characteristic features of the structural glass transition in fully-disordered liquids: 1) rapidly increasing relaxation times as the temperature is lowered toward the glass transition temperature T_g, and 2) increasingly non-Debye relaxation behavior with decreasing temperature. The appearance of these features in a system lacking translational freedom suggests that these materials may be of great interest as model glass systems for theoretical and numerical simulation studies of the glass transition.

However, in addition to displaying the general characteristics of glassy behavior, an ideal model glass system must display structural simplicity. The behavior of a material is critically linked to its structural properties, and a complete dynamical picture can only be achieved by examining the dielectric properties over as wide a frequency range as possible. More specifically, the extension of the cyclo-octanol dielectric measurements to higher frequency revealed the appearance of a complicating β -relaxation process that overlapped the primary α -relaxation at temperatures above T_g . Because the β -relaxation was also observed in the stable crystal as well, it is believed to be associated with the intrinsic flexibility of the cyclo-octanol molecule. Thus, while

cyclo-octanol satisfies the basic requirements for a model glass, its structural complexity and overlapping relaxation processes suggest that it is not an ideal model glass.

The subsequent study of ethanol provided important insights into the nature of the glass transition which could not be gained from cyclo-octanol. First, the intrinsic polymorphic character of ethanol allowed for a quantitative comparison of the glass transition dynamics in the supercooled liquid and rotator crystal phases. The results of the comparison indicate that rotational motion is the dominant dynamical process governing the glass transition in the SCL phase, and that diffusive processes contribute to a lesser extent. Such a result may imply that theories of the glass transition based solely on the diffusive properties of liquids are too general in form, and tend to exclude important contributions from rotational processes.

The structural simplicity of ethanol also provided an opportunity to examine the shape of the α -relaxation without the additional complexity of superimposed relaxation processes (as was the case with cyclo-octanol). Dixon scaling of the RP crystal data showed good agreement with the "master curve" characterizing a wide variety of materials. Equivalently, the power law nature of the relaxation at high frequencies was shown to agree well with the scaling-based predictions of Menon *et al.* The SCL phase appeared to show deviations from the structural glass scaling in the high frequencies, and also displayed steeper power law behavior than the RP crystal.

Based on our results, we conclude that the RP crystal phase of ethanol appears to be the best example of a physical model glass system discovered so far. Thus, the construction of a minimal theoretical model of the glass transition utilizing restricted degrees of freedom appears relevant to the behavior of more complex structural glasses.

A model such as that explored by C. Renner *et al.* [1] should be simple enough to allow a detailed numerical and analytical treatment.

Finally, we have constructed the framework required for the difficult nonlinear measurement. After the resolution of certain experimental obstacles, performing this measurement on an extremely fragile liquid (e.g. propylene carbonate, etc.) may resolve the question of whether or not a thermodynamic phase transition underlies the glass transition in supercooled liquids.

REFERENCES

[1] C. Renner, H. Lowen, and J.L. Barrat, Phys. Rev. E 52, 5091(1995).

Appendix A

DATA CORRECTION METHODS

I. Introduction.

Introductory physics textbooks often leave one with the impression that obtaining accurate measurements of a material's dielectric constant is a simple matter of dividing the measured capacitance with the dielectric in place by that of some appropriate empty cell capacitance. Unfortunately, real-world experiments are complicated by a number of factors including the parasitic effects of lead capacitance and inductance, as well as phase-shifts due to extended cabling between the sample and measuring instrumentation.

These effects become particularly important at high frequencies (> 1 MHz), but also affect the integrity of measurements made at low frequencies as well. Thus, corrections must be applied in order to obtain accurate results in any dielectric spectroscopy experiment. Considerable effort has been put forth in determining a practical scheme for data correction as well as attempting to understand the nature of data corrections from a theoretical perspective. Section II of this appendix will describe the actual empirical correction scheme used for all dielectric data presented in this thesis. Section III of this appendix will outline in detail our theoretical attempt to derive high-frequency data corrections for the Hewlett-Packard HP4192A Impedance Analyzer. These calculations are based on transmission line theory and reasonable assumptions regarding the analyzer's measurement circuitry. Unfortunately, despite a seemingly

satisfactory analysis, the resulting theoretical correction scheme was unable to account for the observed behavior in the experiment.

II. Empirical Dielectric Data Correction.

II. a. Correction of Low-frequency Data.

It was initially thought that empty cell measurements alone would suffice for the correction of parasitic elements in the analysis of the actual dielectric data. In general, the empty cell dielectric measurement can be described by a frequency-dependent magnitude A(f) and phase $\phi(f)$, where these quantities are defined as:

$$(A.1) \quad \phi(f) = tan^{-1} \left(\frac{V_x}{V_y} \right) = tan^{-1} \left(\frac{\epsilon''}{\epsilon'} \right)$$

(A.2)
$$A(f) = \frac{\sqrt{V_x^2 + V_y^2}}{\omega C_0 \beta V_0}$$

As defined in Chapter 4, β is the gain of the current amplifier, C_0 is the capacitance of the empty cell, and V_0 is the voltage of the driving oscillator.

For an ideal capacitor with no dielectric in place, measurement at any frequency should yield zero for V_x and a constant for V_y . Thus, $\phi(f) = 0$ and A(f) = 1 (see eqs. 4.36 and 4.37). However, for the capacitor used in our experiments, the observed empty cell measurements showed a tendency toward negative phase values and increasing amplitudes at the high end of the measurement range. Theoretically, with knowledge of the empty cell phase and magnitude in hand, correction of data taken with the dielectric in place can then be accomplished by first performing a rotation through angle ϕ which corrects for phase errors, and subsequently correcting magnitude using A(f):

(A.3)
$$\begin{pmatrix} V_x' \\ V_y' \end{pmatrix} = \begin{pmatrix} \cos \phi & -\sin \phi \\ \sin \phi & \cos \phi \end{pmatrix} \begin{pmatrix} V_x \\ V_y \end{pmatrix}$$

(A.4)
$$V''_x = \frac{V'_x}{A(f)}$$

(A.5)
$$V_y'' = \frac{V_y'}{A(f)}$$

After the data has been corrected for phase and magnitude, ϵ' and ϵ'' can be determined from eq. 4.36 and 4.37:

$$(A.6) \quad \epsilon' = \frac{V_y''}{\beta \omega V_0 C_0}$$

$$(A.7) \quad \epsilon'' = \frac{V_x''}{\beta \omega V_0 C_0}$$

The problem we encountered with correction of the low-frequency data was the following: Because the high-frequency experiment was performed first, only high-frequency empty cell data was taken before the sample cell was filled and permanently sealed. When the experiment was converted to the low-frequency measurement scheme, we had no opportunity to perform low-frequency measurements on the empty cell. Thus, we had to search for an alternative method of constructing an appropriate "empty cell" data set. To do this, we needed to find a structural phase of the material where ε' was essentially frequency independent and ε'' was zero. Fortunately, at low temperature the stable crystalline phase provided these characteristics. In the end, the measurements used to correct the rotator phase and supercooled liquid data at a given temperature were actually a normalized version of the crystalline dielectric data at a temperature where the sample was known to have no loss. For example, our low-frequency ethanol

measurements were corrected using normalized 90 K crystal data. The only modification to the data correction equations shown above is the inclusion of an appropriate normalization factor in A(f). This method proved to be adequate for data correction, and as will be described in the next section, was used for high-frequency data correction as well.

II. b. Correction of High-Frequency Data.

The correction of high-frequency data obtained from the HP4192A Impedance Analyzer followed the same procedure given in section II.a. for the low-frequency data, however the correction equations are expressed in different variables. Thus, for completeness and future reference the equations will be outlined in this section.

For the empty sample cell, the impedance analyzer measures the capacitance C and conductance G of the sample. The admittance Y of the empty cell is then:

(A.8)
$$Y = G - i\omega C$$

The magnitude and phase are then expressed as

(A.9)
$$A(f) = |Y| = \frac{\sqrt{G^2 + \omega^2 C^2}}{\omega C_0}$$

$$(A.10) \qquad \phi(f) = \tan^{-1} \left(\frac{G}{\omega C}\right)$$

Similar to the section II.a, the data correction process involves both phase correction and magnitude correction using an appropriate set of empty cell data. Unfortunately, the actual empty cell data available was unable to correct the measurements. We believe that the reason for the failure is not due to the correction method described above, but rather because the necessary correction depends upon the impedance of the sample, which of course is much different for a filled capacitor and varies with applied field frequency and

temperature. Thus, we again turned to crystalline phase in order to construct the "empty cell" set. For example, correction of the high frequency ethanol data used crystal measurements taken at 87 K. The correction scheme is then identical to that outlined in the previous section:

(A.11)
$$\begin{pmatrix} G' \\ \omega C' \end{pmatrix} = \begin{pmatrix} \cos \phi & -\sin \phi \\ \sin \phi & \cos \phi \end{pmatrix} \begin{pmatrix} G \\ \omega C \end{pmatrix}$$

$$(A.12) G'' = \frac{G'}{A(f)}$$

(A.13)
$$\omega C'' = \frac{\omega C'}{A(f)}$$

Here, the A(f) in eq. A.12 and A.13 must be appropriately normalized. After correction of the data for phase and magnitude, ε' and ε'' can be extracted using eq. 4.38 and 4.39:

$$(A.14) \qquad \varepsilon' = \frac{C''}{C_0}$$

$$(A.15) \epsilon'' = \frac{G''}{\omega C_0}$$

III. Theoretical Attempts to Correct High-Frequency Data.

The high-frequency measurements (1kHz - 10 MHz) were made exclusively with the Hewlett Packard HP4192A Impedance Analyzer. To determine the behavior of the HP4192A over its listed frequency range, we designed a homemade 512 pF parallel-plate air capacitor of high stability and measured its frequency response. The behavior of the impedance analyzer can be described as follows: At frequencies less than approximately 1 MHz, the measured capacitance C and conductance G of the air capacitor was negligibly different from 512 pF and 0 mho (1mho = 1 Ω^{-1}), respectively, as expected. However, for frequencies above 1 MHz, the measured capacitance would fall steadily

while the conductance measurements took on *negative* values. The reason for this behavior is due to inductance effects in the sample leads and phase shifts in the coaxial cables. For a standard length (1 meter) of coaxial cabling between the impedance analyzer and DUT (Device Under Test), the HP4192A provides an internal correction procedure which automatically compensates for phase and magnitude errors occurring at high frequency. Thus, we wanted to determine the form of the correction used by the analyzer. If it were possible to do so, we would be able to construct our own correction scheme that would work for cabling of arbitrary length.

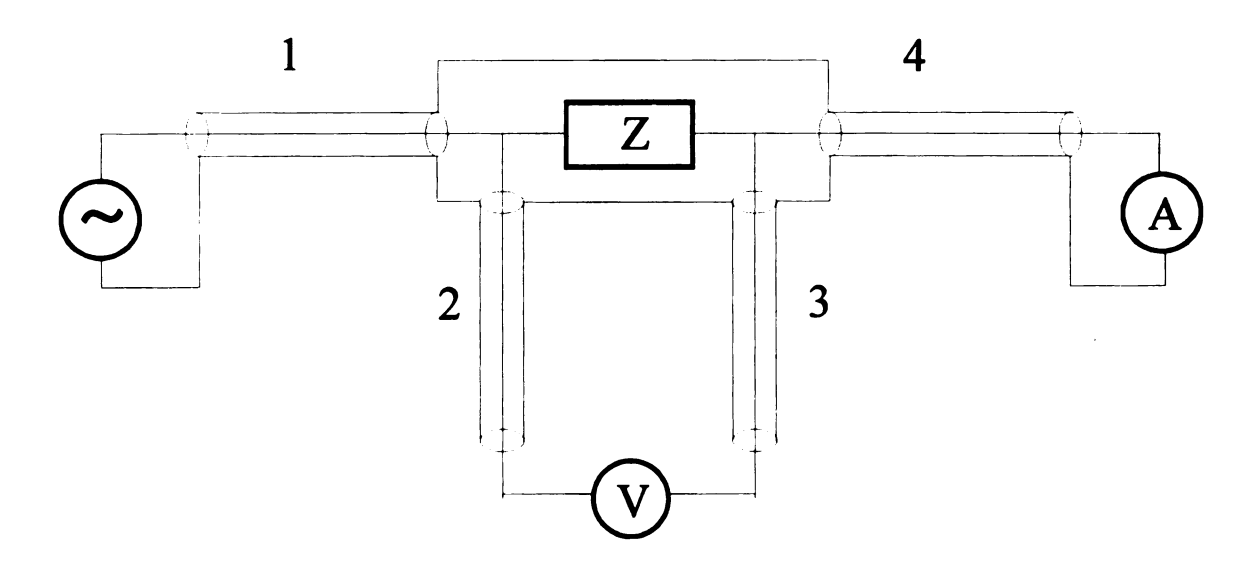


Figure A.1. Circuit diagram for impedance measurement using HP4192A.

A schematic diagram of the HP4192A's impedance measurement circuit can be seen in Figure A.1. To measure the impedance of the sample, the analyzer measures the current through and voltage across the DUT using a four-terminal lead arrangement

consisting of four coaxial cables (1-4 in the diagram). To carry out the analysis of this circuit, we make the following assumptions:

- (1) HP4192A current meter has 50 Ω input impedance, thus, no reflected wave will occur at the input to the meter.
- (2) HP4192A voltmeter has infinite impedance and draws no current.
- (3) All quantities vary in time as e^{-iωt}.
- (4) All cables have same length.
- (5) For each cable, x = 0 is located at the impedance analyzer, x = L is at the DUT.
- (6) In Figure A.1, Current leads are labeled 1 and 4, voltage leads are 2 and 3.
- (7) Measured current and voltage are I_0 and V_0 , respectively.
- (8) The impedance of the coaxial cable is $Z_0 = 50 \Omega$ /meter.
- (9) $k = 2\pi/\lambda$, where λ is the wavelength of the electromagnetic wave in the coaxial cable.

From assumption 1, we can write the voltage and current for cable #4 as:

(A.16)
$$V_4(x) = V_4 e^{-ikx}$$

(A.17)
$$I_4(x) = -\frac{V_4}{Z_0}e^{-ikx}$$

At the impedance analyzer (x = 0), the current in cable #4 will be

$$(A.18)$$
 $I_4(0) = -I_0 \Rightarrow V_4 = I_0 Z_0$

Thus, the current and voltage expressions can now be written as

(A.19)
$$V_4(x) = I_0 Z_0 e^{-ikx}$$

(A.20)
$$I_4(x) = -I_0 e^{-ikx}$$

Using assumption #2 we can write expressions for $V_2(x)$ and $V_3(x)$, which have similar form and will satisfy the boundary conditions at the volmeter:

(A.21)
$$V_{2,3}(x) = V_{2,3}(e^{ikx} + e^{-ikx})$$

(A.22)
$$I_{2,3}(x) = \frac{V_{2,3}}{Z_0} (e^{ikx} - e^{-ikx})$$

The volmeter reading will then be the voltage difference between cables 2 and 3 at x = 0:

(A.23)
$$V_2(0) - V_3(0) = V_0 \implies 2V_2 - 2V_3 = V_0$$

The actual voltage drop at the sample location (x = L) is:

(A.24)
$$V_s = V_2(L) - V_3(L) \Rightarrow V_s = (V_2 - V_3)(e^{ikL} + e^{-ikL})$$

Substituting the result from eq. A.23 into A.24 gives:

(A.25)
$$V_s = \frac{V_0}{2} (e^{ikL} + e^{-ikL}) = V_0 \cos(kL)$$

As it turns out, we do not need to know anything about the wave in cable #1, so we will not introduce expressions for $V_1(x)$ and boundary conditions on the current and voltage at the junction of cables 1 and 2. However, we do need to apply boundary conditions at the junction of cables 3 and 4 in order to find the current through the sample I_s :

(A.26)
$$V_3(L) = V_4(L) \implies V_3(e^{ikL} + e^{-ikL}) = I_0 Z_0 e^{-ikL}$$

(A.27)
$$I_3(L) + I_4(L) + I_s = 0 \implies \frac{V_3}{Z_0} (e^{ikL} - e^{-ikL}) - I_0 e^{-ikL} + I_s = 0$$

Substituting for V_3 in eq. A.27 using A.26, and solving for I_s yields:

$$(A.28) \qquad I_{s} = \frac{-I_{0}e^{-ikL}}{e^{ikL} + e^{-ikL}} \Big(e^{ikL} - e^{-ikL} \Big) + I_{0}e^{-iKL}$$

(A.29)
$$I_s = I_0 e^{-ikL} \left[1 - \frac{e^{ikL} - e^{-ikL}}{e^{ikL} + e^{-ikL}} \right]$$

(A.30)
$$I_s = \frac{2I_0e^{-2ikL}}{e^{ikL} + e^{-ikL}} = \frac{I_0e^{-2ikL}}{\cos(kL)}$$

The actual impedance of the sample, Z_s, can be found by dividing eq. A.25 by A.29:

(A.31)
$$Z_s = \frac{V_s}{I_s} = \frac{V_0 \cos^2(kL)}{I_0 e^{-2ikL}}$$

Defining the impedance as measured by the HP4192A as $Z_m \equiv V_0 / I_0$, we can write the actual sample impedance in terms of Z_m :

(A.32)
$$Z_s = Z_m \left(\frac{\cos^2(kL)}{e^{-2ikL}} \right) = Z_m \cos^2(kL)e^{2ikL}$$

Now that we have the actual sample impedance expressed as a function of the measured impedance, we must supply expressions for Z_s and Z_m . Since the analyzer models the sample in terms of a capacitance C in parallel with a conductance G, we can substitute the general form $Z^{-1} = G - i\omega C$ into eq. A.32:

(A.33)
$$G_m - i\omega C_m = (G_s - i\omega C_s)\cos^2(kL)e^{2ikL}$$

(A.34)
$$G_m - i\omega C_m = (G_s - i\omega C_s)\cos^2(kL)[\cos(2kL) + i\sin(2kL)]$$

Solving A.34 for G_s and C_s provides the expressions for the correction formula:

(A.35)
$$G_s = \frac{1}{\cos^2(kL)} [G_m \cos(2kL) - \omega C_m \sin(2kL)]$$

(A.36)
$$C_s = \frac{1}{\cos^2(kL)} \left[C_m \cos(2kL) + \frac{G_m}{\omega} \sin(2kL) \right]$$

Eq. A.35 and A.36 can then be applied to any set of measurements (C_m , G_m) taken at frequency $\omega = 2\pi f$ to obtain the corrected values.

Despite the apparent consistency of the analysis given above, eq. A.35 and A.36 were unable to satisfactorily correct our measurements. As shown in Figures A.2 and A.3 for measurements made on a 511-pF Air capacitor using 1 meter cables, the capacitance measurements tended to become *over-corrected* and the conductance measurements *under-corrected*. Thus, we must assume that our analysis is somehow flawed.

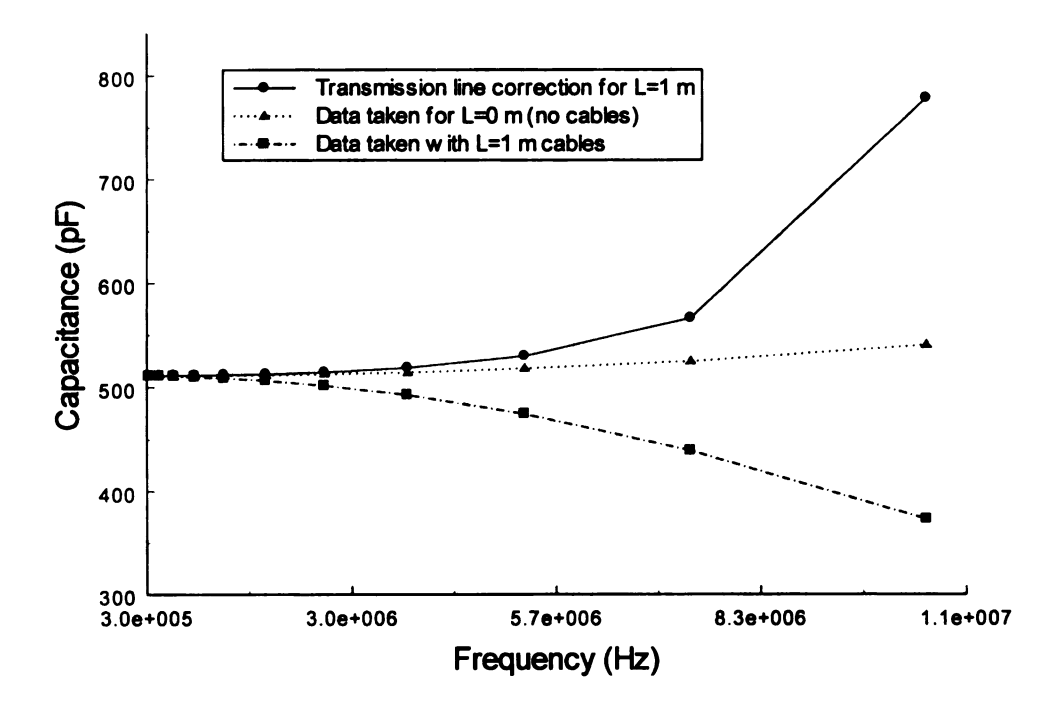


Figure A.2. Transmission line correction of capacitance data for a 511 pF Air capacitor. Correction of the data obtained at 1 meter should match the data obtained at the instrument front panel (L=0 meters). Clearly, the capacitance data is being over-corrected.

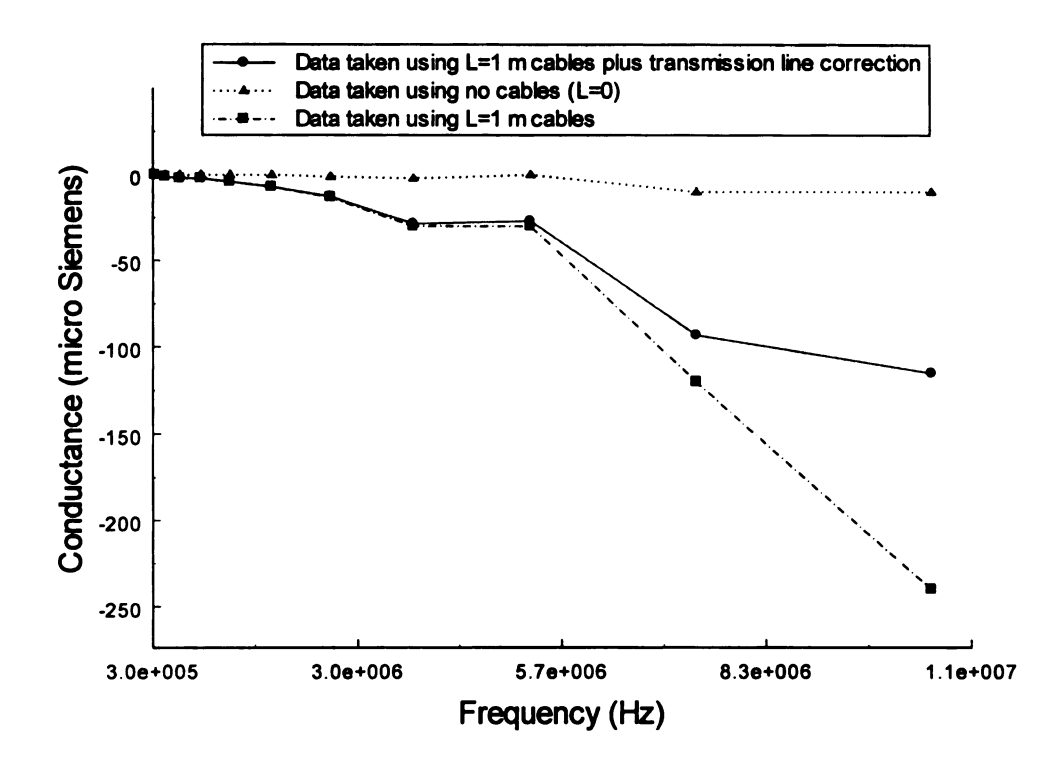


Figure A.3. Transmission line correction of conductance data for a 511 pF Air capacitor. Correction of the data obtained at 1 meter should match the data obtained at the instrument front panel (L=0 meters). Instead, the conductance data is being under-corrected.

